Universitat de Girona

BOND-SLIP AND CRACKING BEHAVIOUR OF GLASS FIBRE REINFORCED POLYMER REINFORCED CONCRETE TENSILE MEMBERS

Irene VILANOVA MARCO

Dipòsit legal: Gi. 2085-2015
http://hdl.handle.net/10803/328720

Universitat de Girona

DOCTORAL THESIS

BOND-SLIP AND CRACKING BEHAVIOUR OF GLASS FIBRE REINFORCED POLYMER REINFORCED CONCRETE TENSILE MEMBERS

Irene Vilanova Marco

2015

Universitat de Girona

BOND-SLIP AND CRACKING BEHAVIOUR OF GLASS FIBRE REINFORCED POLYMER REINFORCED CONCRETE TENSILE MEMBERS

Irene Vilanova Marco

2015

Doctorat en Tecnologia

Advisors: Dr. Lluís Torres Llinàs   Dra. Marta Baena Muñoz

per tu, perquè formes part de la meva vida,

Agraïments - Acknowledgements

First of all, I would like to thank my supervisors Lluís Torres Llinàs and Marta Baena Muñoz for their support, patience and their excellent guidance during this lasts years.

I would also like to thank Professor Gintaris Kaklauskas and Dr. Viktor Gribniak from Vilnius Gediminas Technical University for their support during my research stay in Lithuania.

I would like to acknowledge the Department of Mechanical Engineering and Industrial Construction of the University of Girona, and particularity to the research group Analysis of Advanced Materials for Structural Design (AMADE) for the opportunity given.

Vull donar les gràcies als meus companys d'AMADE pels bons moments que hem passat junts, amb ells els moments complicats han estat més lleugers, especialment a les Cristines i a la Marta pels moments de laboratori. Igualment vull agrair l'ajut d'en Jordi Vicens, en Sergi Saus i en Pere Bellvehí en la realització dels assaigs experimentals.

Vull agrair a la meva família, als meus pares, Josep i Maria Teresa, al meu germà Pau, als meus avis, encara que algun m'ha deixat en el camí, als meus cosins, a tota la família, per tota la confiança que sempre han dipositat en mi ajudant-me en tot moment i fent-me les coses més senzilles. Moltes gràcies.

Igualmente quiero agradecer el soporte recibido por parte de mi familia cubana, Inés, Odalis, Illiana, Jorge, Irma, Yudanis, Nordel y Jorge David, gracias por todo.

Finalment vull agrair a en Takeichi, per tot el que m'ha donat i tot el que espero que em continuï donant, merci Amorsito.

I a tu, Cigroncito, siguis on siguis, ens veurem aviat!

This Ph.D. thesis has been prepared as a compendium of papers, according to the regulations of Universitat de Girona (*Normativa d'ordenació dels ensenyaments universitaris de doctorat de la Universitat de Girona, aprovada pel Consell de Govern en al sessió 3/12, de 26 d'abril de 2012, i modificada pel Consell de Govern en la sessió 5/2013, de 25 de setembre de 2013*). This thesis includes three original papers: Two papers that have already been published in a peer-reviewed journal, and another one that has already been submitted. The complete references of the papers comprising this thesis, the impact factors, quartile, and category of the journals are:

- I. Vilanova, L. Torres, M. Baena, M. Llorens. *Numerical simulation of bond-slip interface and tension stiffening in GFRP RC tensile elements*. Submitted to Composite Structures.

  Impact index 3.120. 1st quartile, Category: Materials Science, Composites.

- I. Vilanova, L. Torres, M. Baena, G. Kaklauskas, V. Gribniak. *Experimental study of tension stiffening in GFRP RC tensile members under sustained load*. Engineering Structures 2014; 79:390-400.

  ISSN: 0141-0296

  doi: 10.1016/j.engstruct.2014.08.037

  Impact index 1.767. 1st quartile, Category: Engineering, Civil.

- I. Vilanova, M. Baena, L. Torres, C. Barris. *Experimental study of bond-slip of GFRP bars in concrete under sustained loads*. Composites Part B: Engineering 2015; 74:42-52.

  ISSN: 1359-8368

  doi: 10.1016/j.compositesb.2015.01.006

  Impact index 2.602. 1st quartile, Category: Engineering, Multidisciplinary.

The three papers have been published in (or submitted to) journals with impact factors within the first quartile, according to the 2013 Journal Citation Reports.

To whom it might concern,

Dr. Lluís Torres Llinàs and Dra. Marta Baena Muñoz, Professors at the Universitat de Girona of the Department of Enginyeria Mecànica i de la Construcció Industrial

CERTIFY that the study entitled "Bond-slip and cracking behaviour of glass fibre reinforced polymer reinforced concrete tensile members" has been carried out under their supervision by Irene Vilanova Marco to apply the doctoral degree with the International Mention.

Girona, September 2015

Dr. Lluís Torres Llinàs
Universitat de Girona, Spain

Dra. Marta Baena Muñoz
Universitat de Girona, Spain

List of Figures

List of Tables

Contents

Resum

L'ús de barres de material compost de matriu polimèrica, generalment conegut en anglès com *Fibre Reinforced Polymers* (FRP), s'ha introduït recentment com a substitució de l'acer en ambients agressius, corrosius o quan és necessària la transparència electromagnètica. La utilització d'aquests nous materials com a reforç intern en estructures de formigó implica majors deformacions comparades amb les estructures convencionals, ja que el seu mòdul elàstic és més baix que el de l'acer. Per aquest motiu l'estudi del comportament en servei adquireixi una importància fonamental en el disseny de les estructures de formigó armat amb barres de material compost.

El comportament estructural dels membres de formigó armat es veu afectat per l'adherència entre les armadures i el formigó que les envolta. Pel que fa a la deformació de l'element estructural, aquesta interacció permet que el formigó traccionat entre fissures contribueixi de manera significativa a incrementar la rigidesa de la peça respecte de la que tindria si estigués constituït per seccions totalment fissurades, fenomen conegut en anglès com *Tension Stiffening*. Com a conseqüència de la diversitat de propietats mecàniques que presenten els diferents tipus de barres de FRP i de la manca d'estandardització en dimensions i acabats superficials, no hi ha encara lleis representatives de la resposta adherència-lliscament que puguin ser aplicades de manera general. Per altra banda, el comportament adherent en el temps en elements amb càrrega mantinguda és un tema encara pendent d'estudi.

Per tal de contribuir al coneixement del comportament de les barres de FRP com a reforç intern d'estructures de formigó, en aquesta tesi es vol aprofundir en l'estudi de la fissuració i el *Tension Stiffening* d'elements de formigó armat amb barres de material compost de fibra de vidre (GFRP) sotmesos a tracció, així com en l'adherència entre armadures i formigó.

En primer lloc, ja que el comportament adherent entre el formigó i l'armadura de FRP varia en funció de diferents paràmetres relacionats amb les característiques de la barra de reforç, s'ha desenvolupat una metodologia que permet la implementació del comportament adherent entre els dos materials en la modelització numèrica amb elements finits, i concretament amb el programa ABAQUS. A partir de resultats experimentals obtinguts d'assaigs de *pull-out* i aplicant un mètode invers s'obtenen les lleis d'adherència aptes per ser incorporades a la modelització numèrica. Per tal de validar la metodologia, s'han modelitzat tirants de

formigó armats amb barres de GFRP obtenint-ne el comportament càrrega-deformació a tracció. Els resultats numèrics s'han comparat amb resultats experimentals mostrant una bona concordança. Per altra banda, la metodologia ha permès la simulació del procés de fissuració i l'obtenció de deformacions, així com les tensions en els dos materials, la tensió d'adherència i lliscament entre barra i formigó al llarg de l'espècimen.

Com a continuació de l'estudi, per tal d'aprofundir en el coneixement del comportament de les estructures de formigó armat amb reforç de GFRP, s'ha portat a terme una campanya experimental amb elements sotmesos a càrrega de tracció mantinguda, amb l'objectiu d'estudiar-ne la resposta a llarg termini. S'ha avaluat el seu comportament i l'evolució del *Tension Stiffening* i s'han comparat els resultats amb la formulació descrita en l'Eurocodi 2 que té en compte els efectes a llarg termini del formigó mitjançant el mètode del mòdul efectiu (*Effective Modulus Method*, EMM). La campanya experimental va consistir en l'assaig d'elements amb reforç de GFRP i formigons de resistències diferents, així com d'espècimens armats amb barres d'acer per tal de comparar-ne els resultats. Alguns dels elements assajats incorporaven galgues extensomètriques instal·lades dins la barra de reforç per tal de poder analitzar amb més precisió les deformacions, el procés de fissuració, el lliscament i l'adherència entre els dos materials. Els resultats mostren un augment de la deformació i una degradació del *Tension Stiffening* degut tant al procés de càrrega com als efectes del període de càrrega mantinguda. Mitjançant l'anàlisi dels resultats, i especialment de les galgues dins de la barra, s'observa un deteriorament de l'adherència en el temps amb increment del lliscament, així com una reducció de les tensions en el formigó, més important per a formigons de menor resistència, que tendeix a estabilitzar-se al cap d'uns 28 dies.

Finalment s'ha portat a terme una campanya experimental per tal d'aprofundir en l'estudi de l'adherència a llarg termini amb càrrega mantinguda. Es va utilitzar l'assaig de *pull-out* i la campanya va consistir en l'assaig de dotze espècimens de formigó amb barres de GFRP en els que es va variar la resistència a compressió del formigó i la longitud d'adherència. Per tal de poder comparar resultats, també es van assajar espècimens armats amb barres convencionals d'acer. Igualment que en l'estudi dels tirants, es va considerar oportú la col·locació de galgues dins d'algunes de les barres de reforç per analitzar més acuradament les deformacions i l'evolució de l'adherència a llarg termini. S'han analitzat els resultats tant en el procés d'aplicació de la càrrega com els resultats a llarg termini, observant una estabilització del lliscament a uns 60 dies després de l'inici dels assaigs, independentment de la resistència a compressió del formigó. Per altra banda, els resultats mostren que la resistència del formigó i la longitud d'adherència tenen una gran influència en la pèrdua d'adherència entre els dos materials a llarg termini.

Resumen

Las barras de material compuesto de matriz polimérica, generalmente conocido en inglés como *Fibre Reinforced Polymers* (FRP), han sido introducidas recientemente como substitución de las barras de acero en ambientes agresivos, corrosivos o cuando se requiere transparencia electromagnética. El uso de estos nuevos materiales como refuerzo interno en estructuras de hormigón implica mayores deformaciones en comparación con las estructuras convencionales, debido a que éstos tienen un menor módulo de elasticidad comparado con el del acero. Es por ello que el estudio del comportamiento en servicio adquiere una importancia fundamental en el diseño de las estructuras de hormigón armadas con barras de material compuesto.

El comportamiento estructural de los elementos de hormigón armado se ve afectado por la adherencia entre la armadura y el hormigón que la envuelve. En lo que se refiere a la deformación del elemento estructural, esta interacción permite que el hormigón traccionado entre fisuras contribuya de forma significativa a incrementar la rigidez de la pieza con respecto de la que ésta tendría si estuviera constituida por secciones totalmente fisuradas, fenómeno conocido en inglés como *Tension Stiffening*. Como consecuencia de la diversidad de propiedades mecánicas que los diferentes tipos de barras de FRP presentan, junto con la ausencia de estandarización en dimensiones y acabados superficiales, todavía no existen leyes representativas de la respuesta adherencia-deslizamiento que puedan ser utilizadas de forma general. Por otro lado, el comportamiento adherente en el tiempo de elementos sometidos a carga mantenida es un tema aún pendiente de estudio.

Con el fin de contribuir al conocimiento del comportamiento de las barras de FRP como refuerzo interno en estructuras de hormigón, en esta tesis se quiere profundizar en el estudio de la fisuración y el *Tension Stiffening* de elementos de hormigón armados con barras de material compuesto de fibra de vidrio (GFRP) sometidos a cargas de tracción. Igualmente, también se estudiará la adherencia entre el refuerzo y el hormigón.

Dado que el comportamiento adherente entre el hormigón y el refuerzo de FRP varía en función de distintos parámetros relacionados con las características de la barra de refuerzo, primeramente se ha desarrollado una metodología que permite la implementación del comportamiento adherente entre los dos materiales en la modelización numérica con elementos finitos, y más concretamente con el programa ABAQUS. A partir

de resultados experimentales obtenidos en ensayos de *pull-out*, y aplicando un método inverso, se obtienen las leyes de adherencia aptas por su implementación en la modelización numérica. Con el fin de validar la metodología se han modelizado tirantes de hormigón reforzados con barras de GFRP obteniendo su comportamiento carga-deformación a tracción. Se han comparado los resultados numéricos y experimentales mostrando una buena relación entre ambos. Por otro lado, la metodología permite la simulación del proceso de fisuración y la obtención de deformaciones, así como de tensiones en los dos materiales, tensión de adherencia y deslizamiento entre la barra y el hormigón a lo largo del espécimen.

Como continuación del estudio y con la finalidad de profundizar en el conocimiento del comportamiento de las estructuras de hormigón armadas con refuerzo de GFRP, se ha llevado a cabo una campaña experimental en elementos de hormigón armados con barras de GFRP sometidos a carga mantenida a tracción. El objetivo principal del ensayo ha sido el estudio del comportamiento a largo plazo de estos elementos. Se ha evaluado el comportamiento y la evolución del *Tension Stiffening* y se han comparado los resultados con la formulación descrita en el Eurocodigo 2, que considera los efectos a largo plazo del hormigón basándose en el método del módulo efectivo (*Effective Modulus Method*, EMM). La campaña experimental consistió en el ensayo de elementos con refuerzo de GFRP con resistencias de hormigones diferentes, así como de especímenes reforzados con acero para la comparación de resultados. Algunos de los elementos ensayados incorporaban galgas extensométricas instaladas dentro de la barra de refuerzo para analizar con más precisión las deformaciones, el proceso de fisuración, el deslizamiento y la adherencia entre los dos materiales. Los resultados muestran un aumento de la deformación y una degradación del *Tension Stiffening* debido tanto al proceso de carga como a los efectos del período de carga mantenida. El análisis de los resultados, y en especial el de las deformaciones registradas por las galgas dentro de la barra, muestra un deterioro de la adherencia en el tiempo con incremento del deslizamiento, así como una reducción de las tensiones en el hormigón, más importante para hormigones de menor resistencia, que tiende a estabilizarse al cabo de unos 28 días.

Finalmente se ha realizado una campaña experimental con el fin de profundizar en el estudio de la adherencia a largo plazo con carga sostenida. Se utilizó el ensayo de *pull-out* y la campaña consistió en el ensayo de doce especímenes de hormigón con barras de GFRP en los cuales se varió la resistencia del hormigón y la longitud de adherencia. Con fines comparativos también se ensayaron especímenes con refuerzo convencional de barras de acero. Del mismo modo que se hizo en el estudio de los tirantes, se consideró oportuna la colocación de galgas dentro de algunas de las barras de refuerzo para analizar mejor las deformaciones y la evolución de la adherencia a largo plazo. Se han analizado los resultados tanto en el proceso de carga como en el proceso a carga mantenida, observando una estabilización del deslizamiento unos 60 días después del inicio de los ensayos, independientemente de la resistencia del hormigón. Por otro lado, los resultados muestran que la resistencia del hormigón y la longitud de adherencia tienen una gran influencia en la pérdida de adherencia entre los dos materiales a largo plazo.

Summary

The use Fibre Reinforced Polymers (FRP) has recently been introduced as an alternative to steel in aggressive or corrosive environments or when the electromagnetic transparency is needed. The use of these new materials as internal reinforcement in reinforced concrete (RC) structures implies major deformation when compared to conventional structures, due to their lower modulus of elasticity compared with steel. Therefore, the study of their behaviour under serviceability conditions is of major importance in the design of FRP RC structures.

Bond between reinforcement and surrounding concrete highly affects the structural behaviour of RC elements. This interaction allows concrete in tension between cracks to significantly contribute to increase the element stiffness when compared to that of an element with fully cracked sections, this phenomenon being known as *Tension Stiffening* effect. Differences in mechanical properties of the available FRP bars as well as the lack of a standardization in their size and surface configuration lead to the existence of different bond-slip responses that do not converge into a unique general response. Besides, there is a gap in the knowledge of long-term bond behaviour under sustained load.

With the aim at contributing to the knowledge of FRP bars as internal reinforcement in concrete structures, this thesis aims at deepen in the study of cracking and the *Tension Stiffening* in concrete elements reinforced with glass fibre reinforced polymer bars (GFRP) under tensile loads, as well as bond between reinforcement and concrete.

Firstly, since bond behaviour between concrete and FRP reinforcing bar depends on many parameters regarding the bar characteristics, a methodology has been developed to implement the bond behaviour between the two materials in the numerical modelling with finite elements, specifically using ABAQUS program. Based on experimental results obtained from pull-out test, and applying the inverse method, the bond law to be used in the numerical model is obtained. The methodology is validated by modelling a total of four concrete ties reinforced with GFRP bars, where the load-strain behaviour under tensile load was recorded. Numerical results were compared with experimental results and good agreement was observed. Moreover, the proposed methodology allows the cracking process to be simulated, making possible to record strains and stresses in both materials, as well as bond stresses and slips between bar and concrete along the speci-

men.

With the aim at deepening in the knowledge of GFRP RC structures, the thesis continues with an experimental campaign on GFRP RC elements under tensile sustained loads. The main objective of the study is to evaluate the long-term behaviour of such elements. The evolution of *Tension Stiffening* effect is analysed and results are compared with Eurocode 2 formulations, which treat long-term effects in concrete by applying the effective modulus method (*Effective Modulus Method*, EMM). The experimental program consisted in testing GFRP RC elements with different target concrete strengths as well as additional steel RC specimens to benchmark the results. Some of the specimens included internally strain gauged reinforcing bars for a better analysis of strains, cracking process, slip and bond between the two materials. Results show an increase of strains and a degradation of *Tension Stiffening* due the loading process and the sustained load. The analysis of results, paying special attention to data obtained from strain gauges in the bar, show bond deterioration with time with an increase of slip, as well as a decrease in concrete stresses, larger for lower strength concretes, which tends to stabilize at approximately 28 days.

Finally, an additional experimental campaign on long-term bond under sustained load was conducted. The experimental campaign consisted on twelve pull-out specimens reinforced with GFRP, with varying target concrete strength and bond length. To benchmark results, some specimens with steel reinforcement were additionally tested. As for the previously presented experimental program on concrete ties, some specimens included strain gauges in the reinforcing bar to better analyse the strains and the evolution of bond under long-term loading. Data was collected and analysed at both the loading process and the sustained load process, and slip stabilization is observed to occur at 60 days after the beginning of the tests. This stabilization of the slip is visible irrespective of concrete strength. Besides, experimental results confirm concrete strength and bond length having an influence on the loss of bond between the two materials.

Chapter 1

Introduction and objectives

1.1 Introduction

The use of Fibre Reinforced Polymers (FRP) as reinforcement for Reinforced Concrete (RC) structures has recently been introduced as an alternative to steel reinforcement in corrosive environments or when the effects of electromagnetic fields may be present [1–4].

FRP bars are made of continuous fibres impregnated with polymeric matrix. The most common types of fibres are carbon, glass and aramid [5]. Lately, basalt fibres have also been investigated [6, 7]. FRP bars are anisotropic with higher modulus in the direction of the reinforcing fibres and are characterized by linear behaviour up to failure, without yielding. Compared to steel, FRP have higher tensile strength and lower modulus of elasticity (Fig. 1.1).
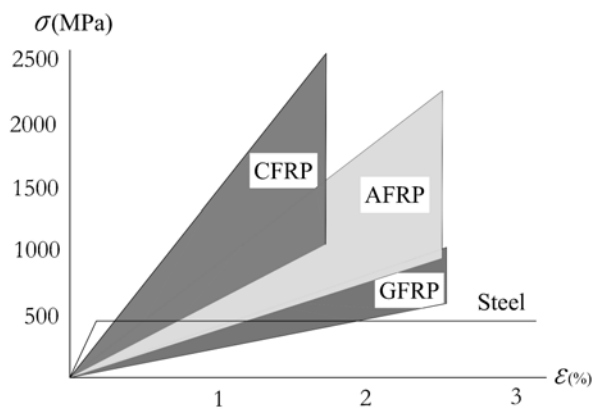
Figure 1.1: Typical stress-strain relationships for FRP and steel bars (after [8]).

The mechanical and bond characteristics of FRP used as internal reinforcement for RC elements result

in larger deflections and crack widths compared to the conventional steel RC elements. Consequently, serviceability requirements may govern the design of such members.

FRPs are new materials that are available in the form of different products with various types of fibres and resins, as well as surface configurations. All these aspects may have influence on the bond behaviour of the reinforcement which may present significant differences among products and compared to traditional steel reinforcement.

Bond-slip interaction between FRP bars and concrete play a fundamental role on the viability of these materials, with an important influence on the tension stiffening effect and therefore on load-deformation behaviour. Several parameters affect the bond-slip response between FRP bars and concrete, as for instance bar diameter, concrete grade, bond length, reinforcing material or even the surface treatment of the reinforcing bar [9, 10]. Due to the number of parameters involved and the lack of standardization in FRP bars' mechanical and geometrical properties, there is not a standard law for characterization of bond between FRP reinforcement and concrete. There are several procedures to experimentally obtain the interface behaviour between reinforcement and concrete, although due to its simplicity the pull-out test [10–16] has been the most widely used.

Bond-slip interaction between reinforcement and concrete is due to the effect of three main components: chemical adhesion, mechanical interaction, and friction [17]. For low bond stress values, the chemical adhesion breaks down (State I in Fig. 1.2); iin deformed bars, the limited wedging action of the lugs is the cause of transverse microcracks which allow bar to slip. In a pull-out failure, for higher bond stress values, the wedging action is enhanced and hoop stresses appear at the surrounding concrete, which at the same time exerts a confinement action on the bar. As a result, bond strength and stiffness are guaranteed (State II in Fig. 1.2). In that case, bond failure being caused by bar pull-out, the force transfer mechanism changes from rib bearing to friction (State III in Fig. 1.2).
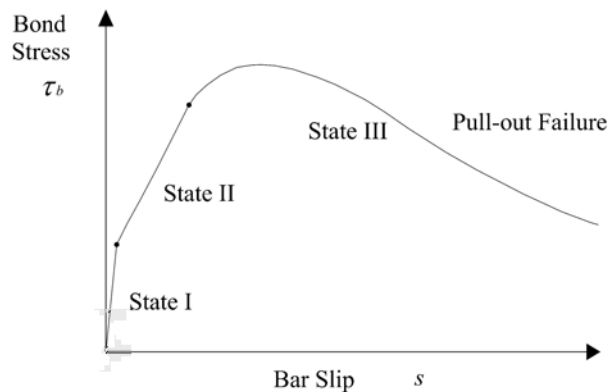
Figure 1.2: Bond stress-slip law for a pull-out failure (after [17]).

There exist a big amount of experimental test and analytical studies in the literature where the bond between the FRP reinforcing bar and concrete is analysed focusing on the short-term response [11, 13, 18–20]. However, a lack of numerical analyses regarding the implementation of bond-slip interface into numerical models is observed.

In the last decades, numerical procedures based on the Finite Element Method (FEM) have been used as a complement of the experimental research, allowing parametric studies for better understanding the influence of different properties and parameters, thus reducing the amount of experimentation. This methodology has started being used to develop numerical approaches to model bar-concrete interface behaviour. The great majority of the available research models the interaction between FRP and concrete assuming a perfect bond, where no slip between both materials is allowed [21–27].

As indicated previously there are many parameters influencing bond behaviour between FRP reinforcement and concrete and this may lead to significant differences among products and compared to traditional steel reinforcement. Since the mechanism of transference of stresses between concrete and reinforcement in a RC structural element is due to bond between both materials, changes in bond behaviour may affect the performance of the element. Likewise bond-slip response of FRP reinforcement in concrete can be obtained in a relatively simple way through the pull-out test, which allows easy comparison among different combinations of concrete and reinforcement. Nevertheless in what concerns the application to numerical simulation, bond-slip obtained from the pull-out test has been claimed to provide distorted responses due to possible effects of confining stresses as well as average behaviour along the bond length instead of local curves (in dependency of the bond length used).

Therefore, a methodology to easily implement a proper bond-slip response from experimental pull-out test in a numerical model would be of major interest for modelling FRP RC structural members. Such a methodology would allow enriching the study of FRP RC elements and obtaining the element response for the specific bond behaviour of an FRP bar and concrete combination.

On the other hand, a number of experimental programmes have been conducted to assess the influence of the different mechanical properties of FRP bars on the deformability and cracking (i.e. crack spacing, crack width and deflections) of FRP RC flexural elements [28–36]. The literature suggests that due to their lower modulus of elasticity, serviceability requirements often govern the design of FRP RC elements. Although the tension stiffening effect is characteristic of tensioned concrete, fewer studies focussed on FRP RC tensile members [37–39], having been proved the major influence of the tension stiffening effect on load-deformation behaviour. Most of this research has focused on the short-term response of RC elements, and limited works on the analysis of long-term performance of FRP RC members under sustained loads are available.

Under sustained load, the deformation of a RC specimen gradually increases with time and eventually

may be many times greater than its initial short-term value. If stress remains constant, the gradual development of strain with time is caused by creep and shrinkage. Creep strain is produced by sustained stress, while shrinkage strain is independent of it. Effects of sustained loads on tensile steel RC elements have been reported to cause a reduction in tension stiffening with time up to approximately half its initial short-term value [40–42]. Under sustained load concrete stresses in a cracked element reduce from the tensile strength to a lower level as cracking progresses; as creep is proportional to concrete stresses its effect might be very small. The results from Scott and Beeby [40–42] showed that effect of creep was insignificant and the reduction of tension stiffening was associated to the progression of the internal damage, although no further analysis regarding bond-slip under sustained load was carried out. On the other hand, although FRPs may experience some creep deformations, existing studies have shown that creep strains under serviceability conditions were not bigger than 5% of the initial strain values [43].

The long-term effects have usually been analytically modelled by using procedures such as the Effective Modulus Method (EMM) or the Age-Adjusted Effective Modulus Method (AAEMM) [44, 45]. The EMM adopts a reduced modulus of elasticity for the concrete dividing the short-term modulus by one plus the creep coefficient, thus considering that concrete stresses are constant along the time [46–48]. The AAEMM uses the same concept but the creep coefficient is reduced by multiplying by the ageing coefficient, which takes into account a predefined evolution of concrete stresses with time, usually that corresponding to relaxation of concrete under constant deformation [49–51]. Due to its simplicity and easiest application, the EMM has been adopted by different codes for steel RC as Eurocode 2 [47] and fib Model Code 2010 [48].

Different experimental campaigns aimed at analysing the influence of long-term effects on cracking, tension stiffening and deformations of FRP RC members have been reported. However, to the best of author?s knowledge, the effects of creep and shrinkage on tensile FRP RC elements have not been analysed neither experimentally nor analytically.

Besides, although some studies have started to analyse bond mechanisms under long-term effects, the existing literature is still limited. The study of bond degradation under sustained load effects was analysed by [52], with different reinforcement material and environmental conditions being considered. The pull-out specimens were loaded for one year. General conclusions of the study indicated that specimens with FRP reinforcement developed larger slips than those with steel reinforcement; stabilization of slips took place between 150 and 250 days after loading; and no influence of the different environments conditions was observed. A more recent work to determine a bond factor for long-term design was carried out by [53]. The authors simulated the behaviour of the bars in cracked concrete under extreme yet realistic environmental conditions. To this end the pull-out specimens were heated to 60°C and were kept water saturated at all times. Under these conditions the obtained design values for the tested FRP bars were found to be similar to steel reinforcement.

The review of the state of the art has shown the lack of studies and information on sustained loading

effects on FRP RC elements, putting in evidence the need of additional studies to deepen the understanding on long-term behaviour of tensile RC members using GFRP bars as internal reinforcement. The analysis would focus on both cracking and bond-slip behaviour of GFRP RC specimens.

The study should allow studying effects on time-dependent stresses and deformations, possible reduction of tension-stiffening, changes in bond-slip, as well as bond deterioration and redistribution of stresses with time. Additionally it could contribute to expand the scarce experimental data collection of long-term effects on FRP RC.

1.2 Objective

The main objective of this work is to study the bond-slip and cracking behaviour of GFRP RC tensile members. To this end, firstly a procedure for including the bond-slip interface behaviour between FRP reinforcement and concrete in a Finite Element (FE) model is presented. The goal is to develop a simple procedure to obtain a bond-slip constitutive law from experimental results of pull-out tests on a specific GFRP product and concrete combination, suitable to be implemented in a standard FE model. The methodology is subsequently applied to numerically simulate the behaviour of FRP RC members subjected to axial load. To better understand the long-term behaviour of these structures under sustained loading, two experimental studies are presented: the first one is focused on the evolution of strains and stresses of members subjected to sustained axial load, whilst the second one is focused on bond interaction in RC elements reinforced with GRFP bars under sustained loads.

According to this, the main tasks of this study are:

- To provide a simplified methodology for including a proper local bond-slip constitutive law derived from data obtained from experimental pull-out tests into a numerical model based on the FEM.

- To validate the applicability of the aforementioned bond-slip constitutive law by numerically modelling the behaviour of GFRP RC elements subjected to axial load and comparing the obtained numerical results with experimental data available in the literature.

- To carry out an experimental study to analyse long-term effects on cracking, stresses, deformations and bond-slip behaviour of GFRP RC specimens subjected to sustained axial load.

- To compare the long-term experimental response of GFRP RC tensile members with existing analytical code procedures for steel RC members (Eurocode 2).

- To carry out an experimental study focused on the analysis of long-term effects on bond-slip

1.3 Thesis layout

The main body of this dissertation consists of the manuscripts of the three journal papers indicated at the beginning, which are included in the document as follows:

In Chapter 2, a methodology to implement a local bond-slip law for GFRP RC, obtained from experimental pull-out tests, into a FE programme is presented. The experimental bond-slip response is separated into two main components: mechanical interaction and friction. The constitutive law for bond interaction is obtained using an inverse method. The methodology is applied to simulate the short-term response of GFRP RC tensile members. Numerical and experimental results are compared in terms of load-deformation response, as well as crack width and crack spacing, to check the validity of the simulation. In addition, the presented methodology allows the study of the strain profile and the analysis of bond and slip along the concrete specimen.

In Chapter 3, an experimental study to evaluate the tension stiffening effect, stresses and deformations of tensile GFRP RC elements under sustained load is conducted. Three concrete grades are considered. Five of the specimens are reinforced with GFRP bars while an additional element is manufactured with steel reinforcement for comparison purposes. The tests were carried out for a period lasting between 35 and 40 days. Creep and shrinkage of concrete were also considered in the programme. Some specimens were internally strain gauged to evaluate the reinforcement strain profile under long-term effects. Results of the loading process, evolution of concrete stresses and deformations, as well as tension-stiffening reduction and bond deterioration, are analysed and discussed. The experimental results are compared with analytical predictions using the Eurocode 2 procedure based on the EMM.

Chapter 4 presents an experimental study of long-term bond performance through pull-out tests on GFRP RC specimens under sustained load. The tests were carried out for a period of 90 and 130 days. As in the previous work, some specimens were internally strain gauged to evaluate long-term strains and bond stresses along the bond length. Creep and shrinkage were also measured during the test. The effects of main parameters that influence long-term bond-slip response (concrete compressive strength, bond length and reinforcement material) are evaluated and discussed. Results of time-dependent slips at the loaded and unloaded end are measured and discussed.

Finally, in Chapter 5 a summary of the main conclusions of this work are presented. Moreover, a proposal for future works is detailed.

Chapter 2

Numerical simulation of bond-slip interface and tension stiffening in GFRP RC tensile elements

This chapter contains the transcription of the submitted paper:

I. Vilanova, L. Torres, M. Baena, M. Llorens *Numerical simulation of bond-slip interface and tension stiffening in GFRP RC tensile elements*. Composite Structures.

Abstract

Bond between reinforcement and concrete highly affects the structural behaviour of reinforced concrete (RC). Introduction of bond-slip models into numerical simulation allows taking into account the bond interaction and analyse its effect on local and global behaviour. Unlike conventional steel reinforcement, no standard bond-slip law exists for FRP reinforcement, as bond is the result of a combination of parameters such as reinforcing material and bar surface configuration, among others. Therefore, there is a need in developing a methodology to easily implement bond-slip response from experimental bond tests.

In this work, a methodology to implement bond-slip behaviour between concrete and reinforcement into a FEM model is presented. The inverse analysis is used to characterize the bond mechanisms active in a pull-out test. The obtained constitutive behaviours are thereafter implemented into a FE program by using *connector* elements and *surface-to-surface* contacts, and GFRP RC tensile elements are modelled. Numerical results are compared to experimental ones available in the literature, showing good accuracy in terms of load-deformation, crack width and crack spacing, as well as strains and bond stress and slip distributions along the reinforcing bar.

2.1 Introduction

The use of Fibre Reinforced Polymers (FRP) in concrete structures has emerged as an alternative to steel due their good behaviour in corrosive environments or when the effects of electromagnetic fields may be present [1, 2, 4]. Bond between FRP bars and concrete play a crucial rule on the viability of these materials. Unlike steel reinforcement, FRP bars present different material and surface properties that directly affect bond mechanisms [9–11]. Because of that, there is not a standardized law for FRP reinforcement to evaluate bond between the two materials. Several experimental researches have focussed on the bond-slip response of the FRP-to-concrete interface. Most of them have been based on data obtained from pull-out testing due to the simplicity of the setup compared to other more complex procedures [11–13, 15, 52–55].

Bond-slip interaction between reinforcement and concrete is characterized by three main components: chemical adhesion, mechanical interaction and friction. It is well known that the chemical adhesion breaks down at low bond stress values where no slip between the reinforcement and the concrete is observed. In a pull-out failure, for higher bond stress values the longitudinal cracks spread radially, owing to the wedding action which is enhanced by the crushed concrete stuck to the front of the lugs. The outward component of the pressure is resisted by the hoop stresses in the surrounding concrete; as a consequence, the surrounding concrete exerts a confinement action on the bar, and bond strength and stiffness are assured mostly by the interlocking among the reinforcement, the concrete struts radiating from the bar and the undamaged outer rings. In that case, bond failure is being caused by a bar pull-out, the force transfer mechanism changes from rib bearing to friction. Most of the published studies, as well as prediction codes, have analytically described pull-out behaviour based on the mechanical interaction, with the ascending branch of the bond-slip curve an extremely important component [56–59].

The use of numerical simulation complements the experimental research allowing parametric studies for better understanding the influence of different properties and parameters and reducing the amount of experimentation. In the last decades, the use of numerical approaches to model bond-slip interface behaviour based on the finite element method (FEM) has exponentially increased due to the extensive development of the models as well as the software applications. Several authors modelled the interface as perfect bond, where no relative slip between the reinforcing bar and concrete is allowed [21–27]. Non-perfect bond models have started to be presented, where special attention to the mechanisms of mechanical interaction and friction is taken [60–63] . A bond interaction study on concrete elements reinforced with FRP bars has been carried out by [60]. The authors modelled four pull-out specimens and two concrete beams. Bond was modelled with a series of non-linear springs, each of them with a load-slip law partially contributing to the experimental one. The authors observed good correlation between analytical and experimental results. The same methodology was applied by the authors to define bond interaction of FRP and concrete in beams where some modifications were introduced in order to incorporate the splitting behaviour of the anchorage bar. Tension stiffening has been deeper studied though the modelling of two concrete ties reinforced with steel bars by [61]. The authors modified the CEB-FIB Model Code 90 [64] bond model to incorporate local

damage and concrete confinement pressure. The methodology provides reasonable good prediction of the variation of steel stress, bond stress and slip between concrete and reinforcement. A good estimation of the crack width and crack opening between primary cracks was found. Zanuy and co-workers [62] developed a finite element approach to predict the bond strength and failure of pull-out elements under variable degree of confinement. The steel-concrete interface is analysed with contact elements whose properties include the influences of the bar ribs. Surface-to-surface contact pair elements were used to implement the friction response. The influence of the embedded length was used to evaluate the proposed methodology. The result indicates that the bond strength is mainly provided by confined zones at the interface. The author concludes that the bond strength is not a constitutive property of the interface but a result of the particular geometry, boundary conditions or load pattern. A study of bond mechanism existing at the steel-concrete interface in reinforced concrete (RC) tensile members has been conducted in [63]. Three types of FE bond models were examined: i) perfect bond, where the same node is shared by the two materials, ii) diagonal link elements, where the angle of bond-bearing stress is analysed, and iii) a bond zone where the material properties of concrete elements close to the reinforcing bar are modified to represent the bond interaction. A parametric study was conducted to determine the peak bond shear stress by using a FE model which included the effect of different clear concrete cover to bar diameter ratios. Finally, as a conclusion, the bond normal stresses were found to be concentrated at the loaded end of the tensile members and the length of the tie member has a negligible influence on the average splitting tensile stresses.

The major part of numerical studies with FEM models which include the bond-slip interaction between reinforcement and concrete have been carried out for steel reinforcement. As mentioned previously, FRP bars present different bond characteristic according to material and surface properties. Therefore, due to the lack of a general bond-slip law, the goodness of the bond law to be implemented in the numerical model should be assessed. Hence, development and validation of methodologies for incorporating bond-slip models in the FEM analysis of FRP RC members is of major interests.

This paper presents a procedure for including the bond-slip interface behaviour between FRP reinforcement and concrete in a FEM model, which is subsequently applied to numerically simulate the behaviour of RC tensile members. Bond-slip relationship is obtained from pull-out tests, which have demonstrated to be a relatively simple methodology for assessing the bond-slip response between concrete and reinforcement. A law that takes into consideration the mechanical interaction and friction effects is obtained through an inverse method and implemented into a numerical model. Numerical results are compared to experimental results from RC tensile members in terms of tension stiffening, crack spacing and crack width. The cracking process, bond stresses and slips along the bond length are analysed showing good correlation between experiments and numerical simulation.

2.2   Description of the model

The parameters of the bond-slip model to be included in the numerical model are deduced from experimental bond-slip laws obtained from standard pull-out tests [65].

2.2.1 FEM Model

Pull-out specimens are modelled with ABAQUS finite element software using explicit dynamic solution technique where the interface bond-slip law is implemented. The specimens are concrete cubes of 200 mm with a single reinforcing bar located in the centre. The bond length is located at the unloaded end of the bar (Fig. 2.1). Taking advantage of the symmetry, only a quarter of the specimens is numerically modelled. Both, concrete and reinforcing bar are modelled by solid elements C3D8R with an approximately element size of 4 mm. In order to simulate the experimental pull-out test, the concrete cube is locked at the side corresponding to the loaded end of the bar at which a displacement is applied at the end of the reinforcing bar (Fig. 2.1). The bond zone is implemented by *connectors* elements and *surface-to-surface* interface where the bond interaction is taken into account.
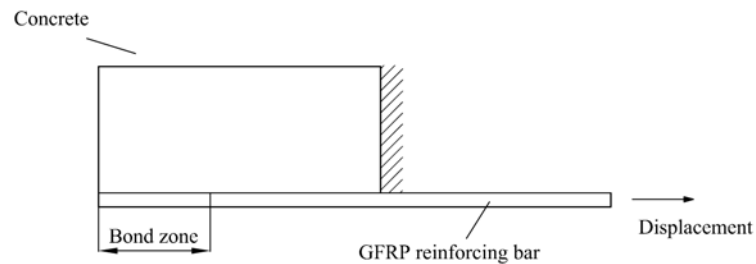
Figure 2.1: Pull-out definition.

2.2.2 Material definition

Concrete Damage Plasticity (CDP) is used to simulate the inelastic behaviour of concrete. The model is a continuum, plasticity-based, damage model for concrete. It assumes that the main two failure mechanisms are tensile cracking and compressive crushing of the concrete material. The evolution of the yield (or failure) surface is controlled by two hardening variables linked to failure mechanisms under tension and compression loading.

The material parameters associated to the CDP model are indicated next:

- Dilatation angle: ψ, is the inclination of the failure surface towards the hydrostatic axis, measured in the meridional plane. It is physically explained as the concrete internal friction angle. In the literature diverse values can be found (from 20 to 45 degrees). In the present work the value of 38º has been used [66–68].

- Flow potential eccentricity: ϵ, the eccentricity is a small positive number that defines the rate of approach of the plastic potential hyperbolic to its asymptote, to define the shape of the plastic potential surface in the meridional plane. When no data is available, a value of 0.1 is proposed to be assumed.

- Stress ratio: σ_{bo}/σ_{co}, is the ratio of the strength in the biaxial state to the strength in the uniaxial state. The CDP default value of 1.16 has been used.

- K_c, is the ratio of the distance between the hydrostatic axis and respectively the compression meridian and tensioned meridian in the deviatoric cross section. K_c values normally ranges between 0.5 and 1. The

recommended CDP value of 2/3 is used.

CEB-FIB Model Code 2010 [48] has been used to model the concrete stress-strain compression relationship (Fig. 2.2a) and the tensile post-cracking behaviour (Fig. 2.2b) of concrete. To define the GFRP reinforcement stress-strain relationship, an isotropic linear elastic law up to failure is used (Fig. 2.2c).
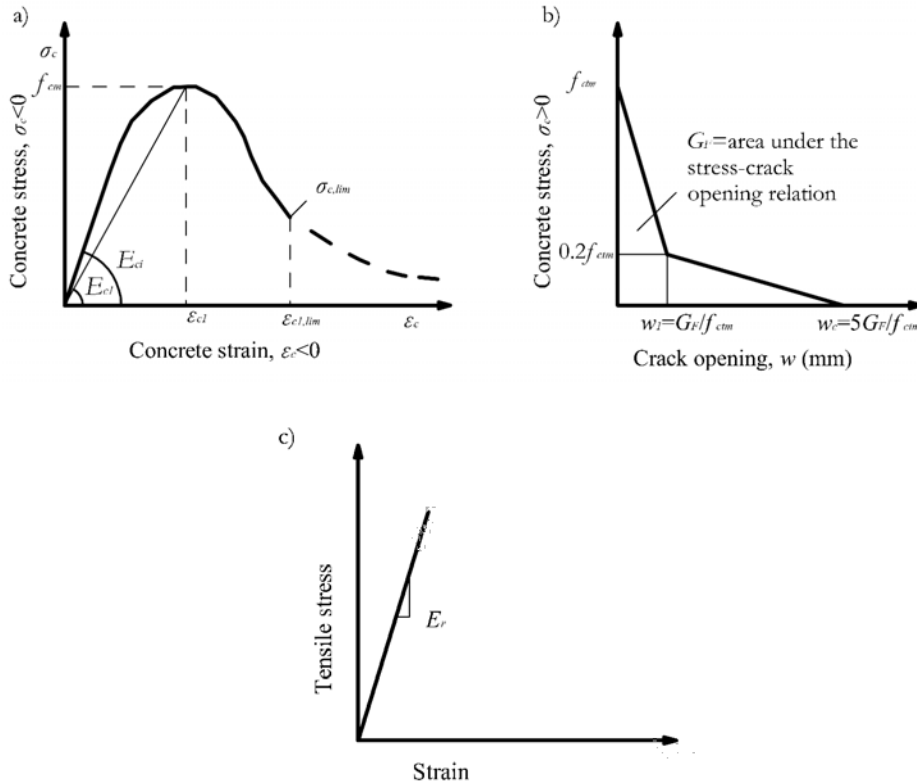
Figure 2.2: Constitutive laws assumed to model the: a) uniaxial stress-strain curve for concrete in compression, b) tensile post-cracking model from MC2010 [48] and c) tensile uniaxial stress-strain curve for GFRP.

2.2.3   Bond model

As started in the literature review, the experimental bond-slip response of a pull-out specimen is mainly characterized by mechanical interaction and friction. Therefore, these are the two mechanisms to be included in the bond interface model presented in this work.

In order to model the bond at the interface between FRP reinforcement and concrete, experimental results

from pull-out tests having a bond length of 5 times the bar diameter are used. In a standard pull-out test, load-slip curves at the loaded and the unloaded end are usually available. In this work, the parameters of the bond-slip interface are obtained by applying the inverse method to the mean of these two curves (Fig. 2.3a). Residual bond stress of the bond-slip experimental curve is considered to depict the friction mechanism (see Fig. 2.3b), whilst mechanical interaction is described by subtracting the frictional component from the total response (see Fig. 2.3c).
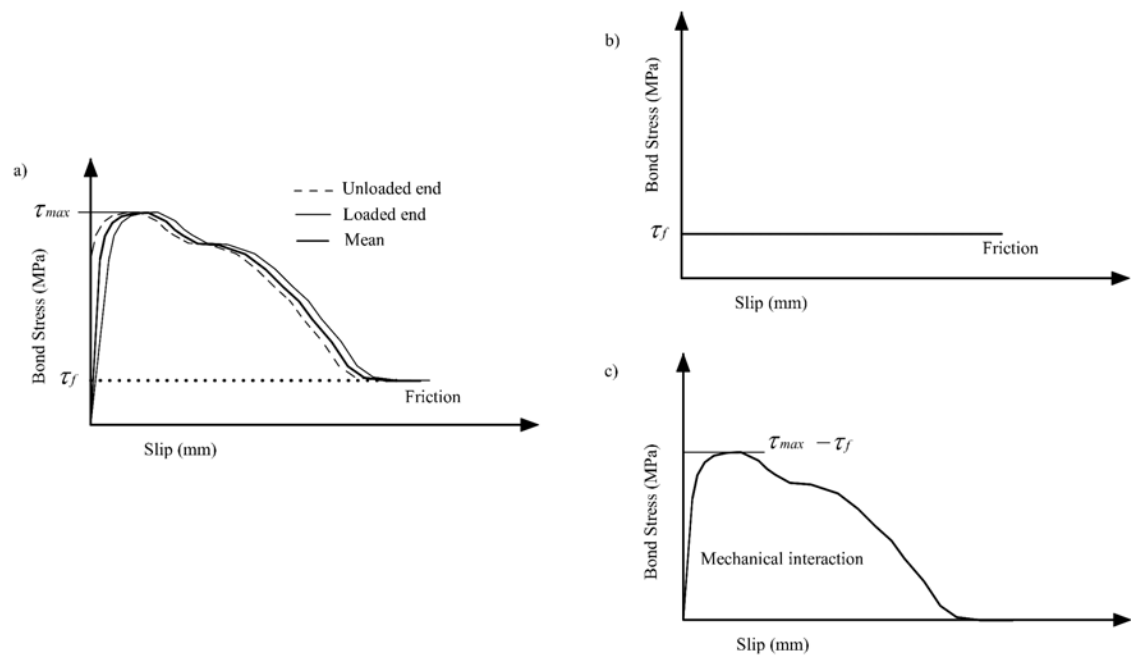
Figure 2.3: Qualitative curves of the bond interface: a) experimental pull-out curves, b) friction and c) mechanical interaction.

Connector elements, CONN3D2, are used to implement the mechanical interaction mechanism. These two-node connectors are placed at the interface with one node belonging to concrete and the other one belonging to reinforcement (the two nodes being placed at the same physical position, see Fig. 2.4a). Their constitutive behaviour is defined with tabular data, with the mechanical interaction curve being defined by the number of pair elements existing in the bond zone (i.e. each pair of nodes partially contributes to the total mechanical interaction). Besides, friction mechanism is implemented with *surface-to-surface* contact interface where a friction coefficient is defined in the whole bond zone (Fig. 2.4b).
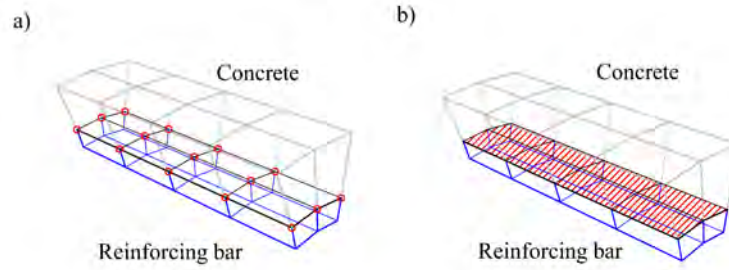
Figure 2.4: Contact definition: a) *connector* elements and b) *surface-to-surface* interface.

The different parameters defining the bond-slip model are adjusted using an inverse method in order to obtain the constitutive law for the numerical model from the experimental test results. As a starting point, it is assumed that friction coefficient can be obtained from the residual bond stress (Fig. 2.3b). Therefore, an initial friction coefficient, μ_0, is assumed and implemented in the model. The program is executed and the numerical results are compared with the experimental pull-out response. If the residual bond stress, τ_f, is well reproduced by the numerical model, the assumed friction coefficient is considered to be valid; otherwise a new coefficient is calculated. To that end, the average normal force in the bond length in the model, N, is estimated from the values of the numerical simulation:

$$F_{Fnum} = N\mu_0 \tag{2.1}$$

where F_{Fnum} is the residual force obtained from the numerical results.

From the calculated value of N and the residual force obtained from the experimental results, F_{Fexp}, a new friction coefficient can be deduced:

$$\mu_1 = \frac{F_{Fexp}}{N} \tag{2.2}$$

where μ_1 is the new friction coefficient to be adopted in the numerical model.

With this new coefficient, the model is executed again and the residual bond stresses compared with the experimental ones, which in general presents a good correlation (otherwise a new iteration should be performed).

Once the friction part is considered to be adjusted, the mechanical interaction part is revised, since in general it is affected by the introduced change in friction coefficient. As for the experimental curves (Fig. 2.3c), the numerical mechanical interaction component is obtained by subtracting the friction force from the total numerical bond-slip response. Numerical and experimental curves for mechanical interaction component are compared and the difference between them is computed. This difference is added to the mechanical interaction data used in the first iteration (i.e. experimental mechanical interaction) and the new model is executed again. The aforementioned procedure has shown its ability to well reproduce the experimental behaviour of the bar-concrete interface.

2.3 Validation of the methodology

To check the validity of the presented methodology to model bond between reinforcement and concrete in RC elements, numerical results are compared to those of an experimental campaign conducted by the authors and reported in a previous work [38]. Four concrete specimens reinforced with GFRP bars were subjected to increasing uniaxial tensile load. The specimens were concrete prisms of 1300 mm long with 1200 mm of effective embedded length, *Leff*. Due to symmetry conditions only a volume corresponding to an eighth of the specimen is modelled (marked area in Fig 2.5). Specimens' identification according to [38] is presented in Table 2.1, along with their geometrical and mechanical properties.
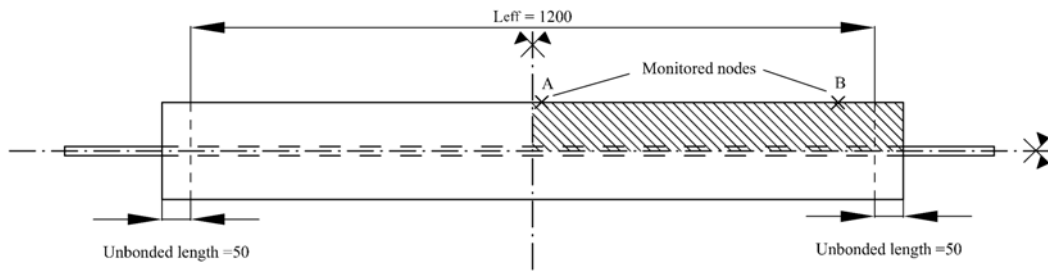
Figure 2.5: GFRP RC tensile specimen (units in mm).

Label in [38]	Cross section	Concrete			Reinforcement	
	(mm)	f_c (MPa)	E_c (MPa)	f_{ct} (MPa)	d experimental (mm)	EA (MN)
16_110	110x110	48.1	27315	1.75	16.11	7.9
13_170	170x170	56.2	33275	2.34	13.73	5.6
16_170	170x170	46.6	34514	2.58	16.11	9.4
19_170	170x170	56.2	33275	2.10	19.14	11.7

Table 2.1: Mechanical properties and test matrix of GFRP RC specimens [38].

State of the art reveals that, bond-slip response is sensitive to changes in bar diameter, concrete grade and reinforcing material. Because of that, when modelling a concrete tie, bond must be modelled with a bond-slip law obtained from a pull-out test with similar components/materials to those of the RC tie to be modelled.

In this study, bond-slip laws to be implemented in the numerical model are obtained from an experimental program on pull-out tests presented in [11]. That program included three nominally equal pull-out specimens for each configuration. The mean of the three curves is used in this work.

Experimental pull-out curves of those bars being used in the RC tensile specimens are shown in Fig. 2.6 (for the sake of simplicity, notation is referred to the nominal diameter of the bar: D13, D16, D19). Since the usual slip of RC elements at service is usually relatively low with respect to that of the complete pull-out failure, detail of the initial part of the curves (up to 2mm slip) is indicated in the upper-right corner [69]. Along with the experimental curves, results of the numerical simulation conducted to adjust the bond model

(following the procedure previously indicated) are also presented in Fig. 2.6. As can be seen, numerical results reproduce the bond-slip response fairly well.
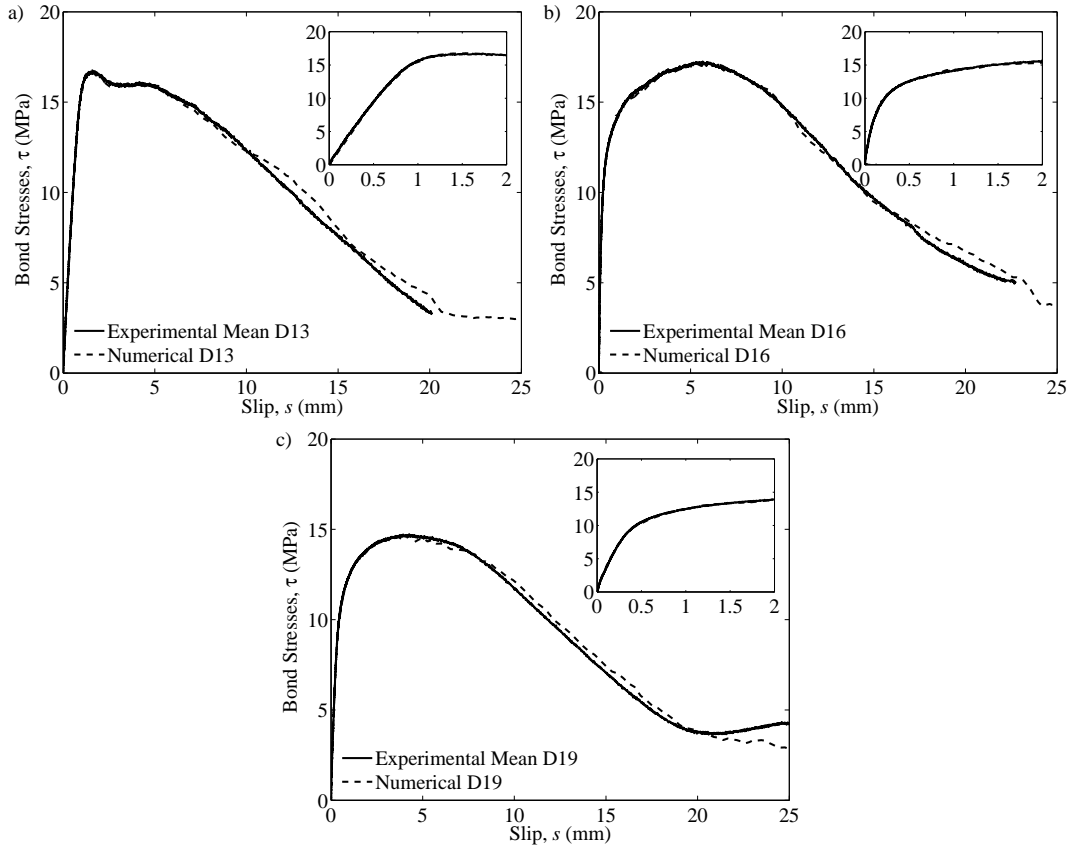
Figure 2.6: Comparison between experimental and numerical bond-slip response.

Once the bond-slip response is perfectly adjusted to the experimental pull-out test with the presented methodology, the law is implemented to the numerical simulation of the concrete ties specimens.

2.3.1   Load-strain response

Once the bond model is properly adjusted, numerical simulations of RC tensile elements, which include the bond model, are conducted. Fig. 2.7 shows the comparison between experimental response and numerical results in terms of axial load-mean strain ($P - \varepsilon_m$). The member mean strain is calculated from the finite element model by dividing the axial displacement between two monitored nodes by the distance between them (see Fig 2.5). The axial load P is the reaction load obtained at the reinforcing bar. For comparison purpose the bare bar response is also plotted. It is seen that the cracking process and the gradual reduction of tension stiffening is well reproduced by the numerical simulations.
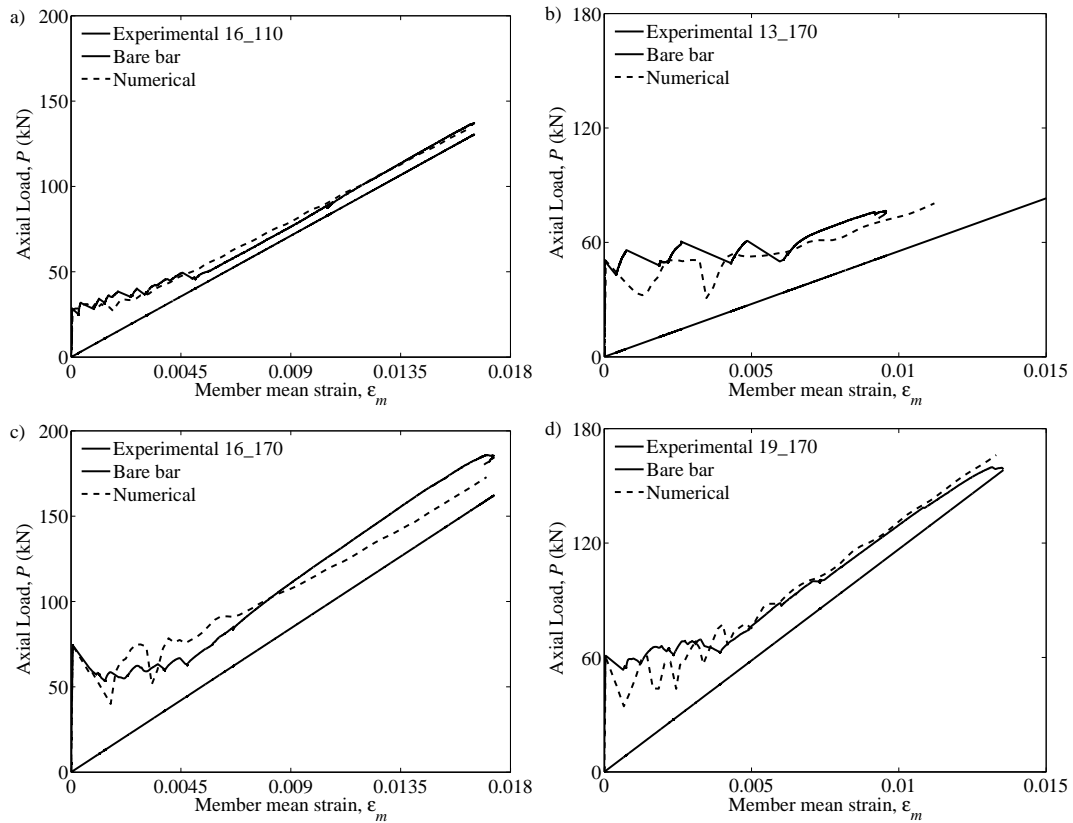
Figure 2.7: Comparison of $P - \varepsilon_m$ numerical prediction and experimental results.

2.3.2 Cracking

The numerical model is also validated by comparison of numerical and experimental results on crack spacing, crack width and number of (see Table 2.2). The average experimental crack width was measured at the concrete surface in the tests and hence the numerical crack width has also been taken from numerical results on the concrete surface. Because of the symmetry condition applied in the numerical models, the number of cracks of the numerical simulation has been doubled so that comparison with experimental results was possible. Numerical results confirm that the implemented model satisfactorily predicts experimental data.

Specimens	Load (kN)	Crack Spacing (mm)		Crack width (mm)		No of cracks	
		Experimental	Numerical	Experimental	Numerical	Experimental	Numerical (entire element)
16_110	87.69	123.34	126.3	1.51	1.16	8	8
13_170	53.84	264.96	330.1	1.95	1.42	4	4
16_170	85.12	227.75	271.2	1.05	1.45	6	4
19_170	100.23	113.27	100.7	0.98	0.90	9	10

Table 2.2: Comparison of crack spacing, crack width and numbers of cracks.

2.3.3 GFRP reinforcement strain distribution

In this section, the numerical methodology is also validated in terms of reinforcement strain distributions. To this end, experimental data of a RC tensile element whose reinforcement was internally strain gauged (specimen with label 16_170_3N in [38]) is used. This specimen was cast using specially manufactured internally strain gauged GFRP bars [38, 55, 70] that allowed monitoring the strain distribution along the bar. Besides, three notches were created to induce experimental cracks at specific sections to obtain a controlled crack pattern.

For the numerical simulations, symmetry conditions are again applied an only a quarter of the specimen is modelled (Fig. 2.8). The interface law to be implemented in this specimen corresponds to the D16 pull-out response (Fig. 2.6b). In order to obtain an order of appearance of cracks similar to that of the experimental results, the concrete tensile strength, f_{ct}, was accordingly reduced at the regions close to the notched sections (areas in grey in Fig. 2.8).
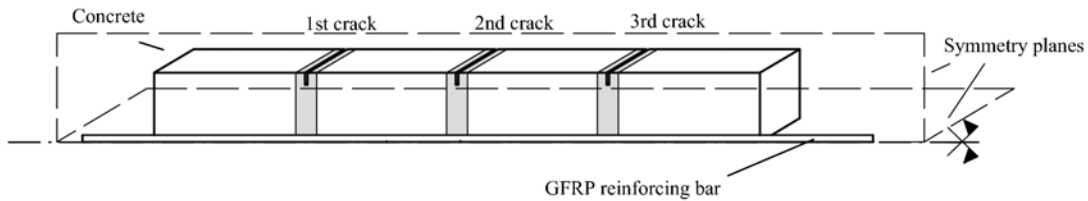
Figure 2.8: Concrete tie model for specimen 16_170_3N.

Previous to the presentation of results on reinforcement strain distribution, comparison of the load-strain response ($P - \varepsilon_m$) is presented in Fig. 2.9, along with the bare bar response. As for the previous specimens, the methodology well reproduces the experimental behaviour.

The evolution of the reinforcement strain distribution throughout the cracking process is presented in Fig. 2.10. Each subfigure represents the state after the formation of a new crack, where an increase of the strains at the reinforcement is observed. Comparison of numerical and experimental results confirms the goodness of the presented methodology.
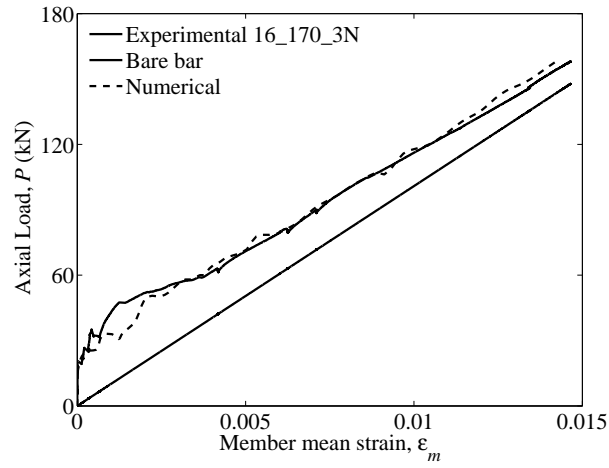
Figure 2.9: Comparison of $P - \varepsilon_m$ numerical prediction and experimental results for specimen 16_170_3N.
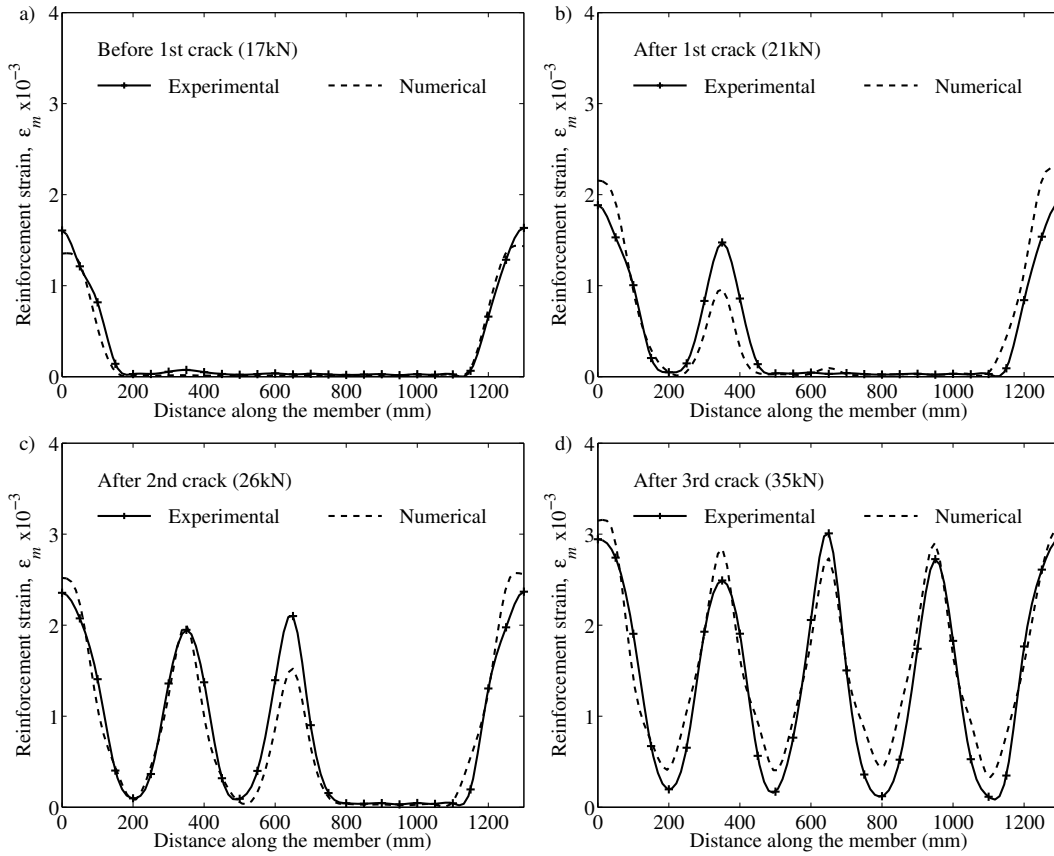
Figure 2.10: Numerical and experimental reinforcement strain distribution at cracking load levels.

The comparison of experimental and numerical reinforcement strain distributions is also presented at the crack stabilization stage, where no more cracks are formed (see Fig. 2.11). In this figure, results corresponding to tensile loads of 40 and 60 kN are shown. The presented methodology well reproduces the strain profile at 40 kN. However, some differences can be observed for results at 60 kN. At this load, the numerical solution is almost perfectly symmetric, while the experimental results show an increase of reinforcement strains at the region between the left-hand side concrete end and the first crack (at 350 mm), probably due to a loss of bond between the two materials.
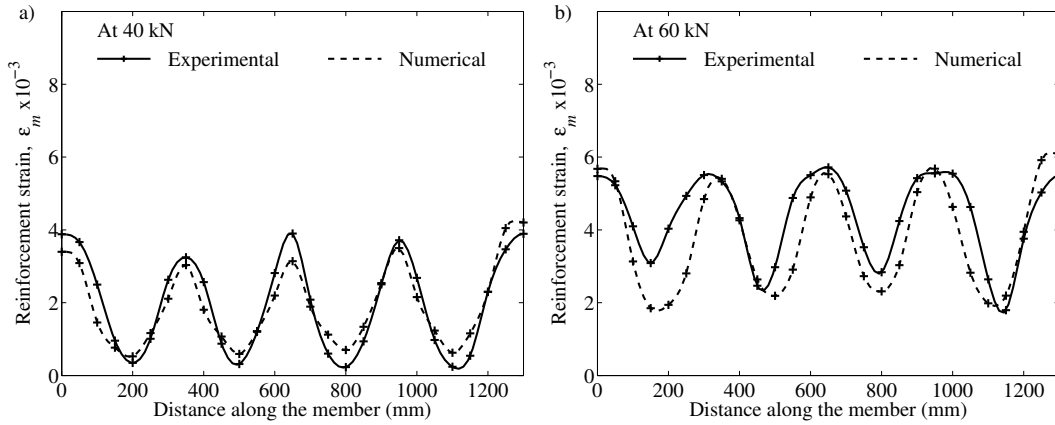
Figure 2.11: Numerical and experimental reinforcement strain distribution at stabilization phase.

2.3.4   Slip and bond stress distribution

As a last validation of the methodology, slip between concrete and reinforcement and bond stresses generated at the interface are analysed at the stabilization phase.

The slip can be defined as the difference between reinforcement displacement (u_r) and concrete displacement (u_c):

$$s = u_r - u_c \tag{2.3}$$

Differentiating Eq. (2.3) leads to:

$$\frac{ds}{dx} = \varepsilon_r - \varepsilon_c \tag{2.4}$$

where ε_r is the reinforcement strain and ε_c is the concrete strain for the same section.

Assuming that concrete strain can be disregarded in front of that of the reinforcement, the slip between concrete and reinforcement can be computed as:

$$s = \int_c^x \varepsilon_r(x)dx \tag{2.5}$$

In Fig. 2.12 results of the numerical simulation are compared to slip obtained from the experimental

reinforcement strain distribution. In each subfigure, cracked sections are properly marked with dotted lines. As in the previous case, good predictions are obtained at a load level of 40 kN (Fig. 2.12a) and some differences can be found at 60 kN (Fig. 2.12b).
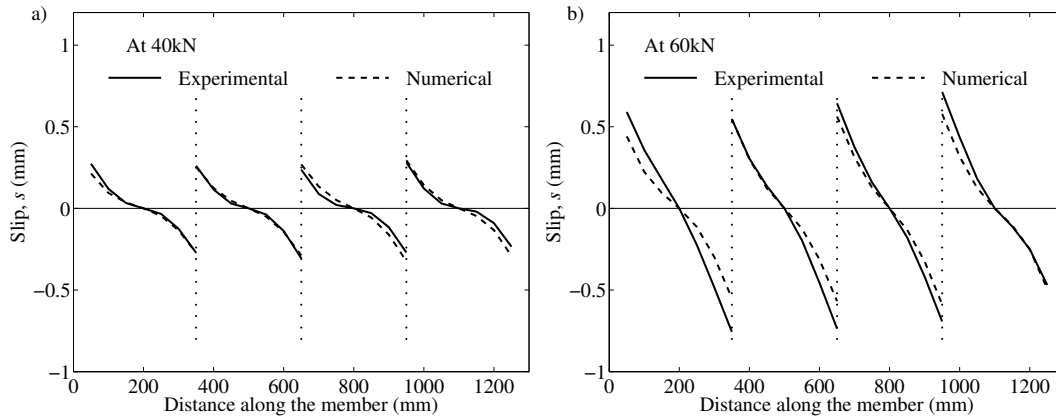
Figure 2.12: Numerical and experimental slip results at stabilization phase.

Bond stresses can also be obtained from experimental data on reinforcement strain distribution. Taking the definition of bond as the force transferred between the reinforcing bar and the concrete per unit surface area, and assuming linear elastic behaviour of the bar, the equilibrium equation on a piece of bar of length dx leads to:

$$\tau = \frac{E_r d_r}{4} \frac{d\varepsilon_r(x)}{dx} \tag{2.6}$$

where τ is the bond stress, d_r is the reinforcing bar diameter and E_r is the elastic modulus of reinforcement.

The comparison of numerical and experimental distributions of bond stress along the reinforcement is shown in Fig. 2.13. Crack locations are properly marked with dotted lines. At 40 kN similar results are observed, with a slight underprediction of bond stresses in the numerical model. The differences between numerical and experimental values at the left-hand side part of the reinforcement strain distribution for a load of 60 kN (visible in Fig. 2.11 b) are the origin of the differences in bond stress distribution at that same location. That said, the numerical results well fit the global experimental response for the rest of the reinforcement length.
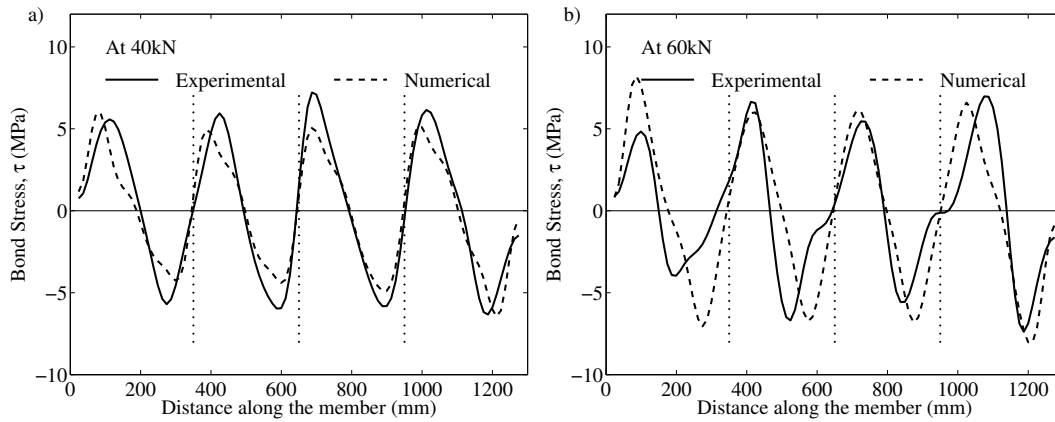
Figure 2.13: Numerical and experimental bond stress results at stabilization phase.

2.4   Conclusions

A methodology has been presented to obtain a local-numerical bond-slip law to model the interaction between concrete and FRP reinforcement and suitable to be implemented in a standard FEM software. An inverse method has been applied to numerically characterize the constitutive law from experimental bond-slip curves obtained from pull-out tests, which have demonstrated to be a simple and widely used methodology for assessing the bond-slip response between concrete and reinforcement. With this method two main issues related to the modelling of bond behaviour between FRP and concrete can be taken into account: the possible different bond-slip response for each GFRP and concrete combination, and the possible distortion of the bond-slip law obtained from pull-out test due to confinement stresses.

The procedure is based on separating the bond response into the two main components of friction and mechanical interaction. Once friction coefficient is adjusted, the mechanical interaction part is adapted so that to reproduce the experimental response for the combination of FRP bar and concrete analysed. The methodology has shown ability to give accurate results with very few iterations being carried out on the relatively small model of the pull-out specimen, with reduced computational costs. In this way a simple procedure is obtained for considering the distinct bond responses that may be obtained using different types of FRP reinforcement.

The applicability of the methodology is validated by numerically modelling the behaviour of a total of four concrete ties reinforced with GFRP bars, being the load-deformation response compared with experimental results available in the literature. The cracking process and the evolution of tension stiffening are in good agreement with experimental data. Besides, numerical predictions on crack width, crack spacing, and number of cracks also compare well with experimental values, this being a sign of the suitability of the bond model.

The procedure is further validated through the simulation of an additional RC tie with three notched sections whose reinforcement was internally strain gauged. The comparison of numerical and experimental

results with regard to reinforcement strain distribution, formation of cracks and redistribution of stresses taking place after a crack creation, confirm the validity of the presented methodology.

Chapter 3

Experimental study of tension stiffening in GFRP RC tensile members under sustained load

This chapter contains the transcription of the published paper:

The paper in journal format is shown in Appendix C

Abstract

Sustained load effects on steel reinforced concrete structures due to creep and shrinkage in the concrete have been widely studied. However, knowledge of behaviour under sustained loads needs extending to the more recently developed fibre reinforced polymer (FRP) reinforced concrete structures. In this experimental study, the effect of tension stiffening on tensile glass fibre reinforced polymer (GFRP) reinforced concrete elements under sustained load is investigated. A total of six specimens with three different concrete strengths were tested for a period of between 35 and 40 days, when it was seen that deformations stabilized. Some of the specimens included internal instrumentation of the reinforcing bar to capture the reinforcement strain profile and analyse long-term effects. Results confirm bond deterioration due to sustained load, with a reduction in the mean bond stress and concrete tensile stress, and showed how deterioration stabilized at approximately 28 days. The influence of concrete strength on the loss of tension stiffening is also confirmed, with higher concrete compressive strength showing the smallest loss of concrete tensile stresses. The results are compared to predictions using Eurocode 2 approach, in which the effects of sustained load are incorporated by applying the effective modulus method (EMM). Predictions using this methodology compare well with experimental results.

3.1 Introduction

The use of fibre reinforced polymer (FRP) bars as reinforcement in reinforced concrete (RC) structures has gradually increased in recent decades due to their electromagnetic transparency and resistance to corrosion in aggressive environments [1, 2, 5, 71]. In line with this trend, research into FRP RC structures has also increased, a fact reflected in design recommendations in the form of codes and guidelines [72–74]. The existing literature mainly addresses the analysis of flexural behaviour in which the effect of the mechanical properties of FRP rebars is analysed [28–36], and concludes that the general assumptions made for steel RC elements are valid for FRP RC members, but that their specific mechanical properties lead to some changes in equations and design philosophy. The literature also suggests that due to their lower modulus of elasticity, serviceability requirements often govern the design of FRP RC elements. Although fewer studies focus on FRP RC tensile members, the major influence of the tension stiffening effect on load-deformations behaviour has been proved [37–39]. Most of the research carried out so far has focussed on the short-term response of FRP RC elements; there are not so many studies focussing on long-term behaviour. The analysis of long-term performance has been mainly approached by both studying material durability issues [75–77] and analysing RC flexural behaviour [78–83].

When analysing time effects on the behaviour of RC elements, concrete creep and shrinkage play a crucial role [84–88]. While creep is associated to sustained stresses, shrinkage may be assumed to be independent of load. Both effects cause long-term deformations in concrete. Existing studies allow the influence of long-term effects on tension stiffening, stresses and deformations [41, 89, 90] to be analysed, but only limited research into the effects of creep and shrinkage on tensile steel RC elements is available.

Scott and Beeby [41] tested a total of twelve steel RC elements in tension for periods of up to 4 months. The results focussed on creep and shrinkage effects and the loss of tension stiffening. Internal instrumentation of the steel reinforcing bars and external strain gauges were used, allowing the cracking process both for instantaneous and sustained loading to be analysed. The results showed an increase in the strain response until tension stiffening decayed and stabilized in less than one month after first loading [42]. Wu and Gilbert [89] carried out an experimental test campaign on six steel RC elements in tension, four subjected to short-term loading and two to long-term loading for a period of about 50 days. The objective was to analyse the influence of creep and shrinkage on long-term behaviour, and to gain a better understanding of the mechanisms involved in tension stiffening, cracking and deformations. According to the experimental results for long-term loading, an increase in reinforcement strain was visible at midway sections between two cracks, and reinforcement strain was found to be approximately constant in cracked sections. Based on the results obtained by Wu and Gilbert [89], Zanuy [90] developed a numerical methodology to predict long-term effects on steel RC elements in tension that included the influence of creep and shrinkage.

The literature dealing with FRP RC elements under sustained loads is even more limited. Nkurunziza et al. [43] tested a total of twenty GFRP bars in tension to study the effect of sustained loads on FRP bars in aggressive environments. The specimens were tested for 417 days at two loading levels (25% and 38% of the ultimate bar tensile strength). The authors observed that long-term loading had a minimal effect on creep strain and elastic modulus, while the effect on residual strength was more dependent on the environmental

conditions. Mazzotti and Savoia [16] tested a total of two concrete specimens externally reinforced with CFRP plates. The specimens were subjected to sustained loading for more than 900 days. Three bonded lengths and two load levels were used to analyse the evolution of axial strain and shear stresses with time. Results showed a redistribution of the shear stresses along the anchorage due to creep deformation at the interface level. To the best knowledge of the authors, no studies have been reported into the long-term behaviour of tensile RC members using FRP bars as internal reinforcement.

In this paper, an experimental campaign to study the evolution of strains and stresses in RC elements reinforced with GRFP bars subjected to sustained axial load is presented. A total of six specimens with three different concrete strengths were tested for a period of between 35 and 40 days, when it was seen that deformations stabilized. Some of the specimens were instrumented with internal strain gauges in the reinforcing bar, to better capture the reinforcement strain profile and analyse the long-term effects. Results in terms of bond, slip, stresses and strains are reported and analysed. Comparison of experimental results with analytical predictions using the effective modulus method (EMM) and Eurocode 2 approach [47] is also reported and discussed.

3.2   Experimental programme

3.2.1   Experimental programme

The experimental programme was designed to investigate the effect of concrete strength and reinforcing material on the long-term performance of reinforced concrete elements in tension. The test matrix consisted of six specimens divided into three groups of two specimens each. All the specimens were rectangular in cross-section (120 x 120 mm) and 1000 mm long with an effective bond length of 900 mm (i.e. 50 mm long plastic tubes were placed at both ends of the specimens before casting to diminish end effects and to try to reproduce bond development better). Two different reinforcing materials (GFRP and steel) and three target concrete strengths (25, 35 and 50 MPa) were used. In order to achieve similar axial stiffness (EA) in all tests, the standardised reinforcement consisted of either a single 16 mm diameter GFRP bar or a single 10 mm diameter steel bar.

Two specimens (Series 1, C1) were cast with a target concrete compressive strength of 50 MPa and GFRP reinforcement. Two specimens (Series 2, C2) were GFRP reinforced and had a target concrete compressive strength of 35 MPa. The last two specimens (Series 3, C3) consisted of one GFRP and one steel RC tie with a target concrete compressive strength of 25 MPa. So that the internal distribution of bond stresses could be analysed, some of the specimens included internal instrumentation in the reinforcing bars. Perimeter notches were included in five of them in order to obtain a controlled crack pattern and force cracks to form at specific locations. The notches were created by placing 3 mm x 2 mm rectangular steel tubes in the moulds prior to casting. A distance of 180 mm between notches was selected based on the cracking results obtained in a previous experimental study [38]. Based on this description, the identification of the tested elements was CxRDni, with Cx standing for the type of concrete (C1, C2, C3), R for the type of reinforcement (F = GFRP, S = steel), D for the reinforcement diameter, with "n" identifying specimens with notched sections, and "i"

specimens with reinforcement internally instrumented. The test matrix is summarised in Table 3.1.

Specimen	Series	Concrete	Target concrete strength (MPa)	Reinforcement	Bar diameter (mm)	Notches	Reinforcement internal instrumentation
C1F16ni	1	C1	50	GFRP	16	Yes	Yes
C1F16	1	C1	50	GFRP	16	No	No
C2F16ni	2	C2	35	GFRP	16	Yes	Yes
C2F16n	2	C2	35	GFRP	16	Yes	No
C3F16n	3	C3	25	GFRP	16	Yes	No
C3S10n	3	C3	25	Steel	10	Yes	No

Table 3.1: Test matrix.

3.2.2 Material properties

Ready-mix concrete was used to cast the specimens. Compressive strength was determined at the time of loading by standard cylinders test (150 x 300 mm) in accordance with UNE 12390-3. The average values of the mechanical properties are summarized in Table 3.2.

Concrete	Compressive strength, f_c (MPa)	Elastic modulus, E_c (GPa)
C1	48.9	33.8
C2	33.7	32.0
C3	28.5	30.1

Table 3.2: Mechanical properties of concrete.

In order to determine the actual characteristics of GFRP and steel reinforcement, three samples for each material were tested under tension in accordance with UNE ISO 15630-1:2011 and ACI 440.3R-12 respectively. The average values of the mechanical properties of the reinforcing bars are presented in Table 3.3.

Material	Elastic modulus, E_r (GPa)	Tensile/Yielding strength (MPa)	Axial Stiffness, EA (MN)
GFRP	66.5 ± 2.5	1200 ± 61	13.5 ± 0.5
Steel	206 ± 5.0	520 ± 10	16.2 ± 0.4

Table 3.3: Mechanical properties of reinforcement.

3.2.3 Test set-up

Two frames with a double lever system were specially designed and manufactured in order to apply a constant tensile load on the specimens (see Fig. A.1). The amplification factor of the mechanical system was 11. Steel housings were glued to both ends of the bars to avoid damaging the bars. The load

was progressively applied until 20-25% of the ultimate capacity of the reinforcing bar was reached (in the upper bound limit of sustained service loads according to recommendations). The load was applied using 400x400x15 mm (18.1 kg) steel plates. Smaller plates of 200x200x15 mm (4.6 kg) were used when approaching the cracking load to determine its value with more accuracy. The tests were stopped whenever a new crack appeared at the concrete surface, and at each stop the strains were recorded in order to plot their evolution. Member strains were measured along the centre line of the element (coinciding with the position of the reinforcing bar) on two opposite faces by means of a mechanical extensometer with a gauge length of 150 mm between Demec points. Additionally, for Series 2 and 3, a linear variable differential transducer (LVDT) was used to measure member deformation; both the mechanical extensometer and the LVDT measured and recorded deformations along the 900 mm bonded length (see Fig. A.3). Specimens C1F16ni and C2F16ni allowed strain distribution along the reinforcing bar to be monitored. To this end, two specially manufactured internally strain gauged reinforcing GFRP bars were used. The original bars were cut into two halves and the strain gauges were placed into of 6x4 mm grooves at intervals of 60 mm. Small holes were drilled every 120 mm to allow the gauge wiring to come out of the bar. After protecting the gauges against possible humidity, the bar was closed, with the two halves glued together, to give the appearance of a normal solid round bar. The bar's surface was not modified, and bond performance was not altered due to its instrumentation.
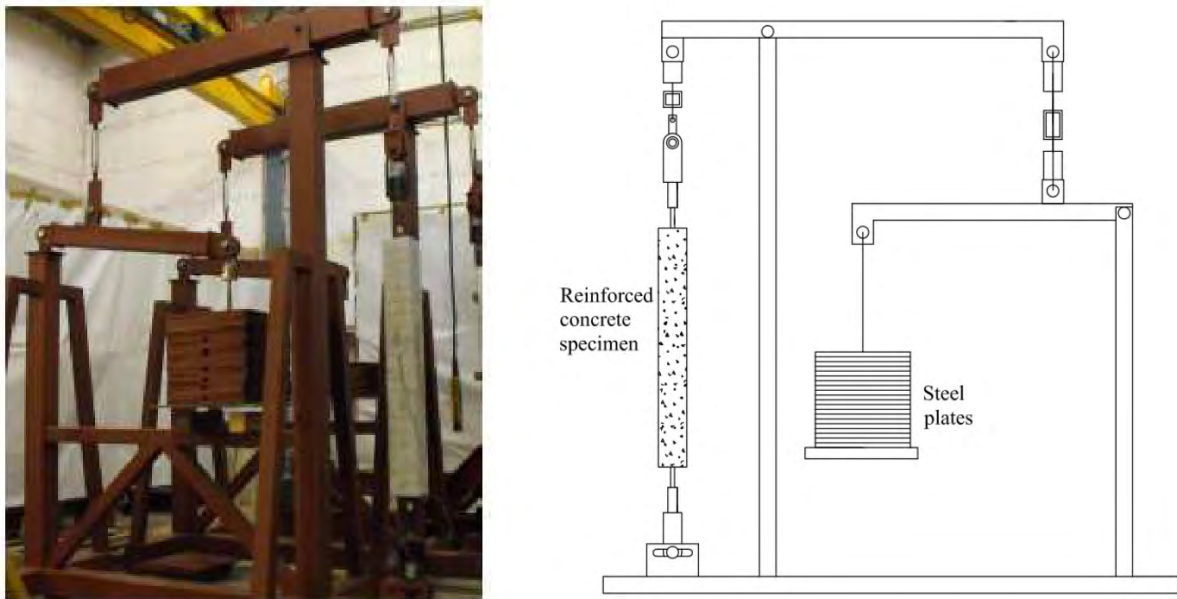
Figure 3.1: Frames for long-term tensile tests.
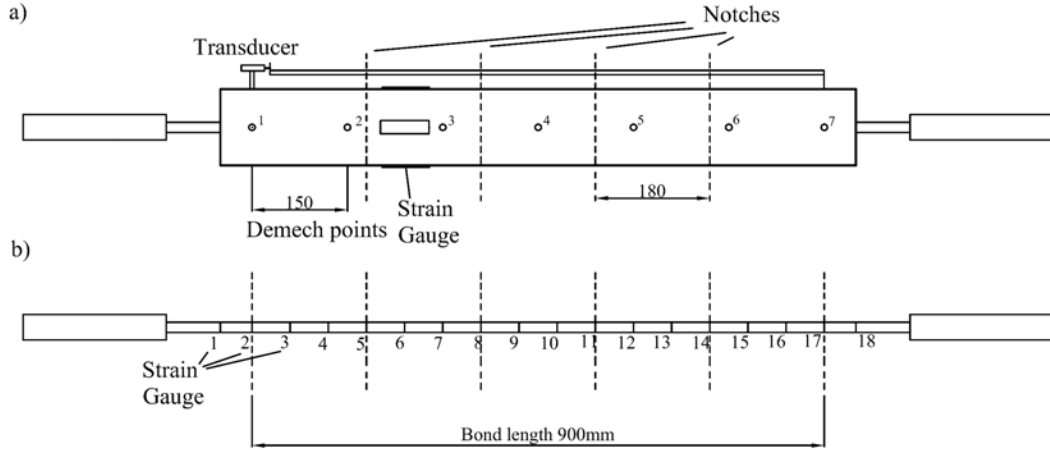
Figure 3.2: (a) External instrumentation of the concrete specimens. (b) Internal instrumentation of the GFRP reinforcing bar.

3.2.4 Creep and shrinkage

Creep coefficient for each series was determined in accordance with ASTM C5 12-02 [91]. Two concrete cylinders (150 mm diameter and 450 mm length) with embedded strain gauges were stacked in a loading frame. The cylinders were loaded at the same time as the tested elements. Additional specimens were left unloaded and were instrumented to determine free shrinkage strain. Temperature and humidity were also recorded.

The evolution of the experimental shrinkage strains of the three types of concrete, C1 (50 MPa), C2 (35 MPa) and C3 (25 MPa), are shown in Fig. A.27a. It is worth mentioning that the different evolution of experimental shrinkage strain for C1, reflected in Fig. A.27a, is related to the greater age of the concrete at the time of loading (t_0). Specimens were loaded at the ages of 63, 28 and 35 days for Series 1, 2 and 3 respectively. The average values of experimental free shrinkage strain at time t ($\varepsilon_{sh}(t, t_0)$) are tabulated in Table 3.4. As can be observed, from 10 to 30 days after loading, the shrinkage strain decreased from -10 $\mu\varepsilon$ to -50 $\mu\varepsilon$ for C1 (50 MPa), from -39 $\mu\varepsilon$ to -95 $\mu\varepsilon$ for C2 (35 MPa), and from -41 $\mu\varepsilon$ to -100 $\mu\varepsilon$ for C3 (25 MPa). Experimental results confirm the influence of concrete strength on the free shrinkage strain, with concrete with lower compressive strengths having higher free shrinkage.

The experimental creep coefficient from the strain measurements of the C1, C2 and C3 cylinders, along with their time evolution, is presented in Fig. A.27b. The coefficient is calculated from the ratio of the creep strain to the instantaneous strain. The creep strain at time t ($\varepsilon_{\varphi}(t)$) is obtained by subtracting the shrinkage strain, $\varepsilon_{sh}(t, t_0)$, from the total strain $\varepsilon_t(t, t_0)$. As seen in the steep slope of Fig. A.27b, at the beginning of the tests (up to approximately 5 days after loading), the creep effect increases significantly over time but thereafter tends to increase slowly. The average values of the experimental creep coefficient ($\varphi(t, t_0)$) are

indicated in Table 3.4. At 10 days after loading, the creep coefficient is 1.06 for C1 specimens, 1.22 for C2, and 1.26 for C3. From 10 to 30 days after loading, the creep coefficient increases from 1.06 to 1.59 for C1, from 1.22 to 1.70 for C2, and from 1.26 to 1.78 for C3, corresponding to an increase of 50%, 39% and 41% of the creep coefficient in C1, C2 and C3 specimens respectively. According to these experimental values, an influence of concrete strength on creep coefficient is observed [92].
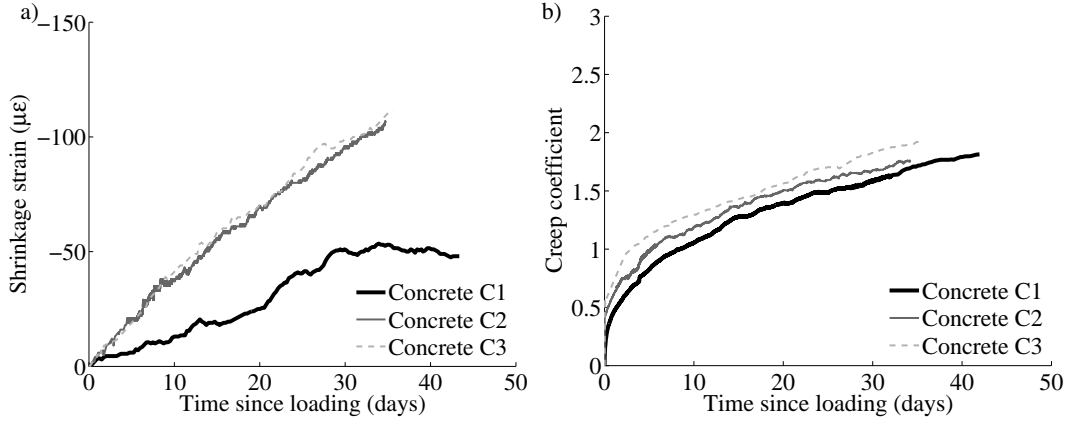
Figure 3.3: (a) Experimental free shrinkage strain. (b) Experimental creep coefficient.

Concrete	Time (days)	Creep coefficient	Shrinkage strain $\mu\varepsilon$
	t	$\varphi(t,t_0)$	$\varepsilon_{sh}(t,t_0)$
C1	10	1.06	-10
C1	30	1.59	-50
C2	10	1.22	-39
C2	30	1.70	-95
C3	10	1.26	-41
C3	30	1.78	-100

Table 3.4: Experimental time-dependent concrete properties (average values) from the loading day.

The effect of shrinkage occurring before initial loading was assessed, since it would be likely to affect test results depending on its absolute value and the sectional characteristics [39, 86]. The reinforcement embedded in the concrete provides restraints to concrete shrinkage, leading to compressive stresses in the reinforcement and tensile stresses in the concrete (see Fig. 3.4). The two main effects of shrinkage on the final response of the RC tie, therefore, are an initial shortening of the member (ε_{mi}) and a lower cracking load (since concrete is under an initial tensile load, hereafter referred to as P_{add}).

$$\varepsilon_{m,i} = \varepsilon_{sh}/(1+n\rho) \tag{3.1}$$

$$|P_{add}| = -\varepsilon_{sh}E_rA_r \tag{3.2}$$

where ε_{sh} is the experimental shrinkage at the time of loading, n is the modular ratio ($n = E_r/E_c$) and ρ is the reinforcement ratio.
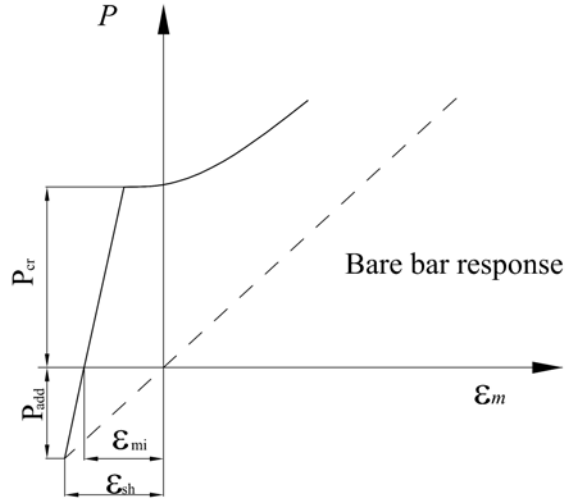
Figure 3.4: Effect of initial shrinkage [39].

As noted above, specimens were loaded at the ages of 63, 28 and 35 days for Series 1, 2 and 3 respectively. The experimental values of the recorded shrinkage at the time of loading are used to estimate the initial shortening, ε_{mi}, in accordance with Eq. (3.1). As shown in Table 3.5, the higher the shrinkage previous to loading, the higher the values of initial shortening (for bars of similar EA stiffness).

Test Series	ε_{sh}^a ($\mu\varepsilon$)	$\varepsilon_{mi}(\mu\varepsilon)$
Series 1	-245	-238
Series 2	-171	-166
Series 3 GFRP	-155	-150
Series 3 Steel	-155	-149

[a]Experimental shrinkage at the time of loading

Table 3.5: Shrinkage influence on ε_{mi}.

Initial member shortening, ε_{mi}, resulting from shrinkage effects is taken into account when representing the member tensile behaviour (Figs. 3.5-3.7) by offsetting the bare bar response with the shortening value ε_{mi} [39].

3.3 Test results

3.3.1 Tensile behaviour

Load-strain responses measured during the experimental tests are presented in Figs. 3.5-3.7. Mean member strain has been computed as member elongation divided by the 900 mm bonded length. For comparison purposes, the theoretical uncracked and the fully cracked responses are also plotted.

All the specimens have an initial linear branch with a steep slope corresponding to the uncracked condition. After cracking load (P_{cr}) is reached, a drop in the slope is observed due to the progressive cracking of the element. At this stage, the load-strain response gradually tends towards fully cracked behaviour. The load was progressively applied until the stress in the reinforcing bar reached 20-25% of its tensile strength. This maximum load was thereafter kept constant until the end of the test. The cracking load, the corresponding tensile strength, the number of cracks that appeared during the loading process and the time under sustained load are summarized in Table 3.6, while Figs. 3.5-3.7 show the load-mean strain response of test specimens. Markers in the curves represent pauses in the specimen loading process for elongation measurements, while sudden elongations indicate the appearance of new cracks. The order of appearance of cracks is indicated by numbers in the figures.

Specimen	P_{cr} (kN)	f_{ct} (MPa)	Number of cracks	Time under sustained load (days)
C1F16ni	19.6	1.46	5	39
C1F16	24.1	1.65	6	39
C2F16ni	19.6	1.46	4	35
C2F16n	23.6	1.76	4	35
C3F16n	15.7	1.31	4	37
C3S10n	17.7	1.16	4	37

Table 3.6: Cracking load, number of cracks and time under sustained load.

Series 1

Experimental responses for Series 1 elements are presented in Fig. 3.5, and similar behaviour can be observed for the two specimens. The differences in cracking load can be attributed to the reduced transversal section and scatter in the cracking load (P_{cr}) of specimen C1F16ni (notched). After cracking, both specimens tend towards fully cracked section behaviour. During the cracking stage, 5 and 6 transversal cracks appeared in specimens C1F16ni and C1F16 respectively. The loading process was stopped at a load of 45.3 kN, equivalent to stress in the reinforcement bar of 225 MPa. At this point, the load was kept constant at a total short-term strain (ε_i) of 2666 $\mu\varepsilon$ and 2716 $\mu\varepsilon$ for specimens C1F16ni and C1F16 respectively, with the load sustained for 39 days for both specimens. The plateau at the end of the load-strain curves shows the deformation increment caused by long-term effects, hereafter referred to as time dependent strain $\Delta\varepsilon$, which was 198 $\mu\varepsilon$ and 274 $\mu\varepsilon$ for specimens C1F16ni and C1F16 respectively.

Figure 3.5: Experimental load-mean strain curves of specimens C1F16ni and C1F16.

Series 2

Experimental responses for Series 2 are presented in Fig. 3.6. During the loading process 4 transversal cracks appeared at the notched sections in both specimens. In this series, the loading process was stopped at a load of 39.3 kN, when there was a stress in reinforcement of 195 MPa. With these loading conditions, the total short-term strains read ε_i=2239 $\mu\varepsilon$ and ε_i=1956 $\mu\varepsilon$ for specimens C2F16ni and C2F16n respectively. From these initial conditions, similar long-term deformations were observed during the 35 days of sustained loading, with time dependent strain reading $\Delta\varepsilon$=388 $\mu\varepsilon$ and 424 $\mu\varepsilon$ for specimens C2F16ni and C2F16n respectively.
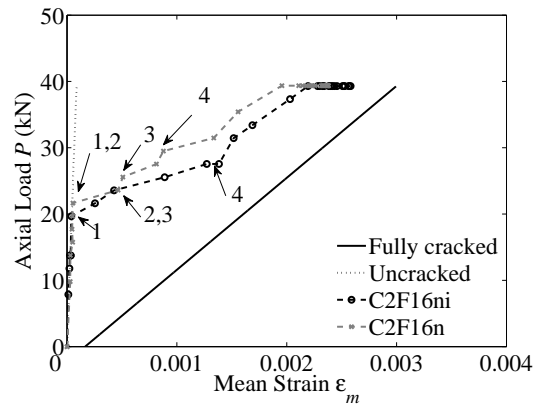
Figure 3.6: Experimental load-mean strain curves of specimens C2F16ni and C2F16n.

Series 3

Experimental responses for Series 3 are presented in Fig. 3.7. One of the specimens in this series was reinforced with a 16 mm GFRP bar and the other with a 10 mm steel bar, so that their axial stiffness was

as similar as possible (see Table 3.3). This can be noticed in the curves for fully cracked behaviour in Fig. 3.7. Despite an unavoidable difference in stiffness, the experimental responses were similar for the two tests, with an analogous cracking load (Pcr) and four transverse cracks at the notched sections. The loading process was stopped at a load of 39.3 kN, meaning there was a stress of 501 MPa in steel reinforcement and 195 MPa in GFRP reinforcement (in accordance with their respective sectional areas). The sustained load was maintained for 37 days under these conditions. The total short-term strains were $\varepsilon_i=1687$ $\mu\varepsilon$ and $\varepsilon_i=2310$ $\mu\varepsilon$ for specimens C3S10n and C3F16n respectively, while the time dependent strains for these two specimens were $\Delta\varepsilon=390$ $\mu\varepsilon$ and $\Delta\varepsilon=375$ $\mu\varepsilon$. According to the experimental results, similar time dependent strain is obtained for a fixed axial stiffness irrespective of the reinforcement material.
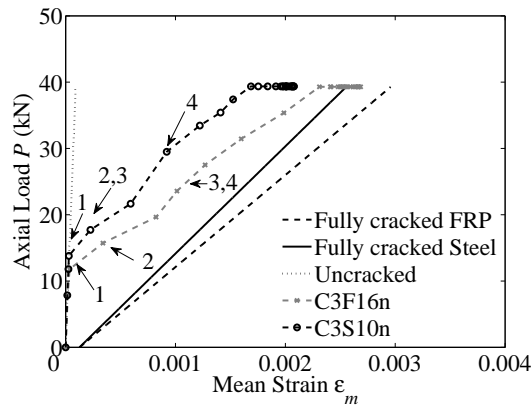
Figure 3.7: Experimental load-mean strain curves of specimens C3S10n and C3F16n.

Table 3.7 presents a summary of long-term behaviour exhibited in all the tests. The total short-term strain was bigger for the specimens in Series 1 because of the larger applied load, (which was adapted to the higher value of the cracking load observed). By contrast, specimens in Series 2 and 3 had larger time dependent strains. This can be explained by the lower compressive strength of the concrete in Series 2 and 3, and it being loaded under sustained loads at an earlier age.

Specimen	ε_i ($\mu\varepsilon$)	$\Delta\varepsilon$ ($\mu\varepsilon$)	Sustained load (kN)	Sustained stress in the bar (MPa)
C1F16ni	2666	198	45.3	225
C1F16	2716	274	45.2	224
C2F16ni	2239	388	39.3	195
C2F16n	1956	424	39.4	196
C3F16n	2310	375	39.3	195
C3S10n	1687	390	39.4	501

Table 3.7: Experimental total short-term strain (ε_i), time dependent strain ($\Delta\varepsilon$), sustained load and sustained stress at reinforcement.

3.3.2 Reinforcement strain and bond stress distributions

The cracking process and the evolution of strains and stresses in the tested specimens can be analysed by looking at the evolution of the reinforcement strain distribution. To this end, two of the GFRP RC elements incorporated internal instrumentation in the reinforcing bar (see Table 3.1). The locations of the strain gauges allowed the reinforcement strain at the four notched sections and the intermediate sections (Fig. A.3b) to be registered.

Experimental reinforcement strain distribution along the bar before and after each crack formation, based on strain gauge readings for specimen C2F16ni, is shown in Fig. 3.8. The vertical dashed lines represent the location of the notches and every marker in the curves represents a reading from a strain gauge. Before the first cracking, a peak in reinforcement strain distribution can be found at both ends of the RC tensile element. The value of this peak in strain corresponds to that of a fully cracked section. From this section on, reinforcement strain decreases until composite action is attained. At this point the reinforcement strain value equals that of an uncracked section. The first crack appears at P=21.61 kN, and a maximum peak in reinforcement strain distribution is displayed at x=770 mm. The second and third cracks, occurring at P=25.55 kN, are captured in reinforcement strain distribution with new peak values of x=230 mm and x=410 mm respectively. Finally, the fourth (and last) crack appears at P=27.55 kN at x=590 mm. This is finally reflected in Fig. 3.8, where the cracking process and experimental distribution on strains along the member are represented for different load levels.
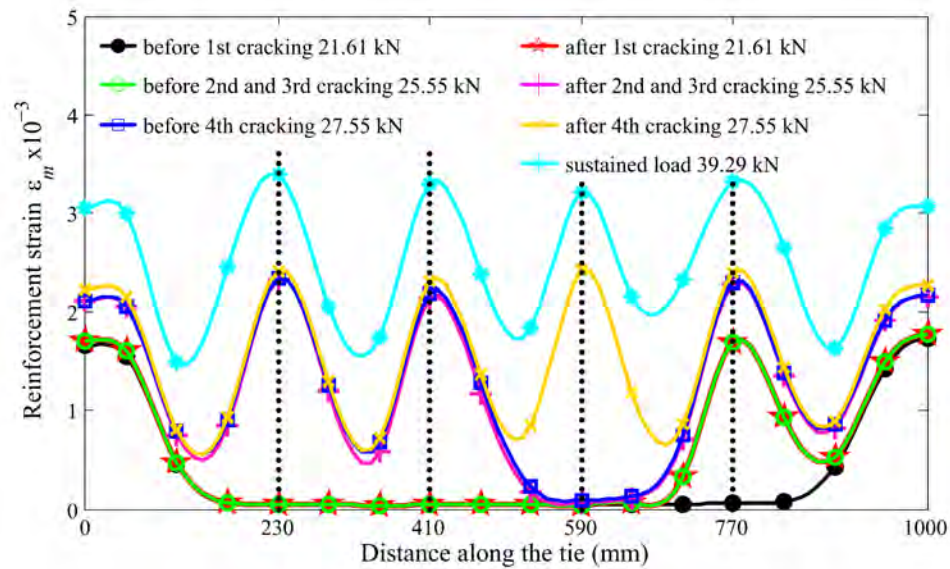
Figure 3.8: Experimental reinforcement strain distribution during crack formation in the loading process for specimen C2F16ni.

Once all the cracks are formed, the load is further increased until it reaches about 39 kN, or 20% of the reinforcement tensile strength. This load was kept constant for long-term testing for 35 days. The

comparison between experimental reinforcement strain distributions at different times of long-term testing is shown in Fig. 3.9. Experimental results show an increase in reinforcement strain due to long-term loading, with higher variations at intermediate sections between cracks. This means a reduction in concrete stresses at these sections, and therefore a reduction in the tension stiffening effect.
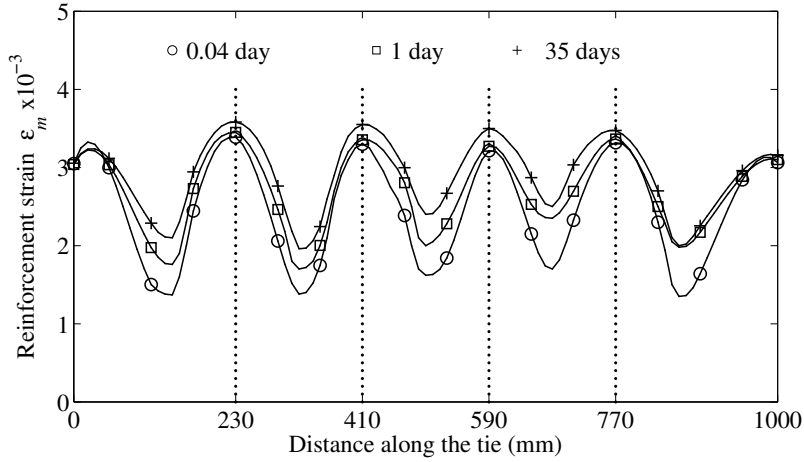
Figure 3.9: Experimental reinforcement strain distribution at different times during long-term testing for specimen C2F16ni.

Further analysis of reinforcement strain distribution makes it possible to study the distribution of bond stresses and concrete-reinforcement slip. The slip can be defined as the difference between the displacement of the reinforcement (u_r) and the displacement of concrete (u_c) as follows:

$$s = u_r - u_c \tag{3.3}$$

Differentiating Eq. (3.3) leads to:

$$\frac{ds}{dx} = \varepsilon_r - \varepsilon_c \tag{3.4}$$

where ε_r is the reinforcement strain and ε_c is the concrete strain for the same section.

Assuming that concrete strain can be disregarded in front of that of the reinforcement, the slip between concrete and reinforcement can be computed as:

$$s = \int_c^x \varepsilon_r(x)dx \tag{3.5}$$

Bond stresses can also be obtained from experimental data on reinforcement strain distribution. Taking the definition of bond as the force transferred between the reinforcing bar and the concrete per unit surface area, and performing equilibrium calculations on a piece of bar of length dx, along with the assumption of linear elastic behaviour of the bar, leads to:

$$\tau = \frac{E_r d_r}{4} \frac{d\varepsilon_r(x)}{dx} \tag{3.6}$$

where τ is the bond stress, d_r is the reinforcing bar diameter and E_r is the elastic modulus of reinforcement.

Using experimental data of specimen C2F16ni and Eqs. (3.5) and (3.6), the experimental slip and bond stress distributions along the reinforcing bar can be obtained as shown in Figs. 3.10 and 3.11, respectively. The vertical dashed lines represent the notched sections. The results in Fig. 3.10 show an increase in slip with time under a sustained load. Moreover, maximum slip matches with the location of the cracks and zero slip values are found in the middle of two consecutive cracks, as expected. Similarly, results in Fig. 3.11 show that maximum bond stresses are located near the cracked sections and zero bond stresses are found at the midway section between two cracks. Comparison between the curves of bond stresses at the time of application of sustained loading and at the end of the test reveals a deterioration in bond performance due to long-term loading. As an example, the mean value for bond stress at 0.04 days reads 5.3 MPa, and decreases to 3.8 MPa at 35 days. Similarly, the mean value for maximum bond stress decreases from 8.4 MPa to 6.2 MPa over the same period - a reduction in bond stresses of 28.30% and 26.19% respectively. Similar tendencies were observed for specimen C1F16ni, with a mean value for bond stress decreasing from 4.7 MPa to 3.4 MPa, and a mean value for maximum bond stress decreasing from 7.9 MPa to 5.7 MPa, meaning a reduction in the two bond stresses of 27.66% and 27.85%, respectively.

Figure 3.10: Experimental slip distribution for specimen C2F16ni at different times during long-term testing.
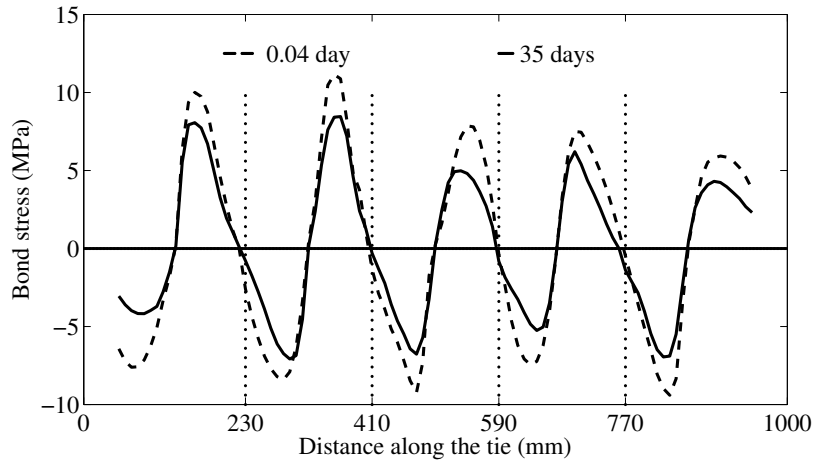
Figure 3.11: Experimental bond distribution for specimen C2F16ni at different times during long-term testing.

3.3.3 Concrete tensile stress

The effects of sustained load on RC tensile elements can also be analysed by studying the evolution over time of concrete tensile stresses. This alternative is based on an equilibrium equation for a block of reinforced concrete reading:

$$P = P_c + P_r \tag{3.7}$$

where P is the applied load, P_c is the force supported by concrete and P_r is the force supported by the reinforcing bar.

Based on Eq. (3.7), the evolution of concrete tensile stresses over time can be analysed by means of two different methodologies. The first uses experimental reinforcement strain values. From these readings, bar tensile stresses can be computed and, consequently, concrete stresses can be obtained. The second method requires the assumption of average reinforcement strain being equal to average surface strains computed by means of a mechanical extensometer as performed in [91]. Using this methodology, readings from the extensometer were averaged over the length of the specimen. Based on these average surface strains, concrete stresses were calculated using the following equations:

$$P_r = E_r \varepsilon_r A_r \tag{3.8}$$

$$\sigma_c = \frac{P - E_r \varepsilon_r A_r}{A_c} \tag{3.9}$$

where A_r is the reinforcement area and A_c is the concrete area.

For comparison purposes, the average reinforcement strain gauge readings and those of the mechanical extensometer at different times after loading are presented for specimen C2F16ni in Table 3.8. There is little difference between the measurements. Therefore, and because not all the specimens included internal instrumentation of the reinforcing bar, readings from the mechanical extensometer are used for the study of the evolution of concrete tensile stress for all the specimens. This evolution is presented in Fig. A.19, where the concrete stress has been normalized to its initial value. As a general trend, there is a marked decrease in concrete stress (of between 20% and 40%) in a short time period immediately after the application of the sustained load (around 10 hours). Stresses continue decreasing over time at a lower rate and stabilise at approximately 28 days. According to the experimental results, Series 1 specimens (with the highest concrete compressive strength) show the smallest variation in concrete tensile stress due to long-term testing, with a decay of around 38%. For Series 2 and 3 specimens, a greater decrease in concrete tensile stress can be observed, with specimens from Series 3 (with the lowest concrete compressive strength) showing the greatest variation with a decay of around 53%. It should be noted that specimens C2F16ni and C3F16n showed splitting cracks during short-term testing, which explains their even larger loss. Based on these results, the influence of concrete strength on the loss of concrete tensile stress, and therefore on the tension stiffening effect, is clear.

Time (days)	Mechanical extensometer ($\mu\varepsilon$)	Strain gauges ($\mu\varepsilon$)	Difference (%)
0.09	2326	2342	0.68
0.16	2342	2374	1.35
0.26	2371	2408	1.54
0.56	2385	2407	0.91
1.93	2427	2519	3.65
3.29	2446	2546	3.93
3.92	2459	2557	3.89
6.92	2478	2648	6.42
7.95	2502	2659	5.90
9.22	2553	2670	4.38
15.92	2562	2709	5.72
20.92	2572	2730	5.79
24.92	2611	2745	4.88
29.97	2612	2756	5.22

Table 3.8: Comparison between experimental mechanical extensometer and strain gauge readings at different testing times (specimen C2F16ni).
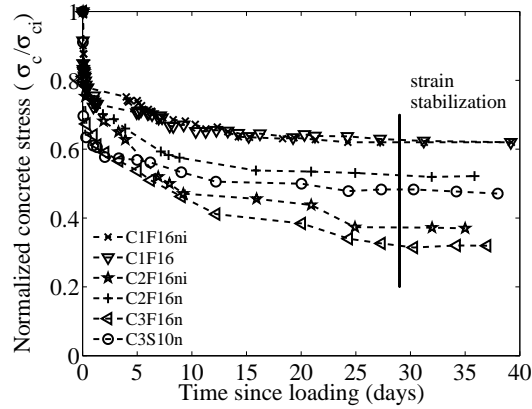
Figure 3.12: Evolution of conrete stress over time.

3.4 Comparison with the EMM approach

In this section, the experimental load-strain behaviour of the tested specimens is compared to theoretical predictions based on the smeared crack approach procedure of Eurocode 2 [47], using the effective modulus method (EMM) for estimating long-term deformations. The mean reinforcement strain at a certain applied load reads:

$$\varepsilon_m = \varepsilon_1 \left[\beta_1 \beta_2 \left(\frac{\sigma_{cr}}{\sigma_r} \right)^2 \right] + \varepsilon_2 \left[1 - \beta_1 \beta_2 \left(\frac{\sigma_{cr}}{\sigma_r} \right)^2 \right] \tag{3.10}$$

where β_1 stands for the bond characteristics of the internal reinforcing bars (1 for ribbed and 0.5 for smooth bars), β_2 represents the loading type (1 for short term and 0.5 for sustained load), σ_{cr} is the tensile stress in the reinforcing bar for a fully-cracked section when the first crack occurs ($\sigma_{cr} = P_{cr}/A_r$), σ_r is the stress in the reinforcing bar for a fully-cracked section at the actual load ($\sigma = P/A_r$), and ε_1 and ε_2 are the reinforcement strains calculated for the uncracked and the fully-cracked states respectively. This equation is applicable both for short and long-term loading.

For the calculation of ε_1 in the uncracked state, the strains between concrete and reinforcement can be considered compatible ($\varepsilon_1 = \varepsilon_c$). To include in Eq. (3.10) long-term effects in accordance with the concrete constitutive relationship used in the EMM, the concrete strain caused by sustained loading can be computed as:

$$\varepsilon_c(t) = \frac{\sigma_c(t)}{E_e(t, t_0)} + \varepsilon_{sh}(t, t_0) \tag{3.11}$$

where $\sigma_c(t)$ is the concrete stress, $\varepsilon_{sh}(t, t_0)$ is the free shrinkage strain and $E_e(t, t_0)$ is the effective modulus of elasticity given by:

$$E_e(t, t_0) = \frac{E_c(t)}{1 + \varphi(t, t_0)} \tag{3.12}$$

where $E_c(t)$ is the modulus of elasticity of concrete at time t and $\varphi(t, t_0)$ the creep coefficient at time t. Taking the equilibrium equation for a block of reinforced concrete:

$$P = \sigma_c(t) A_c + \sigma_r(t) A_r \tag{3.13}$$

the reinforcement strain in the uncracked state is found to be:

$$\varepsilon_1(t) = \frac{P - \sigma_c(t) A_c}{A_r E_r} \tag{3.14}$$

where P is the applied load, A_c is the area of concrete and A_r is the area of reinforcement.

Equating Eqs. (3.11) and (3.14) the following expression can be obtained:

$$\frac{\sigma_c(t)}{E_e(t, t_0)} + \varepsilon_{sh}(t, t_0) = \frac{P - \sigma_c(t) A_c}{A_r E_r} \tag{3.15}$$

Rearranging Eq. (3.15) results in [44]:

$$\sigma_c(t) = \frac{P}{A_c(1 + n^* \rho)} - \frac{\varepsilon_{sh}(t, t_0) E_r \rho}{1 + n^* \rho} \tag{3.16}$$

where n^* is the modular ratio between E_r and $E_e(t, t_0)$ and ρ is the reinforcement ratio. Eq. (3.16) is then substituted in Eq. (3.11), to obtain the strain in the uncracked state due to sustained loading ($\varepsilon_c(t)$), which finally is used to replace ε_1 in Eq. (3.10). The experimental values of the aforementioned parameters have been used in this study.

Predictions using this methodology are presented and compared with experimental results in Figs. 3.13 and 3.14, under the label "EMM, EC2 β_2=0.5". Additionally, Eurocode 2 predictions for a short-term response and the non-inclusion of long-term effects are also plotted under the label "EC2 β_2=1". For comparison purposes, the uncracked and the fully cracked responses are also plotted. It should be noted that the cracking load (P_{cr}) used in the predictions for specimens with notched sections has been normalized in accordance with:

$$P_{cr}^* = P_{cr} \frac{A_2(1 + n\rho_2)}{A_1(1 + n\rho_1)} \tag{3.17}$$

where P_{cr}^* is the normalized cracking load, A_1 is the area of a notched section and A_2 is the area of a section without notches.

Predictions for specimens of Series 1 are presented in Fig. 3.13a. As can be seen in the plot, Eurocode 2 predictions for short-term testing compare rasonably well with experiments. Regarding long-term analysis, the methodology predicts reasonably accurately the effect of long-term testing, with predicted time dependent strains ($\Delta \varepsilon$) being similar to the experimental ones.

Experimental and theoretical values for Series 2 specimens are presented in Fig. 3.13b. While the short-term response for specimen C2F16n is predicted accurately, there is a slight underestimation for specimen C2F16ni. Apart from this, the methodology is again effective in predicting the long-term effects.

Results for Series 3 are plotted in separate Figures (see Figs. 3.14a and 3.14b) due to a stiffness difference

(see Table 3.3). The Figures demonstrate a good prediction of the cracking process in both short-term and long-term testing.
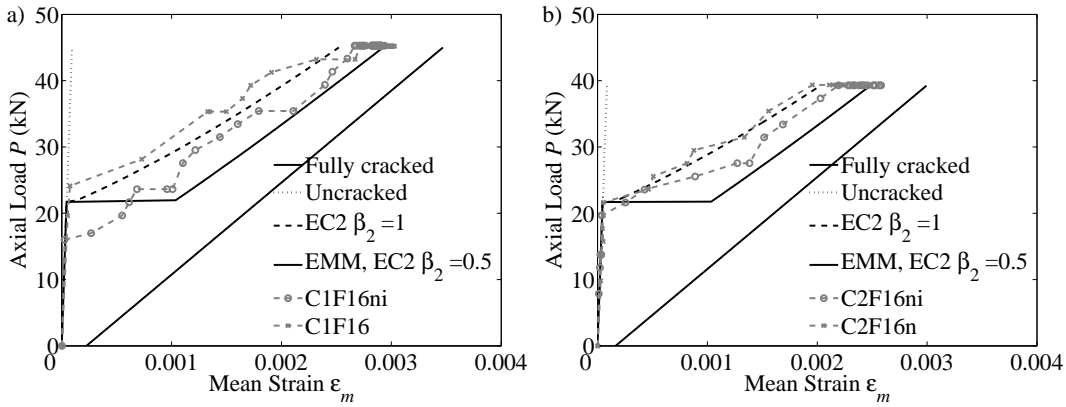
Figure 3.13: Comparison of experimental responses and theoretical predictions for specimens of a) Series 1 and b) Series 2.
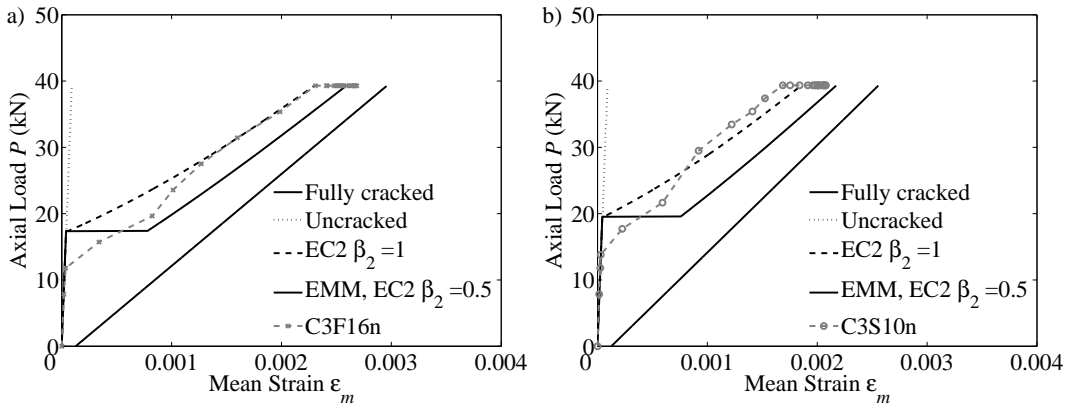
Figure 3.14: Comparison of experimental responses and EMM predictions for specimens a) C3F16n and b) C3F16n.

For the sake of clarity, Table 3.9 presents a summary of experimental and predicted values for short-term strain (ε_i) and the strain after a sustained load (ε_f). This last strain is computed as the sum of short-term strain and time dependent strain (i.e. $\varepsilon_f = \varepsilon_i + \Delta\varepsilon$). The ratios between experimental and predicted strains are also shown along with the mean and the standard deviation. From these ratios, it can be concluded that the combination of the Eurocode 2 proposal and EMM methodology for the analysis of long-term testing is valid.

Specimen	$\varepsilon_{i,exp}(\mu\varepsilon)$	$\varepsilon^*_{i,th}(\mu\varepsilon)$	$\varepsilon^*_{i,th}/\varepsilon_{i,exp}$	$\varepsilon_{f,exp}(\mu\varepsilon)$	$\varepsilon^{**}_{f,th}(\mu\varepsilon)$	$\varepsilon^{**}_{t,th}/\varepsilon_{t,exp}$
C1F16ni	2666	2522	0.95	2864	2925	1.02
C1F16	2716	2522	0.93	2990	2925	0.98
C2F16ni	2239	2028	0.91	2626	2482	0.95
C2F16n	1956	2028	1.04	2380	2482	1.04
C3F16n	2310	2295	0.99	2685	2586	0.96
C3S10n	1687	1854	1.09	2077	2172	1.05
Mean			0.97			1.00
Standard deviation			0.07			0.04

*EC2, β_2=1

**EMM, EC2, β_2=0.5

Table 3.9: Comparison between experimental and analytical long term predictions.

3.5 Conclusions

An experimental study to investigate the tension stiffening effect on GFRP RC tensile elements under sustained loading has been presented. The experiment consisted of an initial short-term loading and a subsequent test under sustained load for a period of between 35 and 40 days. A total of six tensile members with three concrete strengths were tested and analysed. Two specimens included internal instrumentation of the reinforcing bar that allowed monitoring of the strain distribution in both the short-term and the long-term tests.

Based on data from the internal strain gauges, the slip and the bond stresses were computed and analysed. Results show an increase in reinforcement strain due to sustained loading and a degradation in the tension stiffening effect. This reflects the impact of long-term loading on bond deterioration, with 28% reduction in mean bond stresses and increase in slip along the specimen.

Behaviour under sustained load was also studied by analysing the evolution of concrete tensile stresses. A sharp decrease in such stresses was found during the first 10 hours after imposing the sustained loading, followed by a smaller reduction that stabilized at approximately 28 days. The experimental results confirm the influence of concrete strength on the loss of tension stiffening, with higher concrete compressive strength showing the smallest decrease of concrete tensile stresses, with a value of around 38% compared to approximately 53% for the lowest concrete strength.

Experimental results from both short and long-term tests have been compared to predictions using Eurocode 2 by applying EMM methodology. The predictions using the methodology compare well with experimental results.

Nomenclature

A_1	area of a notched section
A_2	area of a section without notches
A_c	concrete area
A_r	reinforcement area
d_r	reinforcement diameter
E_c	concrete modulus of elasticity
$E_c(t)$	concrete modulus of elasticity at time t
$E_e(t,t_0)$	concrete effective modulus of elasticity
E_r	reinforcement modulus of elasticity
f_c	concrete compressive strength
n	modular ratio between E_r and E_c
n^*	modular ratio between E_r and E_e
P	applied load
P_{add}	initial tensile load due to shrinkage
P_c	load supported by concrete
P_{cr}	cracking load
P_{cr}^*	normalised cracking load
P_r	load supported by reinforcement
s	slip between concrete and reinforcement
t	time
t_0	time of loading
u_c	displacement of concrete
u_r	displacement of reinforcement
β_1	bond characteristics coefficient in EC2 propoal
β_2	loading type coefficient in EC2 proposal
$\Delta\varepsilon$	time dependent strain
ε_1	reinforcement strain for uncracked section
ε_2	reinforcement strain for fully cracked section
ε_c	concrete strain
$\varepsilon_c(t)$	concrete strain due sustained loading
$\varepsilon_{f,exp}$	experimental strain after sustained loading
$\varepsilon_{f,th}$	theoretical strain after sustained load
ε_r	reinforcement strain
ε_i	total short-term strain before sustained loading
$\varepsilon_{i,exp}$	experimental values of strain before sustained loading
$\varepsilon_{i,th}$	theoretical strain before sustained load

ε_m	analytical final strain response
ε_{mi}	initial shortening due to shrinkage
ε_{sh}	experimental shrinkage
$\varepsilon_{sh}(t, t_0)$	free shrinkage strain
$\varepsilon_\varphi(t)$	creep strain
$\varepsilon_t(t, t_0)$	total strain
$\varphi(t, t_0)$	creep coefficient
P	reinforcement ratio
$\sigma_c(t)$	concrete stress
σ_{cr}	reinforcement stress at cracking load
σ_r	reinforcement stress at actual load
τ	bond stress

Chapter 4

Experimental study of bond-slip of GFRP bars in concrete under sustained loads

This chapter contains the transcription of the published paper:

The paper in journal format is shown in Appendix D

Abstract

The structural behaviour of reinforced concrete (RC) elements depends heavily on the bond performance between the concrete and the reinforcing material. Bond behaviour under short-term testing has been extensively analysed for steel reinforcement and many studies have been carried out for fibre reinforced polymer (FRP) reinforcement. However, there has only been limited investigation of the long-term effects of this interaction. Several factors can affect the long-term bond behaviour of these elements, the most important being bond length and the immediate and time-dependent properties of reinforcement and concrete (concrete grade, creep, shrinkage and stiffness). This time-dependent behaviour is likely to cause changes and redistributions in bond stresses not properly considered in the limited existing literature. In this experimental study, the bond performance of GFRP RC under sustained load is investigated through pull-out tests. A total of 12 pull-out specimens were tested for a period of between 90 and 130 days. Two concrete strengths (35 MPa and 50 MPa), two bond lengths (5 and 10 times the diameter of the reinforcing bar) and two reinforcing materials (glass fibre reinforced polymer (GFRP) and steel) were used. Experimental results regarding immediate and time-dependent slip are presented and analysed here. In addition, some specimens were instrumented, with internal strain gauges in the reinforcing bar to provide data on the reinforcement strain, thus allowing the distribution of bond stresses and their evolution during sustained loading to be also presented and analysed.

4.1 Introduction

Fibre reinforced polymer (FRP) bars are increasingly being used as an alternative to steel reinforcement for reinforced concrete (RC) elements in corrosive environments or when the effects of electromagnetic fields may be present [1, 2, 4]. This has led to an increasing interest in the knowledge of properties and the study of different aspects of behaviour of FRP RC structures [29–32, 93–99]. The viability of these recently introduced materials largely depends on the effectiveness of the bond between the FRP bar and the concrete. In this regard, pull-out tests are probably one of the tests most extensively used to characterize the behaviour of the interface between the reinforcement and the concrete by means of bond-slip response. In the last two decades, considerable experimental research has gone into investigating the short-term response of FRP-to-concrete interfaces [10–15, 18–20, 37], with it being generally concluded that the pull-out mechanism of the many existing types of FRP reinforcement differs from that of deformed steel bars and is dependent on even more parameters [9, 10].

When analysing time effects on the behaviour of RC elements, concrete creep and shrinkage play a crucial role [82–88]. While creep is associated with sustained stresses, shrinkage may be assumed to be independent on load, but both cause long-term deformations in concrete. For common steel RC no additional long-term effects need to be considered because steel undergoes neither shrinkage nor creep. Few studies have focused on the possible effect of creep in FRP reinforcement. An experimental programme with regard to such an effect in aggressive environments was presented in Ref. [43]. The programme consisted of testing twenty GFRP bars in tension for 417 days at two loading levels (25% and 38% of the ultimate bar tensile strength). The results showed that creep strain in the GFRP bars was less than 5% of the initial strain value. It was also concluded that long-term loading had a minimal effect on the elastic modulus, whilst the effect on residual strength was more dependent on the environmental conditions. A more recent programme was presented in Ref. [100], where GFRP pultruded laminates were tested under a tensile sustained load for 500 days. The authors observed that the largest increments in longitudinal stresses due to long-term testing were less than 2%. The components (matrix and reinforcement or polyester resin and glass fibres) were tested separately to check their individual long-term responses. A significant increase in longitudinal strain was observed for the polyester resin while only a negligible increase was obtained for the glass fibres.

The literature dealing with time effect on the bond behaviour of FRP reinforcement and concrete is also limited in extent [16, 52, 53, 70]. An experimental study of long-term behaviour of CFRP externally reinforced concrete elements covering three bond lengths and two loading levels was presented in Ref. [16], where the evolution of reinforcement axial stresses and bond stresses under constant tensile load was analysed over 900 days of testing. Results showed a redistribution of bond stresses along the anchorage due to creep deformations at the interface. In respect of internal reinforcement, degradation of the bond between FRP bars and concrete under sustained load was analysed in Ref. [52] through a pull-out testing procedure. The experimental work included four different reinforcing materials as well as different environmental conditions, with pull-out specimens being loaded for one year at different loading levels. Results showed an increase in slip with time, with this increase being dependent on the bar surface treatment and the level of sustained load. A more recent experimental study of the bond behaviour of internal GFRP reinforcement

and concrete under sustained loading was presented in Ref. [53]. The pull-out specimens, which combined three different bar diameters, were pre-loaded until one millimetre of slip was observed at the unloaded end. Following this, the specimens were loaded until slip stabilization. The tests were considered to be acceptable if no increase in slip was observed after 2000 h. To simulate accelerated long-term testing, the tests were conducted at 60°C, and a design value of bond strength was proposed by the authors based on the experimental data. The long-term effect on steel and GFRP internally reinforced concrete members under tension has been analysed in a study made by the present authors [70]. The experimental programme included three different concrete strengths and two different reinforcing materials. The evolution of reinforcement strains was monitored, and slips and bond stresses were analysed. Results showed that long-term testing caused a reduction in mean bond stress of about 28%, which highlights the importance of analysing and understanding bond behaviour in the long term. Since limited literature exists on this issue, an experimental long-term bond test programme is needed.

This paper presents the results of an experimental campaign consisting of twelve pull-out specimens tested under sustained axial load for a period between 90 and 130 days. The programme included two concrete strengths, two reinforcing materials and two bond lengths. The sustained load level was set at 15% of the ultimate capacity of the GFRP reinforcing bar to ensure it corresponded to the service load range. Experimental results in terms of immediate and time-dependent slip are presented and analysed. Some specimens were instrumented, with internal strain gauges in the reinforcing bar, to provide data on the reinforcement strain, thus allowing the distribution of bond stresses and their evolution during sustained loading to be analysed.

4.2   Experimental programme

4.2.1   Test matrix

The experimental programme was aimed at studying the effect of concrete strength, reinforcing material and bond length on the bond response of pull-out tests under sustained loading. Two different target concrete compressive strengths (35 and 50 MPa), two different bond lengths (equal to $5d_r$ and $10d_r$, with d_r being the nominal diameter of the reinforcing bar) and two reinforcing materials (GFRP and steel) were considered. So that axial stiffness (EA) would be similar in all tests, the reinforcement consisted of either a single 16 mm diameter GFRP bar or a single 10 mm diameter steel bar. The combination of these variables gave a total of eight specimens. So that the internal distribution of bond stresses could be analysed, four additional specimens were manufactured that included internal instrumentation of the GFRP reinforcing bar. Thus, the test matrix consisted of twelve pull-out specimens divided into two groups of six specimens each according to concrete grade.

Based on this description, the tested elements are identifiable by the formula CxBRi, with Cx standing for the type of concrete (C1=35 MPa, C2=50 MPa), B for the bond length (S=$5d_r$, L=$10d_r$), R for the type of reinforcement (F=GFRP, S=Steel), and "i" for the identification of specimens with internally instrumented reinforcement. The test matrix is summarized in Table 4.1.

Specimen	Concrete	Bond length, l_b (mm)	Reinforcement	Reinforcement internal instrumentation
C1SS	C1	50	Steel	No
C1SF	C1	80	GFRP	No
C1SFi	C1	80	GFRP	Yes
C1LS	C1	100	Steel	No
C1LF	C1	160	GFRP	No
C1LFi	C1	160	GFRP	Yes
C2SS	C2	50	Steel	No
C2SF	C2	80	GFRP	No
C2SFi	C2	80	GFRP	Yes
C2LS	C2	100	Steel	No
C2LF	C2	160	GFRP	No
C2LFi	C2	160	GFRP	Yes

Table 4.1: Test matrix.

All the specimens were cubic (200 mm sides) with a 600 mm bar located in the middle. Before casting, the bond length was appropriately marked, and a plastic tube was positioned to prevent contact along the remaining bar length. Steel housings were glued to the GFRP bars so that the pull-out load could be applied without damaging the bars.

4.2.2   Material properties

Ready-mixed concrete was used to cast the specimens. Compressive strength was determined at the time of loading (35 days after casting) by a standard cylinder test (150 x 300 mm) according to UNE 12390-3 [101]. The average values of the mechanical properties are summarized in Table 4.2.

Concrete	Compressive strength, f_c (MPa)	Elastic modulus, E_c (GPa)
C1	35.5	32.1
C2	48.5	35.3

Table 4.2: Mechanical properties of concrete.

In order to determine the characteristics of the GFRP and steel reinforcement, three samples for each material were tested under tension according to UNE ISO 15630-1:2011[102] and ACI 44.3R-12 [103] respectively. The average values of the mechanical properties of the reinforcing bars are given in Table 4.3.

Material	Elastic modulus, E_r (GPa)	Tensile/Yielding strength (MPa)	Axial Stiffness, EA (MN)
GFRP	66.5 ± 2.5	1200 ± 61	13.5 ± 0.5
Steel	206 ± 5.0	520 ± 10	16.2 ± 0.4

Table 4.3: Mechanical properties of reinforcement.

4.2.3   Test set-up

Three frames with a double lever system were used to apply a constant tensile load on the pull-out specimens (see Fig. B.1). The amplification factor of the mechanical system was 11. In each frame, two pull-out specimens with the same reinforcing bar and concrete grade but of different bond length were connected in series (i.e. specimen C1SS was connected in series with specimen C1LS), which meant that the same load was applied to both specimens. A maximum load equal to 15% of the ultimate capacity of the GFRP bar was selected (see Table 4.4), in order to correspond to the service load range (ACI 440 1.R-06 [72] fixes a limit of 20% for GFRP bars). The sustained load applied to the steel reinforced specimens was adapted (by means of the bond perimeter) so as to obtain similar bond stresses to those of GFRP reinforced pull-outs.
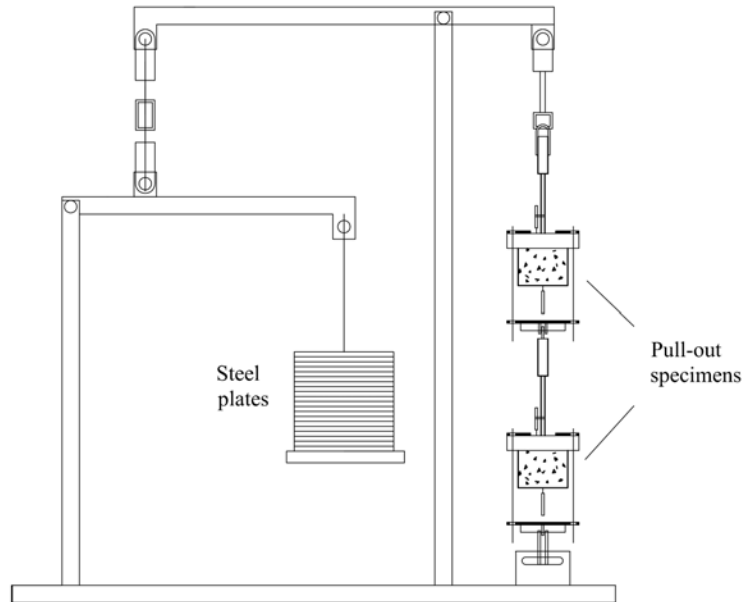
Figure 4.1: Frame for long-term testing.

Specimens	P_{max} (kN)
C1SS, C1LS	10.5
C1SF, C1LF	29.5
C1SFi, C1LFi	29.5
C2SS, C2LS	10.5
C2SF, C2LF	29.5
C2SFi, C2LFi	29.5

Table 4.4: Maximum loads.

To perform the test the load was applied progressively using 400x400x15 mm (18.1 kg) steel plates, until

the loads indicated in Table 4.4 were reached. These maximum loads were thereafter sustained for 90 days in the case of series C1 and 130 days in series C2.

To measure the slip at both the loaded and the unloaded end, two displacement transducers (HLS) were used for each pull-out specimen (see Fig. 4.2a). Four of the twelve pull-out specimens allowed monitoring of the strain distribution along the bar. These specimens were cast using specially manufactured internally strain gauged GFRP bars [70, 104]. The location of the internal instrumentation is shown in Fig 4.2b. In the case of the short bond length specimens, four and two strain gauges were placed along and outside the bond length respectively. For long bond length specimens, the number of gauges located along the bond length was doubled to eight.
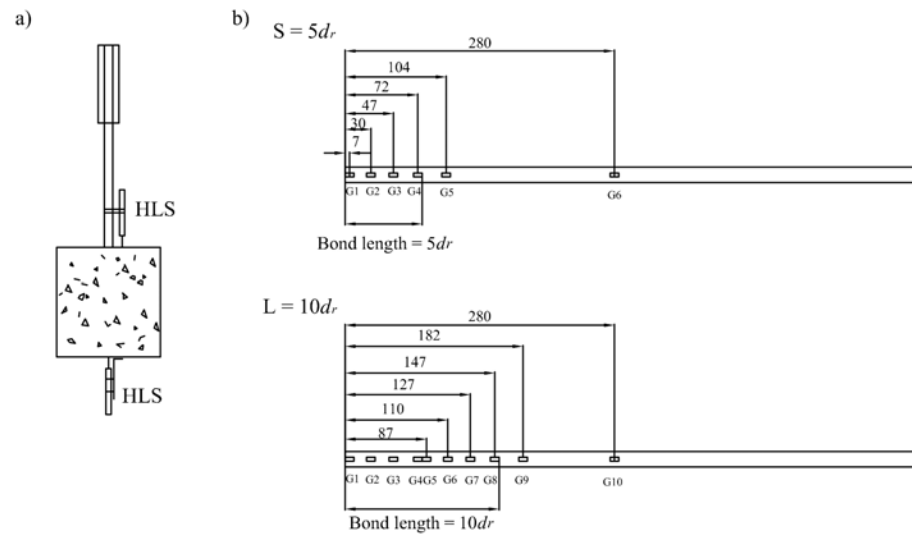
Figure 4.2: a) Experimental instrumentation of the pull-out specimens. b) Internal instrumentation of the GFRP reinforcing bar (distance in mm).

4.2.4 Shrinkage and Creep

The creep coefficient for each series was determined in accordance with ASTM C5 12-02 [91]. Two concrete cylinders (150 mm in diameter and 450 mm in length) with embedded strain gauges were stacked in a loading frame. The cylinders were loaded at the same time as the pull-out specimens. An additional 200 mm cubic concrete specimen was instrumented and left unloaded to determine free shrinkage strain.

Temperature and humidity were also recorded. An average temperature and relative humidity of $16 \pm 2.5°C$ and $40 \pm 23.5\%$ were registered for the C1 series. These registers changed to $27 \pm 3.5°C$ and $49 \pm 15\%$ for the C2 series. Recorded values are shown in Fig. B.9.

Figure 4.3: Temperature and relative humidity registered in the laboratory during a) C1 tests and b) C2 tests.

The evolution of the shrinkage strains recorded for the two types of concrete is shown in Fig. B.11a. The values of free shrinkage strains recorded at time t ($\varepsilon_{sh}(t, t_0)$) are indicated in Table 4.5. As can be observed, from 10 to 90 days the shrinkage strain increased from -46 $\mu\varepsilon$ to -190 $\mu\varepsilon$ for C1 (35 MPa), and from -36 $\mu\varepsilon$ to -182 $\mu\varepsilon$ for C2 (50 MPa). At 90 days, the shrinkage strain of concrete C1 was 4.2% greater than that of concrete C2.
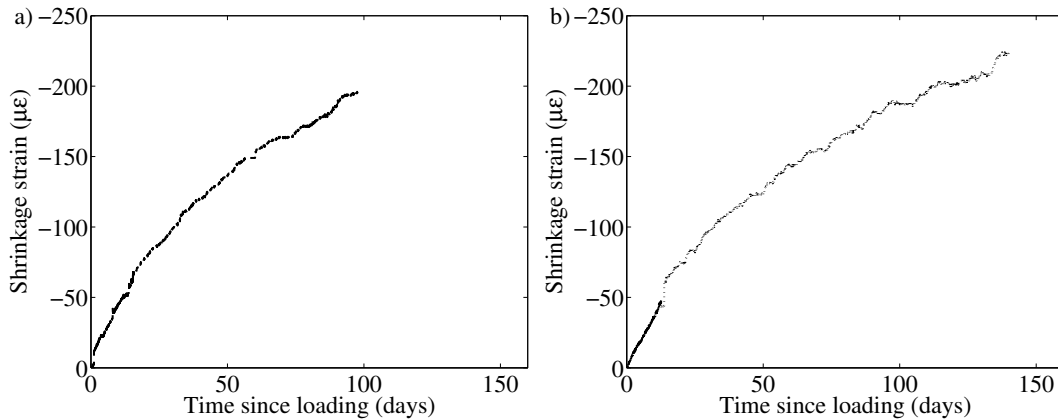
Figure 4.4: Experimental free shrinkage strain of a) C1 series and b) C2 series.

The experimental creep coefficient obtained from the strain measurements of the C1 and C2 series, calculated from the ratio of creep strain to instantaneous strain, is shown in Fig. B.13. The creep strain at time t ($\varepsilon_{\varphi}(t)$) is obtained by subtracting the shrinkage strain, $\varepsilon_{sh}(t, t_0)$ from the total strain $\varepsilon_t(t, t0)$ [70, 83]. At the beginning of the test the creep effect increases considerably with time, but thereafter tends to increase slowly. The average values of experimental creep coefficient ($\varphi(t, t0)$) are indicated in Table 4.5. At 10 days after loading, the creep coefficient reads 1.00 and 0.74 for C1 and C2 respectively. From 10 to 90 days after loading, it increases from 1.00 to 1.88 for C1 and from 0.74 to 1.37 for C2, corresponding to increases of

88% and 85% respectively. The influence of concrete strength on creep coefficient is observable in these values, with the creep coefficient at 90 days of C1 being around 1.37 times greater than that of C2.
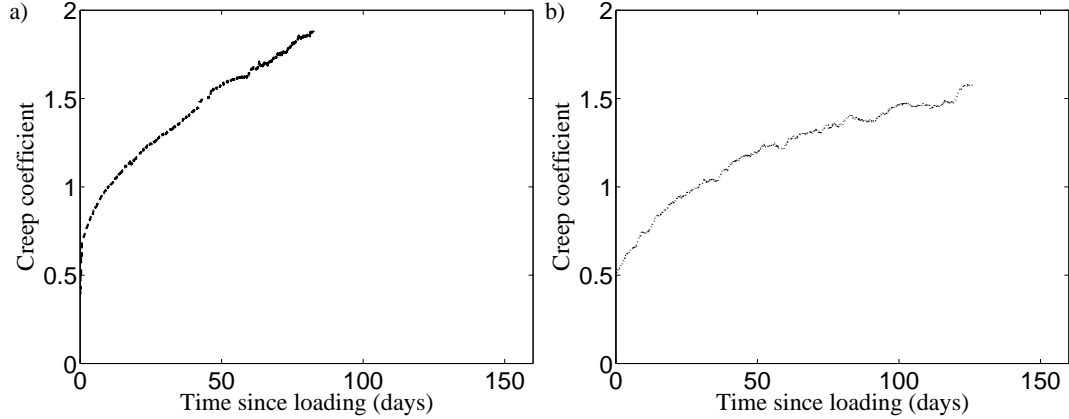
Figure 4.5: Experimental creep coefficient of a) C1 series and b) C2 series.

Concrete	Time, t (days)	Creep coefficient, $\varphi(t, t_0)$	Shrinkage strain, $\varepsilon_{sh}(t, t_0)(\mu\varepsilon)$
C1	10	1.00	-46
C1	50	1.57	-134
C1	90	1.88	-190
C2	10	0.74	-36
C2	50	1.19	-123
C2	90	1.37	-182
C2	130	1.57	-223

Table 4.5: Experimental time-dependent concrete properties (average values) from the loading day.

4.3 Test results

The results obtained in the experimental tests described in Section 4.2 are presented and discussed in the following. Particularly, the immediate value and the time-development of the relative slip measured at the bar-concrete interface are particularly considered. As stress distribution is not constant along the bond length in a pull-out test, an average bond stress is defined as:

$$\tau_{av} = \frac{P_{max}}{\Pi d_r l_b} \tag{4.1}$$

where τ_{av} is the average bond stress applied to the interface, P_{max} is the maximum load applied to the bar, d_r is the bar diameter and l_b is the bond length.

For the test set-up, the pull-out specimens were loaded in pairs of equal concrete grade and with the same reinforcing bar, but different bond length (i.e. specimen C1SS and C1LS in series, specimens C1SF

and C1LF in series, and so on). As a result, the average bond stress induced in short bond length specimens was twice that in long bond length specimens (see Table 4.6).

Specimen	P_{max} (kN)	Average bond stress, τ_{av}(MPa)
C1SS	10.5	6.71
C1SF	29.5	7.33
C1SFi	29.5	7.32
C1LS	10.5	3.35
C1LF	29.5	3.67
C1LFi	29.5	3.66
C2SS	10.5	6.71
C2SF	29.5	7.33
C2SFi	29.5	7.32
C2LS	10.5	3.35
C2LF	29.5	3.67
C2LFi	29.5	3.66

Table 4.6: Maximum applied loads and average bond stresses at the interface.

Experimental total slips versus time after loading are shown in Figs. B.15 and B.17. The total slip includes both the immediate slip due to instantaneous loading and the time-dependent slip due to sustained loading. As can be observed, the curves have a similar trend, with a larger immediate slip for short bond length specimens.

Figure 4.6: Experimental total slip vs. time after loading for C1 specimens with a) short bond length and b) long bond length.
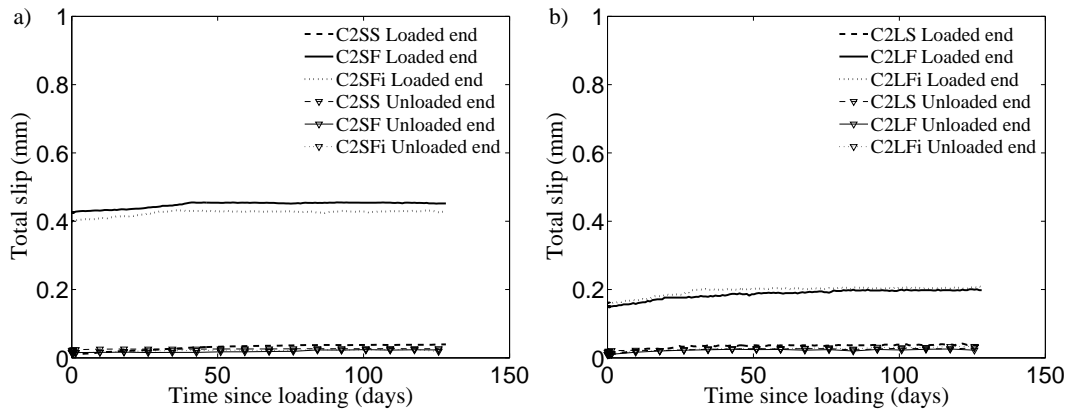
Figure 4.7: Experimental total slip vs. time after loading for C2 specimens with a) short bond length and b) long bond length.

4.3.1 Immediate slip

Experimental data on the immediate response is given in Table 4.7 and analysed in this section. As can be seen values of registered slips are influenced by bond length, concrete strength and type of bar as has been reported in previous studies [10, 11, 15, 19, 20, 37].

Specimen	Immediate slip (mm)	
	Loaded end	Unloaded end
C1SS	0.028	0.025
C1SF	0.590	0.019
C1SFi	0.591	0.021
C1LS	0.018	0.006
C1LF	0.216	0.014
C1LFi	0.233	0.015
C2SS	0.021	0.006
C2SF	0.424	0.016
C2SFi	0.401	0.015
C2LS	0.016	0.002
C2LF	0.148	0.010
C2LFi	0.158	0.009

Table 4.7: Experimental results for immediate slip.

Irrespective of the type of bar and bond length, slips are larger for lower concrete strength which is a consequence of larger local deformability and damage in the concrete surrounding the bar. Likewise, slips are larger for specimens with lower bond lengths due to the higher bond stresses needed to transfer similar loads. It is also observed that the difference in slips between loaded and unloaded end is larger for the FRP bars as reported in Refs. [19, 37]. This may be attributable to the higher deformability of the FRP bars jointly with a more effective mechanical interlock between bars and concrete due to the material and surface

characteristics. Comparing similar specimens with different type of bar, slips are generally higher for the FRP bars, which indicates a lower slope in the bond stress-slip response. The only exception is for the slip at the unloaded end in specimens with short bond length and C1 concrete, which may be attributable to the combination of higher bar stiffness and damage introduced in the concrete for this short bond length. Globally, these differences in slips between both ends indicate a non-uniform distribution of stresses along the bonded length, which is more pronounced for larger bond lengths [11, 20].

4.3.2   Time-dependent slip

For the sake of clarity and to make analysing the long-term experimental results easier, in Figs. B.19 and B.21 the immediate slip has been removed, so that only the experimental time-dependent slip (Δs) is presented. In addition, representative time-dependent slips at different times during long-term testing have been tabulated in Table 4.8.

Both Figs. B.19 and B.21 and Table 4.8 confirm the minimal effect of long-term testing on the slip at the unloaded end. As an example, time-dependent slip at 90 days (Δs_{90}) is below 0.012 mm for steel specimens and below 0.022 mm for GFRP specimens. Larger time-dependent slips are observed for the loaded end. An analysis of the evolution of these slips is presented below.

Experimental time-dependent slip results for C1 specimens are given in Fig. B.19. As can be seen in the slopes of the curves, at the beginning of the sustained loading test the slip increases considerably over time, but thereafter tends to increase more slowly. Changeover takes place at around 60 days, when an average of 89.7% and 97.8% of the time-dependent slip at 90 days (Δs_{90}) is achieved for short and long bond length specimens respectively. Finally, the time-dependent slip at 90 days (Δs_{90}) for specimens with a long bond length is 1.94 times that of specimens with a short bond length.
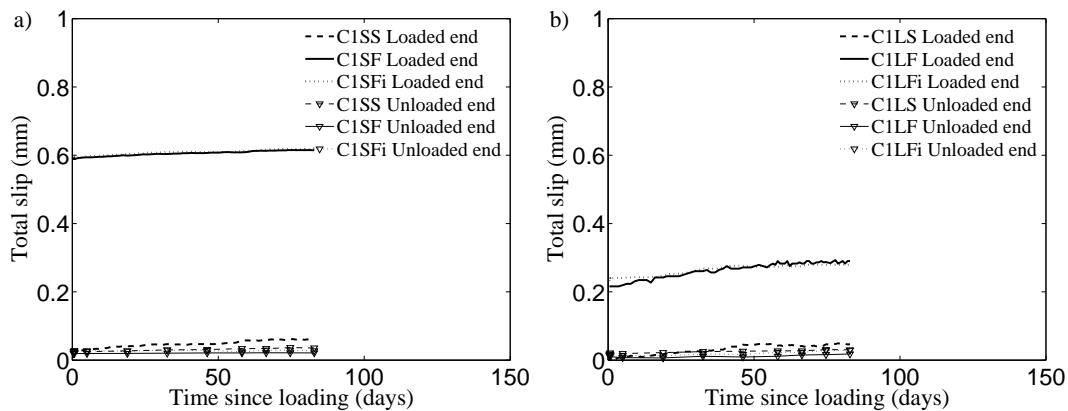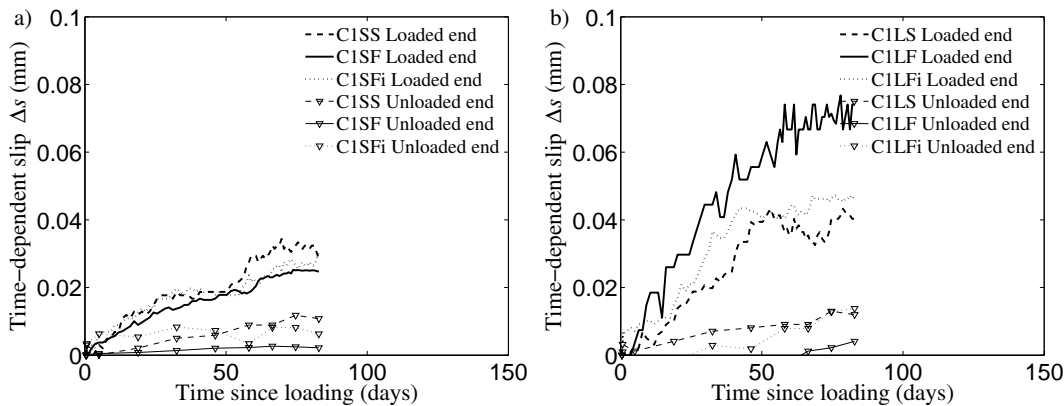

Figure 4.8: Experimental time-dependent slip vs. time after loading for C1 specimens with a) short bond length and b) long bond length.

Similar trends can be observed in C2 specimens (see Fig. B.21 and Table 4.8). In this series, the sustained load was applied for a total of 130 days, making stabilization much clearer. In fact, based on the stabilization

observed previously in this series, the C1 series was designed to consist of 90 days' testing. At 60 days an average of 95.5% and 95.9% of the time-dependent slip at 90 days (Δs_{90}) was achieved for short and long bond length specimens respectively. In this series, the time-dependent slip at 90 days (Δs_{90}) for specimens with long bond length was 1.49 times that of short bond length specimens. According to these results, the time-dependent slip at 90 days (Δs_{90}) in the C2 series is around 23.3% lower than in the C1 series. This difference could be attributable to the mechanical properties of concrete (immediate and time-dependent), where lower concrete strength produces higher time-dependent slips, as would be expected.

A summary of experimental time-dependent slips at 60 and 90 days after loading (Δs_{60}, and Δs_{90}) is shown in Table 4.8. Additionally, the time-dependent slip at 130 days (Δs_{130}) is also reported for the C2 series.
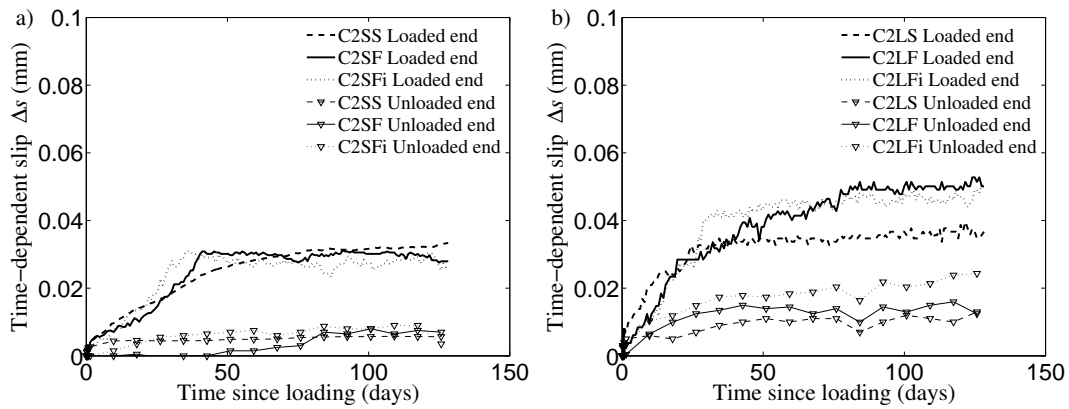
Figure 4.9: Experimental time-dependent slip vs. time after loading for C2 specimens with a) short bond length and b) long bond length.

Specimen	Δs_{60} (mm)		$\Delta s_{90} (mm)$		$\Delta s_{130} (mm)$	
	Loaded	Unloaded	Loaded	Unloaded	Loaded	Unloaded
C1SS	0.029	0.009	0.029	0.011	-	-
C1SF	0.023	0.002	0.024	0.002	-	-
C1SFi	0.022	0.007	0.030	0.006	-	-
C1LS	0.040	0.009	0.040	0.012	-	-
C1LF	0.074	0.003	0.074	0.004	-	-
C1LFi	0.044	0.008	0.047	0.010	-	-
C2SS	0.028	0.005	0.031	0.006	0.030	0.006
C2SF	0.030	0.002	0.030	0.007	0.031	0.008
C2SFi	0.026	0.008	0.027	0.008	0.030	0.009
C2LS	0.036	0.010	0.036	0.010	0.037	0.011
C2LF	0.043	0.014	0.049	0.014	0.050	0.013
C2LFi	0.046	0.018	0.046	0.022	0.048	0.021

Table 4.8: Experimental time-dependent slip at different times during long-term testin.

4.3.3   Bond stresses-distribution and evolution

Experimental results show an increase in pull-out slips due to sustained loading, attributable to bond deterioration. There are no means of directly registering the bond taking place at an interface, but bond can be estimated from strain distribution along the bond length, as shown in previous works [16, 70, 91].

As indicated previously, this experimental investigation included four pull-out specimens whose reinforcement was internally strain gauged so that data on the reinforcement strains along the bond length would be available. In this section, the reinforcement strain distributions are presented and analysed. In a further step, these strain distributions are used for the analysis of the bond profile and redistribution of bond stresses over time which take place due to sustained loading.

Reinforcement strain distribution

Fig. B.25 shows the strain gauge readings at various locations along the bond and unbonded length (see Fig. 4.2b), with location 0 mm representing the unloaded end of the pull-out specimen. The figure includes two different sets of information. First, strain development with load is represented at the very first curves (plotted at 0 days after loading). These curves were registered during the instantaneous test, where load was progressively applied until 15% of the ultimate capacity of the GFRP reinforcing bar was reached. Second, strain development with time is represented with the help of the third axis. These curves were registered during the long-term test, when load was sustained for 90 days in the case of the C1 series and 130 days for the C2 series. For practical reasons, only data regarding specimen C1LFi is shown in Fig. B.25, although this information is also available for specimens C1SFi, C2SFi and C2LFi.

Fig. B.29 shows the reinforcement strain distribution at different load levels at the time of loading (instantaneous pull-out corresponding to 0 days in Fig. B.25), with location 0 mm representing the unloaded end of the pull-out specimen and the vertical dashed lines representing the location of strain gauges (see Fig. 4.2b). The bond length is clearly marked to help in the analysis of the results. Some of the strain gauges failed during the test, and therefore no data is recorded at some locations. For example, the strain gauge at 104 mm from the unloaded end of specimen C1SFi failed, and this is evident in Fig. B.29a, where no marker exists at that location. In this case, for illustrative purposes, and because this gauge was located outside the bond length, its value was assumed to be the same as that of location 280 mm, also located outside the bond length.

A significant difference can be observed between Figs. B.29a and B.29b. The loading process in the short bond length is characterized by a quasi linear distribution of strains (see Fig. B.29a) along the bond length, whereas in the case of long bond length a clearer non-linear distribution is obtained (see Fig. B.29b). According to these results, bond stresses are more evenly distributed in a short bond length, with the entire bond region contributing to the stress transfer process. On the other hand, for specimens with long bond

length the transfer length increases with the applied load.
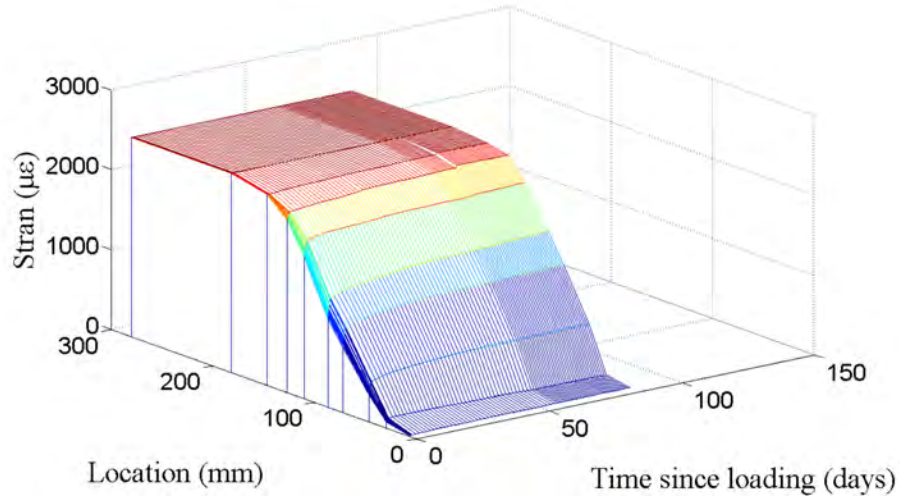
Figure 4.10: Experimental reinforcement strain distribution over time for specimen C1LFi.
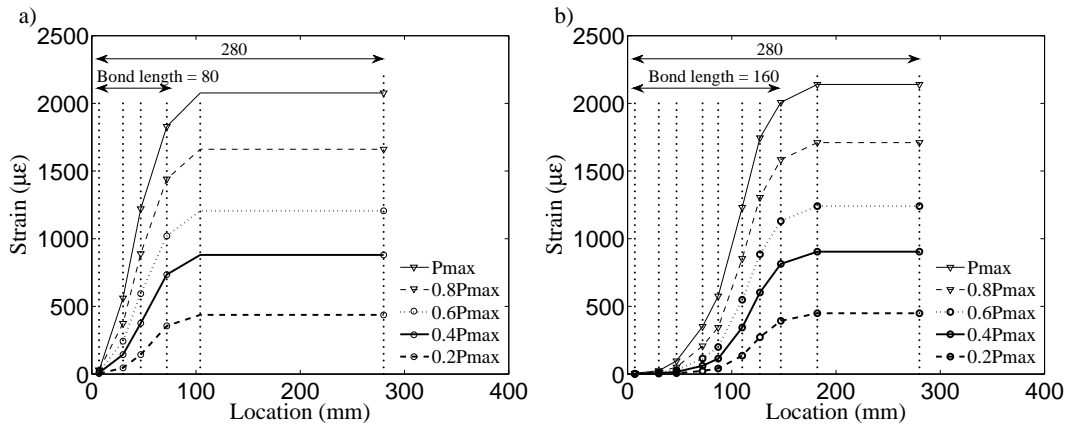
Figure 4.11: Experimental reinforcement strain distribution at different loads during instantaneous pull-out test for specimen with a) short bond length (C1SFi) and b) long bond length (C1LFi).

Reinforcement strain distribution at different times during long-term testing is shown in Table 4.9 and Figs. B.31 and B.33. As in previous figures, location 0 mm represents the unloaded end, vertical dashed lines represent the location of strain gauges and bond length is clearly marked.
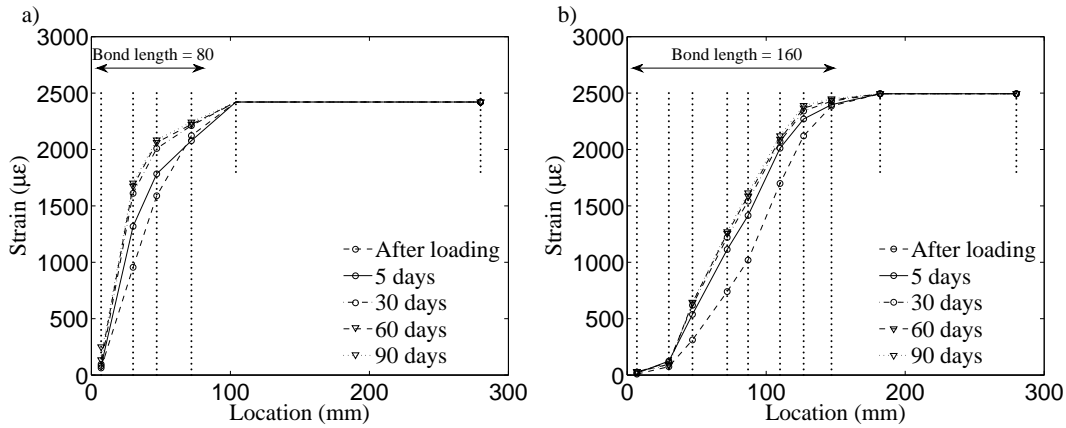
Figure 4.12: Experimental reinforcement strain distribution at different times during long-term testing for specimen a) C1SFi and b) C1LFi.
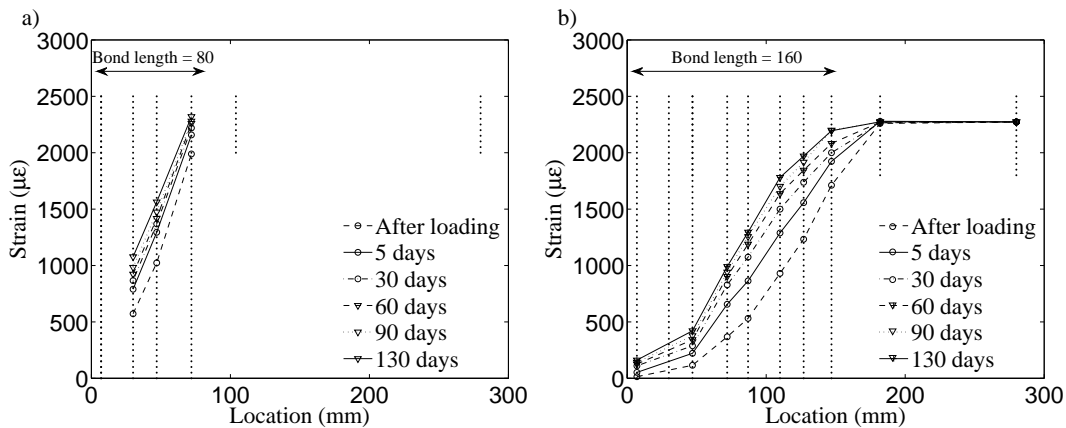
Figure 4.13: Experimental reinforcement strain distribution at different times during long-term testing for specimen a) C2SFi and b) C2LFi.

Irrespective of the length of the bond zone and the concrete grade, experimental results show that no significant increase in the readings of the strain gauges located in the unbonded zone is visible at the service load levels applied in the present work (see section 4.2.3). This means that no appreciable creep due to sustained loading occurred in the GFRP bar as expected. In the region within the bond length, the effect of sustained load is reflected in an increase in the strain gauge readings, with higher rates occurring at the intermediate zone between loaded and unloaded ends. This can be attributed to bond deterioration and redistribution of stresses, which is lower in more damaged zones (i.e. close to loaded end) and in zones with low levels of stress (i.e. unloaded end in specimens with larger bond length). This is indicated by the area between curves after loading and 90 days in Figs. B.31 and B.33. The stabilization of this redistribution occurs at approximately 30 days after loading in the case of the C1 series (see Fig. B.31). For the C2 series, the increase in strains slows down and stabilizes at the end of long-term testing (see Fig. B.33). In

situations in which creep could not be ignored, higher deformations and therefore larger redistributions and slips would be expected.

Reinforcement strains both at the beginning (ε_{inst}) and at 90 days (ε_{90}) of the sustained loading tests are greater for C1 series specimens, as might be expected. However, larger increments in strains due to long-term testing ($\Delta\varepsilon_{90}$) are found for C2 series specimens with long bond lengths (see Table 4.9). This is a sign of greater stress transfer, which is related to better bond behaviour attributable to a higher concrete grade.

Specimen	Strain gauge	Position (mm)	Instantaneous strain, $\varepsilon_{inst}(\mu\varepsilon)$	Strain at 60 days, $\varepsilon_{60}(\mu\varepsilon)$	Strain at 90 days, $\varepsilon_{90}(\mu\varepsilon)$	Strain at 130 days, $\varepsilon_{130}(\mu\varepsilon)$
C1SFi	G1	7	63	150	276	-
	G2	30	948	1680	1702	-
	G3	47	1582	2070	2084	-
	G4	72	2123	2250	2243	-
	G5	104	Failed			
	G6	280	2421	2422	2423	-
C1LFi	G1	7	8	30	31	-
	G2	30	73	90	87	-
	G3	47	307	660	645	-
	G4	72	731	1260	1270	-
	G5	87	1008	1590	1615	-
	G6	110	1688	2091	2121	-
	G7	127	2115	2370	2390	-
	G8	147	2385	2438	2449	-
	G9	182	2494	2496	2497	-
	G10	280	2493	2496	2495	-
C2SFi	G1	7	Failed			
	G2	30	567	930	983	1077
	G3	47	1013	1417	1474	1563
	G4	72	1981	2260	2280	2319
	G5	104	Failed			
	G6	280	Failed			
C2LFi	G1	7	14	126	142	161
	G2	30	Failed			
	G3	47	115	342	377	422
	G4	72	368	902	941	990
	G5	87	531	1189	1256	1319
	G6	110	930	1637	1702	1781
	G7	127	1233	1845	1916	2037
	G8	147	1711	2082	2239	2215
	G9	182	2269	2270	2272	2274
	G10	280	2272	2273	2273	2274

Table 4.9: Experimental instantaneous strain and time-dependent strain at different times during long-term testing.

Bond stress distribution

The experimental data shown in the previous section was used to analyse bond deterioration due to sustained loading. Taking the definition of bond as the force transferred between the reinforcing bar and the concrete per unit of surface area, and performing equilibrium calculations on a piece of bar of length dx, along with the assumption of linear elastic behaviour of the bar, leads to:

$$\tau = \frac{EA}{\Pi d_r} \frac{d\varepsilon_r(x)}{dx} \tag{4.2}$$

where τ is the bond stress, EA is the axial stiffness of the reinforcement and d_r is the nominal bar diameter.

Eq. (4.2) was applied to experimental reinforcement strains registered during long-term testing, and experimental bond stress distributions were obtained for internally strain-gauged specimens (i.e. specimens C1SFi, C1LFi, C2SFi and C2LFi). Information regarding bond stress distributions for specimens of series C1 and C2 at different stages of long-term testing is presented in Figs. B.35 and B.37 respectively, with location 0 mm representing the unloaded end as in previous figures. When Eq. (4.2) is applied between two consecutive strain gauges, dx = Δx, dε_r = $\Delta\varepsilon_r$, and discrete constant values of bond stresses are obtained. It should be noted that bond stress distributions for specimen C2SFi is only partially represented due to the failure of one of the strain gauges (Fig. B.37a).

Figure 4.14: Experimental bond stress distribution at different times during long-term testing for specimen a) C1SFi and b) C1LFi.

Comparison of the plots of bond stresses at the time of application of sustained loading and at 90 days reveals a general trend of redistribution of bond stresses due to long-term loading. Within this redistribution, different trends can be found if short and long bond specimens are compared.

For short bond length specimens, bond stresses decrease at the loaded end and increase near the unloaded end, which is due to an increase of bar-concrete interface damage in the loaded end zone. This is a sign of the whole bond length contributing to the bond phenomenon. As an example, bond stress decreases from 5.9 MPa to 1.7 MPa at the loaded end and increases from 10.8 MPa to 18.5 MPa at the unloaded end in

specimen C1SFi (see Fig. B.35a), meaning a decrease of 70% and an increase of 7% respectively. Similar trends can be observed for specimen C2SFi (see Fig. B.37a), with bond stress at the loaded end decreasing from 10.7 MPa to 8.9 MPa, a reduction of 16%. No percentage can be defined at the unloaded end due to the failure of one of the strain gauges.
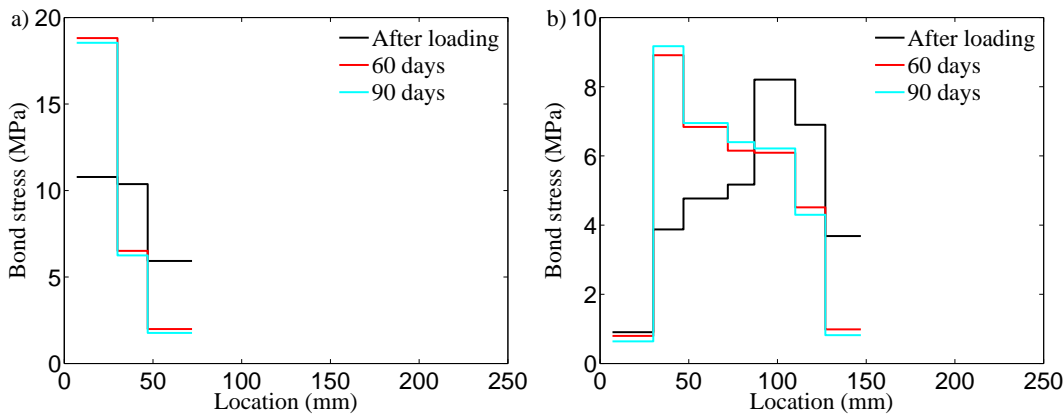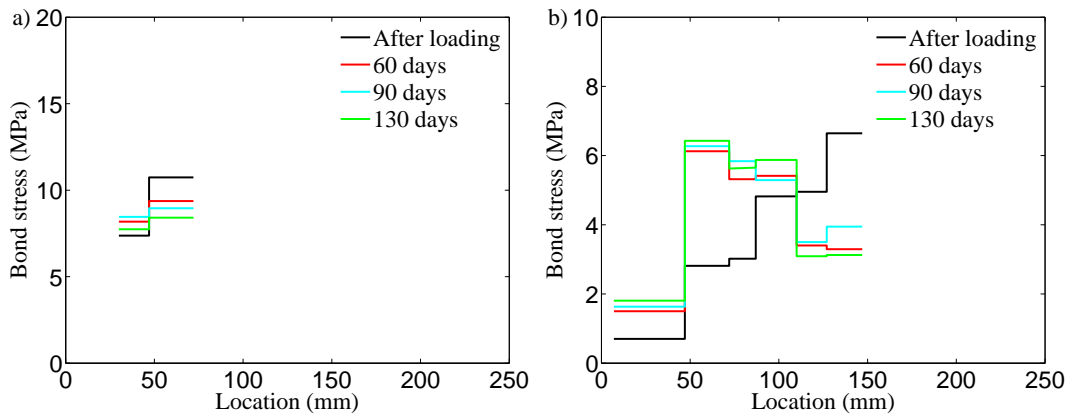

Figure 4.15: Experimental bond stress distribution at different times during long-term testing for specimens a) C2SFi and b) C2LFi.

In the case of long bond length specimens, a redistribution of bond stresses is also visible, with bond stresses decreasing at the loaded end, and larger bond stresses developing in neighbouring sections. As an example, bond stress at the loaded end decreases from 3.7 MPa to 0.8 MPa and from 6.6 MPa to 3.9 MPa in specimens C1LFi (see Fig. B.35b) and C2LFi (see Fig. B.37b) respectively, representing a reduction in bond stress of 78% and 41% respectively. However, such redistribution does not take place at the unloaded end of the specimens, indicating that the stress transfer process does not affect the entire length of the bond in the same way.

4.4 Conclusions

The results of an experimental programme to investigate the bond stress-slip behaviour of GFRP bars in concrete under sustained load have been presented and discussed. A total of 12 pull-out specimens with two concrete strengths (35 and 50 MPa), two bond lengths ($5d_r$ and $10d_r$) and two reinforcement materials (GFRP and steel) were tested. The specimens were initially subject to short-term loading, which was sustained for a period of between 90 and 130 days. A load corresponding to 15% of the ultimate capacity of the GFRP bar was selected so as to correspond to the service range. Based on the results of this study, the following conclusion can be drawn:

-Experimental results on immediate slip due to short-term loading confirm results from previous studies with larger slips for specimens with either lower concrete compressive strength or shorter bond length, attributable to larger local deformability and damage in the concrete surrounding the bar. At the same time

the tendency for GFRP pull-out specimens to bars to have larger slips than steel specimens is also confirmed, which may attributed to the deformability jointly with the mechanical interlock characteristics of the bars. Globally, the differences in slips between both ends indicate a non-uniform distribution of stresses along the bonded length, which is more pronounced for larger bond lengths.

-Data from the internal strain gauges during short-term testing shows that bond stresses are more evenly distributed in a short bond length where a quasi linear distribution of strains can be observed. This is not the case in a long bond length, where distribution is more clearly non-linear.

-As regards time-dependent slip due to sustained loading, results show an increase in the slip that stabilizes at approximately 60 days after loading, irrespective of the concrete strength, with higher increments for long bond length specimens. This can be attributed to bond deterioration and redistribution of stresses, which is more pronounced at the intermediate zone between loaded and unloaded ends. The experimental results confirm the influence of concrete strength on the deterioration of bond performance, with higher concrete compressive strength showing a time-dependent slip around 23.3% lower than that of lower concrete compressive strength.

-The evolution of bond stresses under sustained load was analyzed using data from internal strain gauges. The experimental results confirm the influence of concrete strength on the stress transfer process and the redistribution of stresses along the bond length, decreasing in neighboring loaded end zones due to an increase of bar-concrete interface damage. Specimens with the greatest concrete compressive strength showed a smaller loss of bond stresses at the loaded end, with values of 16% and 41% (for short and long bond length respectively) compared to 70% and 78% for the lowest concrete strength. In addition, irrespective of the concrete compressive strength, bigger variations of bond stresses were found in long bond length specimens, a sign of greater bond stress redistribution along the bond length.

Chapter 5

Conclusions and Future work

5.1 Summary

The present thesis focuses on the study of bond-slip and cracking behaviour between GFRP reinforcement and concrete under tensile loads. Firstly, a numerical methodology to implement the interface bond-slip law between concrete and reinforcement into a FE programme is presented. The interface law is obtained from experimental pull-out test through an inverse method. The proposed methodology is thereafter applied to simulate the short-term behaviour of GFRP RC tensile elements and the numerical results are compared with the experimental ones, in terms of load-deformation, tension stiffening, cracking process, and bond stresses and slip along the reinforcing bar. The thesis continues with an experimental campaign to analyse long-term effects on GFRP RC elements under tensile load. Data on load-deformation response and cracking behaviour is presented and discussed. Results are compared with analytical predictions using the Eurocode 2 provisions based on the EMM. Response shows changes in tension stiffening and concrete stresses as well as reduction in bond stresses between concrete and reinforcement along time. These results lead to an additional experimental campaign focused on the long-term effects on bond performance, where the influence of concrete strength, reinforcing material and bond length is investigated.

5.2 Concluding remarks

Numerical simulation of bond-slip interface and tension stiffening in GFRP RC tensile elements:

A methodology has been presented to easily implement into a standard FE program the local-numerical bond-slip laws to model the interaction between FRP reinforcement and concrete. The constitutive laws are derived from bond-slip response obtained from the widely used pull-out test procedure using an inverse method. The method is able to take into account the particular behaviour of each GFRP and concrete combination as well as to consider the possible confinement effect in the pull-out test curves. The procedure allows taking into account in an easy and reliable way bond-slip between FRP reinforcement and concrete

in the numerical modelling of GFRP RC structural members.

The most relevant conclusions from the numerical modelling of bond-slip interface between GFRP bars and concrete and its application to GFRP RC tensile members can be summarized as follows:

- A simple procedure for obtaining a local bond-slip constitutive law based on separating the bond-slip response of the experimental pull-out test into the two main components of friction and mechanical interaction has been successfully developed.

- With few iterations, the procedure reproduces well the experimental pull-out response that takes into consideration the different bond responses that may be obtained using FRP reinforcement.

- The methodology has been validated by comparing the load-deformation behaviour obtained from the numerical model with experimental data on GFRP RC tensile members available in the literature. The numerical simulation satisfactorily reproduces the response of the analysed GFRP RC elements proving the suitability of the presented procedure.

- Numerical simulation of the cracking process as well as predictions of crack width, crack spacing and number of cracks are in good agreement with experimental values, this being a sign of the suitability of the bond model.

Experimental study of tension stiffening in GFRP RC tensile members under sustained load:

An experimental programme was carried out with the objective of deepening the understanding on long-term behaviour of GFRP RC tensile members under sustained loading and the effects on stresses and strains, tension-stiffening and bond-slip along time. The programme comprised five GFRP RC elements and one additional steel RC element tested under sustained load for a period between 30 and 35 days. Three target concrete strengths (25, 35 and 50 MPa) were used. Creep and shrinkage of concrete were also considered in the programme.

The most relevant conclusions from the experimental programme on GFRP tensile members under sustained load presented in Chapter 3 can be summarized as follows:

- The evolution of stresses in concrete was analysed. A sharp decrease was observed at the first 10 hours of sustained loading and the reduction stabilized at 28 days.

- Tension stiffening reduced with time, observing an influence of concrete compressive strength. A reduction of concrete tensile stress was obtained as a result of sustained load, with reductions of 38% and 53% for the highest and lowest concrete strengths, respectively.

- As a result of long-term testing, reinforcement strain increased, this being a sign of bond deterioration. According to experimental data of this study, a reduction of 28% of bond between concrete and reinforcement took place.

- The Eurocode 2 equations based on the EMM to include long-term effects were able to reproduce experimental results with good accuracy.

Experimental study of bond-slip of GFRP in concrete under sustained loads:

An experimental programme comprising twelve pull-out specimens was conducted to evaluate bond under sustained load effects. Eight of the specimens were manufactured with GFRP bars whereas the remaining four were made using steel reinforcement for comparison purposes. The specimens were subjected to a sustained load in the serviceability range (15% of the ultimate capacity) for a period between 90 and 130 days. Two target concrete strengths (35 and 50 MPa) and two bond lengths (5 and 10 times the reinforcement diameter) were considered.

The most relevant conclusions from the bond-slip behaviour of the pull-out specimens under sustained load can be summarized as follows:

- The analysis of experimental results during the application of the load (short-term testing) confirms slip to be influenced by reinforcing material, concrete compressive strength and bond length. Larger slips were obtained for specimens with lower concrete compressive strength or shorter bond length.

- A non-uniform distribution of stresses along the bond length is confirmed by the differences in slips between the two ends of the specimens.

- The analysis of experimental data on reinforcement strains during the application of the load reveals bond length to influence the stress transfer process; a quasi linear distribution of strains was observed for short bond length, whilst non-linear distributions were obtained for long bond lengths.

- As regards time-dependent slip due to sustained loading, an increase in the slip that stabilizes at approximately 60 days was observed irrespective of the concrete strength.

- Time-dependent slip of higher concrete compressive strength specimens was approximately 23.3% lower than specimens with lower concrete compressive strength confirming an influence of concrete strength on the deterioration of bond.

- The evolution of bond stresses under sustained load was analysed using data from internal strain gauges. The experimental results confirm the influence of concrete strength on the stress transfer process and the redistribution of stresses along the bond length. Specimens with the highest concrete compressive strength showed a smaller loss of bond stresses of 16% and 41% at the loaded end for short and long bond length, respectively, whereas specimens with the lowest concrete compressive strength showed comparative values of 70% and 78%. Larger redistribution of bond stresses was observed for specimens with longer bond lengths.

5.3 Future work

Based on the results of this research the following points are proposed as future work:

- To carry out a parametric study of the influence of bond-slip behaviour, combined with concrete cover, reinforcement ratio and reinforcement stiffness on crack formation, crack spacing and crack width of tensile elements.

- To apply the presented methodology to implement bond-slip laws obtained in pull-out tests in numerical models to simulate RC flexural elements, with varying reinforcing materials and reinforcement ratios.

- To expand/adapt the methodology so that to include long-term effects in the numerical simulation.

- To design and conduct an experimental programme on pull-out tests and tensile members, where long-term effects are combined with varying environmental conditions (i.e. temperature and humidity).

- To study the effects of cyclic loading and fatigue on bond interaction between FRP bars and concrete.

Bibliography

[1] LC. Bank. *Composites for construction: Structural design with FRP materials.* 560. John Wiley & Sons, New Jersey, 2006.

[2] HVS. GangaRao, N. Taly, and PV. Vijay. *Reinforced concrete design with FRP composites.* London: Taylor & Francis Group, 2006.

[3] FIB Bulletin 40. *FRP Reinforcement in RC structures.* Task Group 9.3, International Federation for Structural Concrete, Lausanne, Switzerland., 2007.

[4] A. Nanni, A. De Luca, and HJ. Zadeh. *Reinforced Concrete with FRP Bars: Mechanics and Design.* CRC Press, 2014.

[5] LC. Hollaway. A review of the present and future utilisation of FRP composites in the civil infrastructure with reference to their important in-service properties. *Construction and Building Materials*, 24(12):2419–45, 2010.

[6] A. Serbescu, M. Guadagnini, and K. Pilakoutas. Mechanical characterization of basalt FRP rebars and long-term strength predictive model. *Journal of Composites for Construction*, 19(2):04014037, 2015.

[7] F. Elgabbas, EA. Ahmed, and B. Benmokrane. Physical and mechanical characteristics of new basalt-FRP bars for reinforcing concrete structures . *Construction and Building Materials*, 95:623–635, 2015.

[8] K. Pilakoutas, Z. Achillides, and P. Waldron. *Non-ferrous reinforcement in concrete structures.* In: Topping, E.M.L.&.B, editor. Centenary Conference on Innovation in Civil and Structural Engineering. Civil-Comp Ltd; p. 47-58, 1997.

[9] R. Tepfers. Bond clause proposal for FRP-bars/rods in concrete based on CEB/FIP Model Code 90. Part 1: Design bond stress for FRP reinforcing bars. *Structural concrete*, 7(2):47–55, 2006.

[10] Z. Achillides and K. Pilakoutas. Bond behaviour of fiber reinforced polymer bars under direct pull out conditions. *ASCE Journal of Composites for Construction*, 8(2):173–181, 2004.

[11] M. Baena, L. Torres, A. Turon, and Barris. Experimental study of bond behaviour between concrete and FRP bars using a pull-out test. *Composites Part B: Engineering*, 40(8):784–797, 2009.

[12] J. Larralde and R. Silva-Rodriguez. Bond and slip of FRP rebars in concrete. *ASCE Journal of Materials in Civil Engineering*, 5(1):30–40, 1993.

[13] B. Benmokrane, B. Tighiouart, and O. Chaallal. Bond strength and load distribution of composite GFRP reinforcing bars in concrete. *ACI Materials Journal*, 93(3):246–253, 1996.

[14] B. Tighiouart, B. Benmokrane, and D. Gao. Investigation of bond in concrete members with fiber reinforced polymer (FRP) bars. *Construction and Building Materials*, 12:453–462, 1998.

[15] JY. Lee, TY. Kim, TJ. Kim, CK. Yi, JS. Park, YC. You, and YH. Park. Interfacial bond strength of glass fiber reinforced polymer bars in high-strength concrete. *Composites Part B: Engineering*, 39: 258–270, 2008.

[16] C. Mazzotti and M. Savoia. Stress redistribution along the interface between concrete and FRP subjected to long-term loading. *Advances in Structural Engineering*, 12(5):651–661, 2009.

[17] FIB Bulletin 10. *Bond of Reinforcement in Concrete, State-of-the-Art Report*. FIP. Fédération International de la Précontraint. Lausanne, Switzerland. p. 34, 2000.

[18] E. Cosenza, G. Manfredi, and Realfonzo. Behavior and modeling of bond of FRP rebars to concrete. *ASCE Journal of Composites for Construction*, 1(2):40–51, 1997.

[19] M. Pecce, G. Manfredi, R. Realfanzo, and E. Cosenza. Experimental and analytical evaluation of bond properties of GFRP bars. *Journal of Materials in Civil Engineering*, 13(4):282–290, 2001.

[20] H. Mazaheripour, J. Barros, J. Sen-Cruz, M. Pepe, and E. Martinelli. Experimental study on bond performance of GFRP bars in self-compacting steel fiber reinforced concrete. *Composite Structures*, 95:202–212, 2013.

[21] HM. Gomes and AM. Awruch. Some aspects on three-dimensional numerical modelling of reinforced concrete structures using the finite element method. *Advances in Engineering Software*, 32(4):257–277, 2001.

[22] S. Khalfallah. Modeling of bond for pull-out test. *Building research journal*, 56(1):37–48, 2008.

[23] AR. Khaloo, I. Eshghi, and P. Piran Aghl. Study of behaviour of reinforced concrete beams with smart rebars using finite element modelling. *International Journal of Civil Engineering*, 8(3):221–231, 2010.

[24] HR. Valipour and SJ. Foster. Finite element modelling of reinforced concrete framed structures including catenary action. *Computers & Structures*, 88(9-10):529–538, 2010.

[25] S. Alih and A. Khelil. Behavior of inoxydable steel and their performance as reinforcement bars in concrete beam: Experimental and nonlinear finite element analysis. *Construction and Building Materials*, 37:481–492, 2012.

[26] M. Guerra, F. Ceia, J. de Brito, and E. Júlio. Anchorage of steel rebars to recycled aggregates concrete. *Construction and Building Materials*, 74:113–123, 2014.

[27] C. Oliver-Leblond, A. Delaplace, and F. Ragueneau. Modelling of three-dimensional crack patterns in deep reinforced concrete structures. *Engineering Structures*, 83:176–186, 2015.

[28] B. Benmokrane, O. Chaallal, and R. Masmoudi. Flexural response of concrete beams reinforced with FRP reinforcing bars. *ACI Structures Journal*, 91(2):46–55, 1996.

[29] S. Matthys and L. Taerwe. Concrete slabs reinforced with FRP grids. I: One-way bending. *Journal of Composites for Construction*, 4(3):145–152, 2000.

[30] M. Pecce, G. Manfredi, and E. Cosenza. Experimental response and code models of GFRP RC beams in bending. *ASCE Journal of Composites for Construction*, 4(4):182–190, 2000.

[31] R. Al-Sunna, K. Pilakoutas, I. Hajirasouliha, and M. Guadagnini. Deflection behaviour of FRP reinforced concrete beams and slabs: an experimental investigation. *Composites Part B: Engineering*, 43(5):2125–34, 2012.

[32] PH. Bischoff. Deflection calculation of FRP reinforced concrete beams based on modifications to the existing Branson equation. *ASCE Journal of Composites for Construction*, 11(1):4–14, 2007.

[33] R. Muhamad, A. MS Mohamed, D. Oehlers, and A. Hamid Sheikh. Load-slip relationship of tension reinforcement in reinforced concrete membres. *Engineering Structures*, 33(4):1098–1106, 2011.

[34] C. Barris, L. Torres, M. Baena, K. Pilakoutas, and M. Giadagnini. Serviceability limit state of FRP RC beams. *Advances in Structural Engineering*, 15:653–663, 2012.

[35] C. Barris, L. Torres, C. Miàs, and I. Vilanova. Design of FRP reinforced concrete beams for serviceability requirements. *Journal of Civil Engineering and Management*, 18(6):843–857, 2012.

[36] V. Gribniak, G. Kaklauskas, L. Torres, A. Daniunas, E. Timinskas, and E. Gudonis. Comparative analysis of deformations and tension-stiffening in concrete beams reinforced with GFRP or steel bars and fibers. *Composites Part B: Engineering*, 50:158–170, 2013.

[37] AM. Aiello and M. Leone. Bond performances of FRP rebars-reinforced concrete. *ASCE Journal of Materials in Civil Engineering*, 19(3):205–213, 2007.

[38] M. Baena, L. Torres, A. Turon, and C. Miàs. Experimental study and code predictions of fibre reinforced polymer reinforced concrete (FRP RC) tensile members. *Composite Structures*, 93:2511–2520, 2011.

[39] PH. Bischoff. Effects of shrinkage on tension stiffening and cracking in reinforced concrete. *Canadian Journal of Civil Engineering*, 28(3):363–374, 2001.

[40] AW. Beeby and RH. Scott. *Tension stiffening of concrete: Behaviour of tension zones in reinforced concrete including time dependent effects.* The Concrete Society, Camberley, UK, 2002.

[41] RH. Scott and AW. Beeby. Long-term tension-stiffening effects in concrete. *ACI Structural Journal*, 102(6):904–905, 2005.

[42] RH. Scott and AW. Beeby. Mechanisms of long-term decay of tension stiffening. *Magazine of Concrete Research*, 58(5):255–266, 2006.

[43] G. Nkurunziza, B. Benmokrane, AS. Debaiky, and R. Masmoudi. Effect of sustained load and environment on long-term tensile properties of glass fiber-reinforced polymer reinforcing bars. *ACI Structural Journal*, 102(4):615–621, 2005.

[44] R. Gilbert. *Time effects in concrete structures*. Amsterdam: Elsevier., 1988.

[45] A. Ghali and R. Favre. *Concrete Structures: Stresses and Deformations*. 2nd edn. E & FN Spon, London, 1994.

[46] O. Faber. Plastic yield, shrinkage, and other problems of concrete, and their effect on design. *Minutes of proceedings of the Institution of Civil Engineers*, 225, Part I, London:27–73, 1927.

[47] CEN. *Eurocode 2 Design of concrete structures- part 1: general rules and rules for buildings*. ENV 1992-1-1 Brussels, 1992.

[48] CEB-FIB. *CEB-FIB Model code for Concrete Structures 2010*. p. 120 Ernst & Sohn, Lausanne, 2010.

[49] H. Trost. Auswirkungen des superpositionsprinzips auf kriech-und relaxations-probleme bei beton und spannbeton. *Beton-und Stahlbetonbau*, 62(10):230–238, 1967.

[50] ZP. Bazant. Prediction of concrete creep effects using Age-Adjusted Effective Modulus Method. *Journal of the American Concrete Institute*, 69:212–217, 1972.

[51] CEB-FIB. *Manual Structural Effects on Time-dependent Behaviour of Concrete (142)*. 1984.

[52] F. Shahidi. *Bond degradation between FRP bars and concrete under sustained loads*. PhD Thesis. University of Saskatchewan, Saskatoon, Canada, 2003.

[53] A. Juette, A. Weber, and C. Witt. *Long-term bond behaviour of GFRP rebars in severe environments Quebec City, Canada*. p.10. July 2011.

[54] V. Carvelli, MA. Pisani, and C. Poggi. High temperature effects on concrete members reinforced with gfrp rebars. *Composites Part B: Engineering*, 54:125–132, 2013.

[55] I. Vilanova, M. Baena, L. Torres, and C. Barris. Experimental study of bond-slip of GFRP bars in concrete under sustained loads. *Composites Part B: Engineering*, 74:45–52, 2015.

[56] LJ. Malvar. Bond stress-slip characteristics of FRP rebars. Technical report, TR2013-SHR Naval Facilities Engineering Service Center, Port Huneme, California, 1994.

[57] E. Cosenza, G. Manfredi, and R. Realfonzo. *Analytical modelling of bond between FRP reinforcing bars and concrete*. p. 164-171. In: Taerwe L, editor. Proceedings of second international RILEM symposium (FRPRCS-2). London: E and FN Spon, 1995.

[58] VA. Rossetti, D. Galeota, and MM. Giammatteo. Local bond stress-slip relationships of glass fibre reinforced plastic bars embedded in concrete. *Materials and Structures*, 28(6):340–344, 1995.

[59] E. Cosenza, G. Manfredi, and R. Realfonzo. Development length of FRP straight rebars. *Composites Part B: Engineering*, 33:493–504, 2002.

[60] Z. Achillides and P. Pilakoutas. FE modelling of bond interaction of FRP bars to concrete. *Structural Concrete*, 7(1):7–16, 2006.

[61] HQ. Wu and RI. Gilbert. Modelling short-term tension stiffening in reinforced concrete prisms using a continuum-based finite element model. *Engineering Structures*, 31:2380–2391, 2009.

[62] C. Zanuy, M. Curbach, and A. Lindorf. Finite element study of bond strength between concrete and reinforcement under uneven confinement condition. Technical paper. *Structural Concrete*, 14: 260–270, 2013.

[63] A. Ziari and R. Kianoush. Finite-element parametric study of bond and splitting stresses in reinforced concrete tie members. *ASCE Journal of Structural Engineering*, p. 140, 2014.

[64] CEB-FIB. *Model Code 1990*. Comité Euro-International du Béton. Fédération Internationale de la Précontrainte, Thomas Telford House, London, England, 1990.

[65] ACI comitte 440. *ACI 440.3R-12 Guide test methods for fiber-reinforced polymers (FRP) composites for reinforcing or strengthening concrete and masonry structures*. ACI Committee 440, American Concrete Institute, 2012.

[66] J. Fink, TH. Petraschek, and L. Ondris. *Push-out test parametric simulation study of a new sheet-type shear connector*. p. 131-153. in: Projekte an den zentralen Applikationsservern, Berichte, 2006, Zentraler Informatikdienst (ZID) der Technischen Universität Wien, Wien, 2007.

[67] P. Kmiecik and M. Kaminski. Modeling of reinforced concrete structures and composite structures with concrete strength degradation taken into consideration. *Archives of Civil and Mechanical Engineering*, 3,(Wroclaw University of Technology, Poland), 2011.

[68] M. Rezazadech, I. Costa, and J. Barros. Influence of prestress level on NSM CFRP laminates for the flexural strengthening of RC beams. *Composite Structures*, 116:489–500, 2014.

[69] R. Jakubovskis, G. Kaklauskas, V. Gribniak, A. Weber, and M. Juknys. Serviceability analysis of concrete beams with different arrangements of GFRP bars in the tensile zone. *ASCE Journal of Composites for Construction*, 18(5):04014005, 2014.

[70] I. Vilanova, L. Torres, M. Baena, G. Kaklauskas, and V. Gribniak. Experimental study of GFRP RC tensile members under sustained load. *Engineering Structures*, 79:390–400, 2014.

[71] A. Nanni. *Fiber reinforced plastic (FRP) reinforcement for concrete structures: properties and applications*. Amsterdam: Elsevier, 1993.

[72] ACI 440.1R-06. *Guide for the Design and Construction of Concrete Reinforced with FRP Bars*. Formington Hills: American Concrete Institute, 2006.

[73] CSA (2012). *Design and Construction of Building Structures with Fibre-Reinforced Polymers (CAN/CSA-S806-012)*. Canadian Standards Association, Mississauga, Ontario, Canada, 2012.

[74] CNR (2007). *Guide for the Design and Construction of Concrete Structures Reinforced with Fiber-Reinforced Polymer Bars CNR-DT (203/2006)*. National Research Council, Rome, Italy, 2007.

[75] M. Robert and B. Benmokrane. Combined effects of saline solution and moist concrete on long-term durability of GFRP reinforcing bars. *Construction and Building Materials*, 38:274–284, 2013.

[76] R. Masmoudi, A. Masmoudi, MB. Ouezdou, and A. Daoud. Long-term bond performance of GFRP bars in concrete under temperature ranging from $20°$C to $80°$C. *Construction and Building Materials*, 25(2):486–493, 2011.

[77] M. Robert and B. Benmokrane. Effect of aging on bond of GFRP bars embedded in concrete. *Cement and Concrete Composites*, 32(6):461–467, 2010.

[78] T. Hall and A. Ghali. Long-term deflection prediction of concrete members reinforced with glass fibre reinforced polymer bars. *Canadian Journal of Civil Engineering*, 27(5):890–898, 2000.

[79] M. Arockiasamy, S. Chidambaram, A. Amer, and M. Shahawy. Time-dependent deformations of concrete beams reinforced with CFRP bars. *Composites Part B: Engineering*, 31(6-7):577–592, 2000.

[80] YA. Al-Salloum and TH. Almusallam. Creep effect on the behavior of concrete beams reinforced with GFRP bars subjected to different environments. *Construction and Building Materials*, 21(7): 1510–1519, 2007.

[81] C. Miàs, L. Torres, A. Turon, M. Baena, and C. Barris. A simplified method to obtain time-dependent curvatures and deflections of concrete members reinforced with FRP bars. *Composite Structures*, 92: 1833–1838, 2010.

[82] L. Torres, C. Miàs, A. Turon, and M. Baena. A rational method to predict long-term deflections of FRP reinforced concrete members. *Engineering Structures*, 40:230–239, 2012.

[83] C. Miàs, L. Torres, A. Turon, and IA. Sharaky. Effect of material properties on long-term deflections of GFRP reinforced concrete beams. *Construction and Building Materials*, 41:99–108, 2013.

[84] AR. Marí. Numerical simulation of the segmental construction of three dimensional concrete frames. *Engineering Structures*, 22:585–596, 2000.

[85] L. Torres, F. López-Almansa, X. Cahís, and Bozzo. A numerical model for sequential construction, repairing and strengthening of 2-D concrete frames. *Engineering Structures*, 25(3):323–336, 2003.

[86] G. Kaklauskas, V. Gribniak, D. Bacinskas, and Vainiunas. Shrinkage influence on tension stiffening in concrete members. *Engineering Structures*, 31(6):1305–1312, 2009.

[87] P. Visintin, DJ. Oehlers, and M. Haskett. Partial-interaction time dependent behaviour of reinforced concrete beams. *Engineering Structures*, 49:408–420, 2013.

[88] V. Gribniak, D. Bacinskas, R. Kacianauskas, G. Kaklauskas, and L. Torres. Long-term deflections of reinforced concrete elements: accuracy analysis of predictions by different methods. *Mechanics of Time-Dependent Materials*, 17(3):297–313, 2013.

[89] HQ. Wu and RI. Gilbert. *An experimental study of tension stiffening in reinforced concrete members under short-term and long-term loads*. Technical report. The University of New South Wales, 2008.

[90] C. Zanuy. Analytical approach to factors affecting long-term tension stiffening. *Magazine of Concrete Research*, 62:869–878, 2010.

[91] ASTM. *Standard Test Method for Creep of Concrete in Compression*. 04.02, 2008.

[92] AM. Neville. *Properties of concrete. 4th ed*. Harlow, England: Longman Group Limited, 1995.

[93] SH. Alsayed, YA. Al-Salloum, and TH. Almusallam. Performance of glass fiber reinforced plastic bars as a reinforcing material for concrete structures. *Composites Part B: Engineering*, 31(6-7):555–567, 2000.

[94] C. Barris, L. Torres, A. Turon, M. Baena, and A. Catalan. An experimental study of the flexural behaviour of GFRP RC beams and comparison with prediction models. *Composite Structures*, 91(3): 2125–2134, 2009.

[95] IF. Kara, AF. Ashour, and C. Dundar. Deflection of concrete structures reinforced with FRP bars. *Composites Part B: Engineering*, 44(1):375–84, 2013.

[96] M. Pepe, H. Mazaheripour, J. Barros, J. Sena-Cruz, and E. Martinelli. Numerical calibration of bond law for GFRP bars embedded in steel fibre-reinforced self-compacting concrete. *Composites Part B: Engineering*, 50:403–412, 2013.

[97] C. Miàs, L. Torres, A. Turon, and C. Barris. Experimental study of immediate and time dependent deflections of GFRP reinforced concrete beams. *Composite Structures*, 96:279–285, 2013.

[98] HJ. Zadeh and A. Nanni. Reliability analysis of concrete beams internally reinforced with fiber-reinforced polymer bars. *ACI Structural Journal*, 110(6):1023–1031, 2013.

[99] M. Hassan, EA. Ahmed, and B. Benmokrane. Punching-shear design equation for two-way concrete slabs reinforced with FRP bars and stirrups. *Construction and Building Materials*, 66:522–532, 2014.

[100] L. Ascione, VP. Berardi, and A. Dapont. Creep phenomena in FRP materials. *Mechanics Research Communications*, 43:15–21, 2012.

[101] UNE-EN 12390-3:2003. *Testing hardened concrete - Part 3: compressive strength of test specimens*. AENOR, 2003.

[102] UNE-EN ISO 15630-1:2011. *Steel for the reinforcement and prestressing of concrete - test methods - Part 1: reinforcing bars, wire rod and wire*. AENOR, 2011.

[103] ACI 440.1R-03-12. *Guide test methods for fiber-reinforced polymer (FRPs) composites for reinforcing or strengthening concrete structures*. American Concrete Institute, 2012.

[104] M. Baena, L. Torres, A. Turon, and C. Miàs. Analysis of cracking behaviour and tension stiffening in FRP reinforced concrete tensile elements. *Composites Part B: Engineering*, 45:1360–1367, 2013.

Appendixes

Appendix A

Experimental details of long-term tests on GFRP RC ties
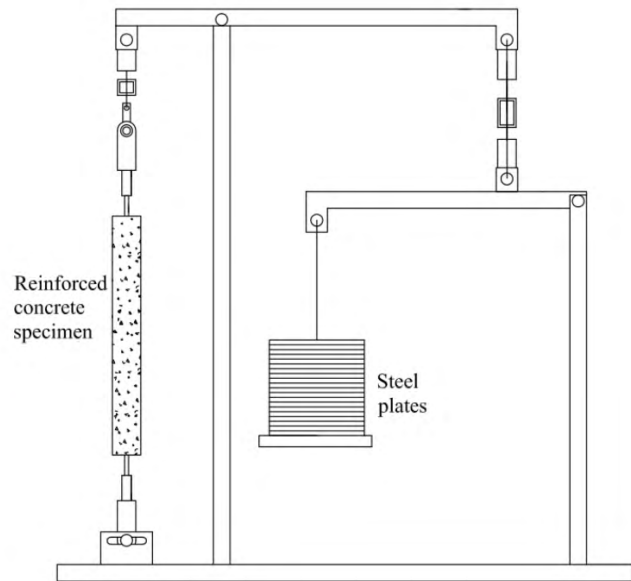
A.1 Test set-up

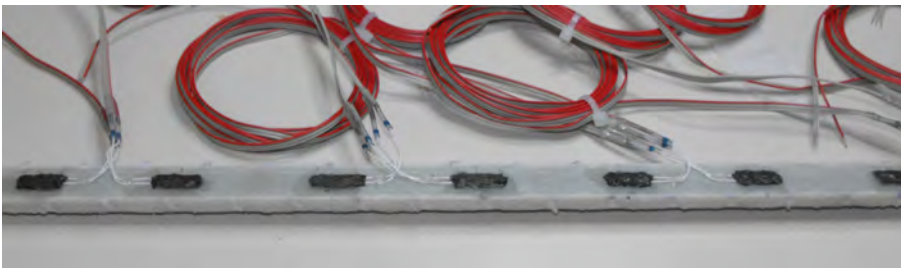Figure A.1: Frames for long-term tensile tests.

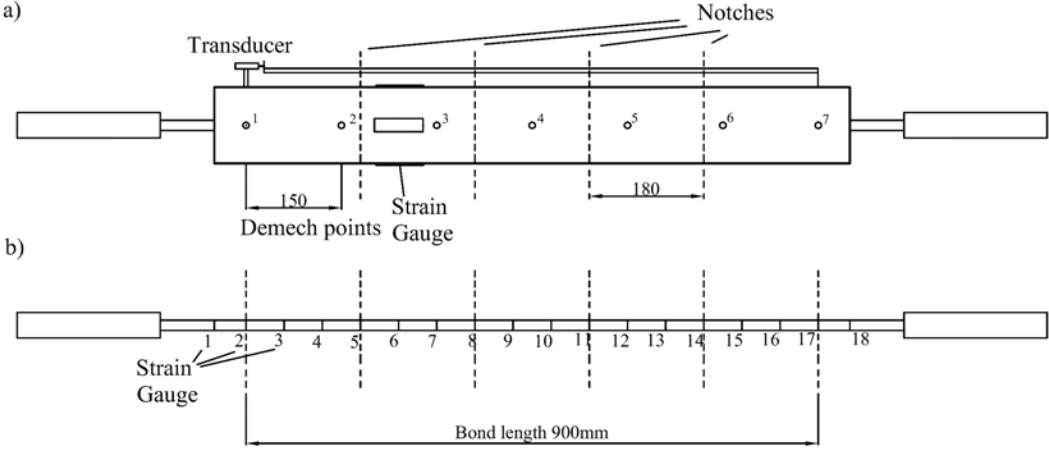Figure A.2: GFRP bar internal instrumentation (Specimens C1F16ni and C2F16ni).

Figure A.3: (a) External instrumentation of the concrete specimens. (b) Internal instrumentation of the GFRP reinforcing bar.
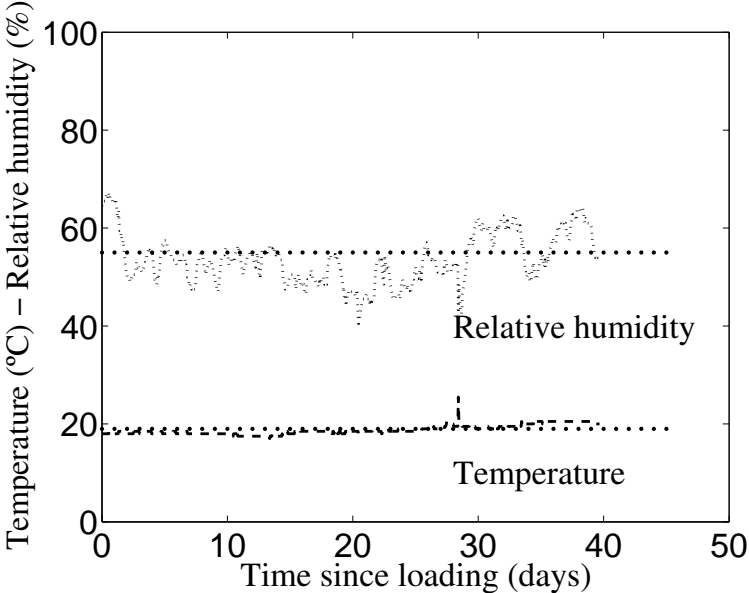
A.2 Creep and shrinkage

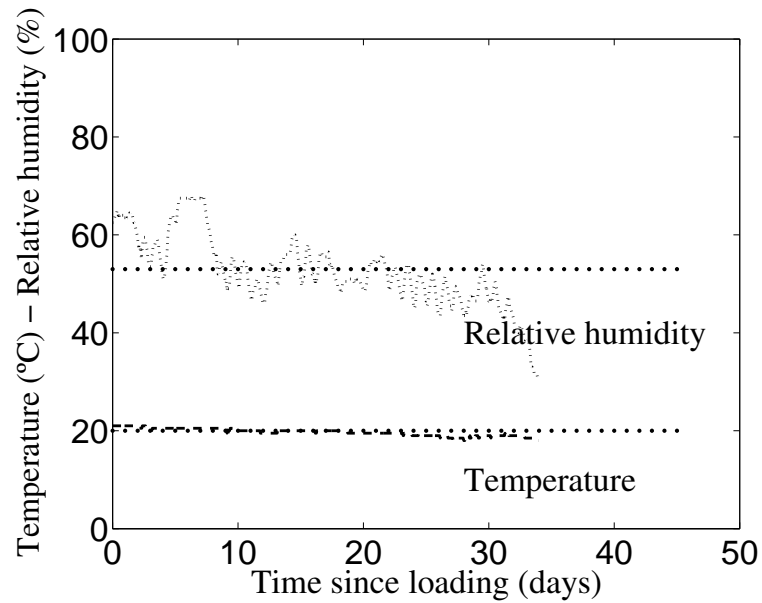Figure A.4: Temperature and relative humidity registered in the laboratory during C1 tests.

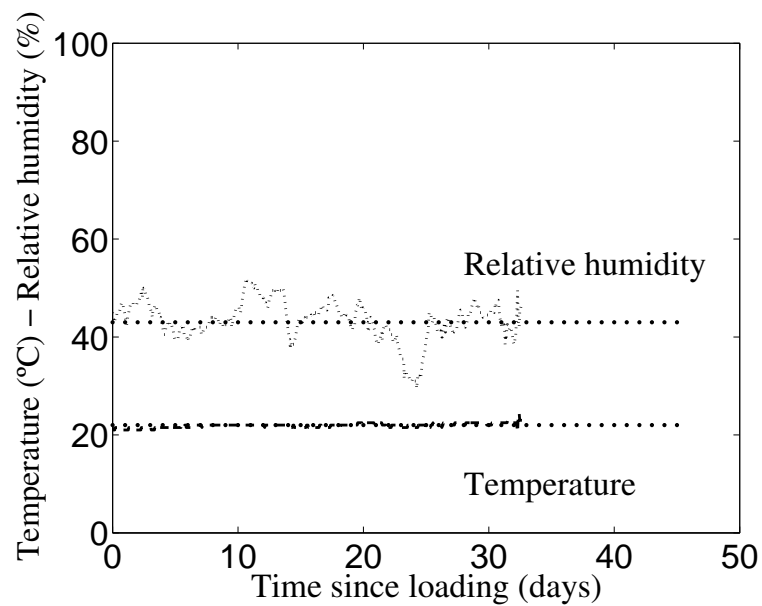Figure A.5: Temperature and relative humidity registered in the laboratory during C2 tests.

Figure A.6: Temperature and relative humidity registered in the laboratory during C3 tests.
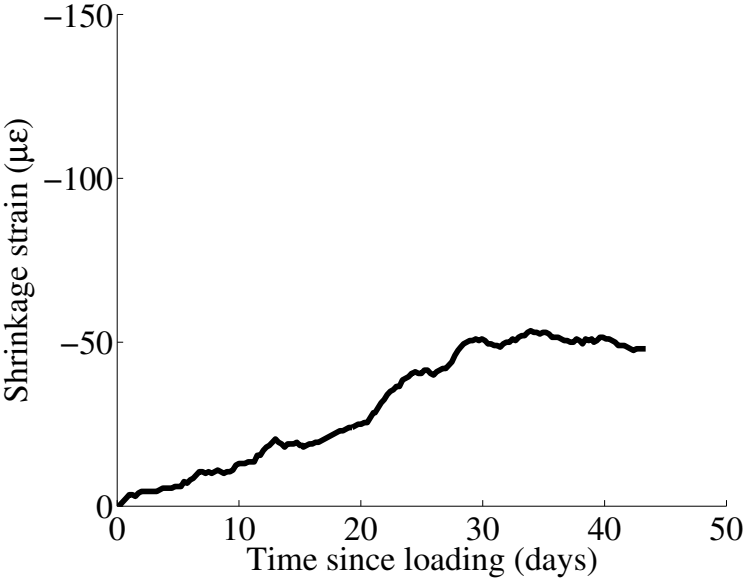
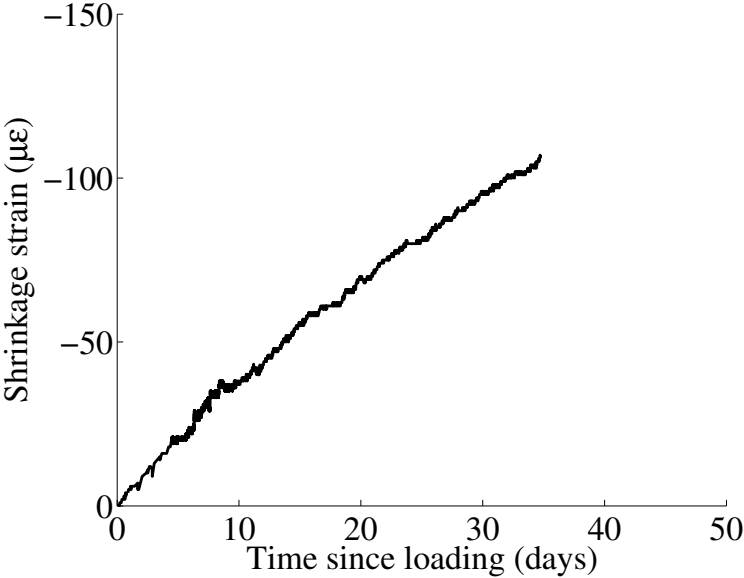Figure A.7: Experimental free shrinkage strain during C1 tests.

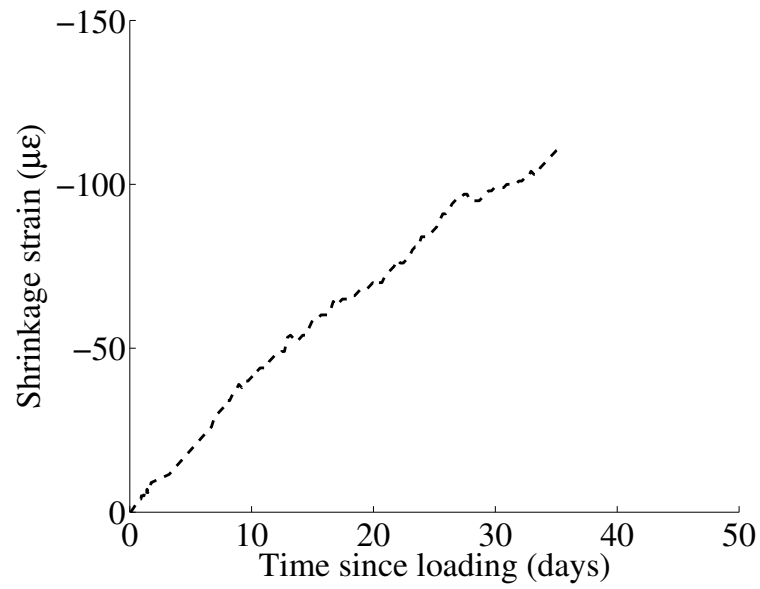Figure A.8: Experimental free shrinkage strain during C2 tests.

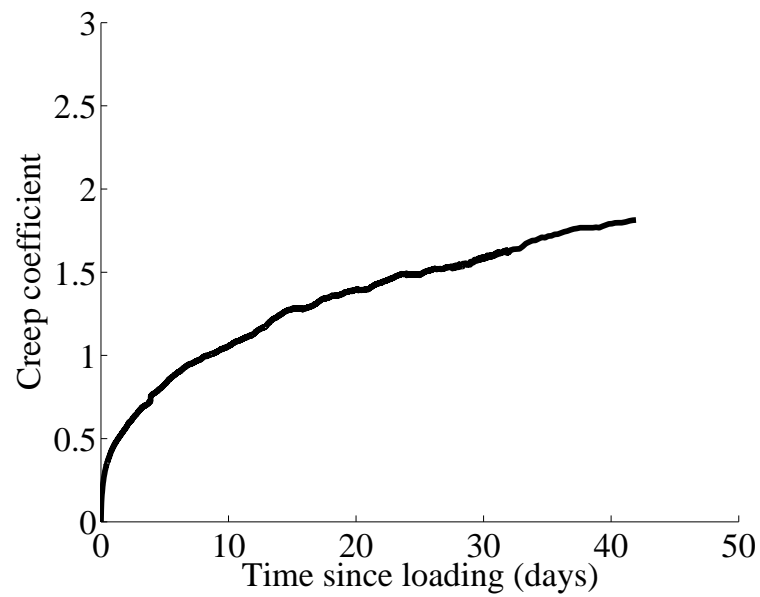Figure A.9: Experimental free shrinkage strain during C3 tests.

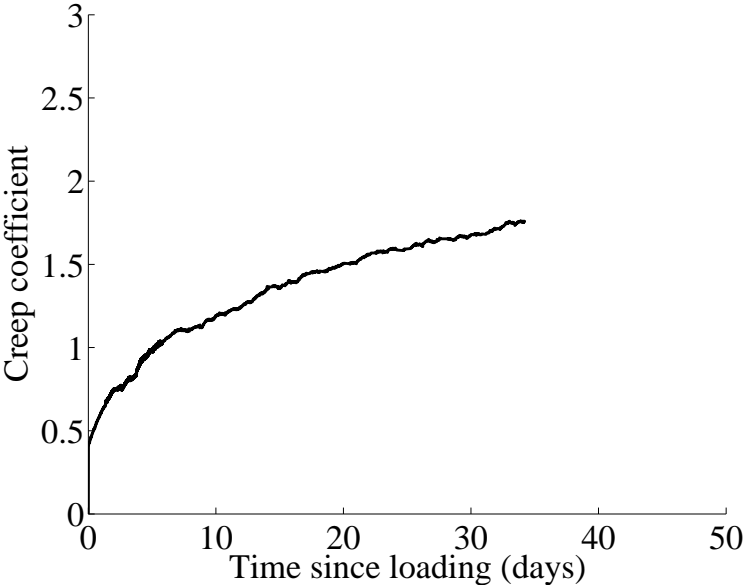Figure A.10: Experimental creep coefficient during C1 tests.

Figure A.11: Experimental creep coefficient during C2 tests.

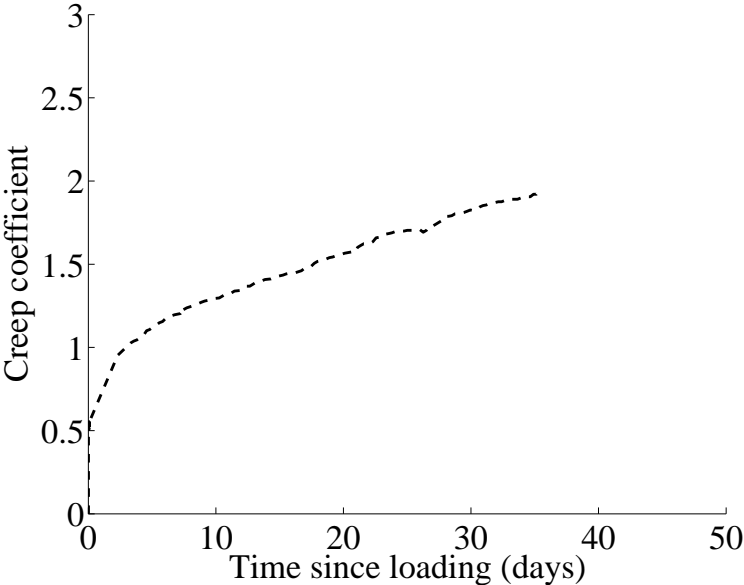Figure A.12: Experimental creep coefficient during C3 tests.

A.3   Results

A.3.1   Tensile behaviour

Figure A.13: Experimental load-mean strain curves of specimens C1F16ni.
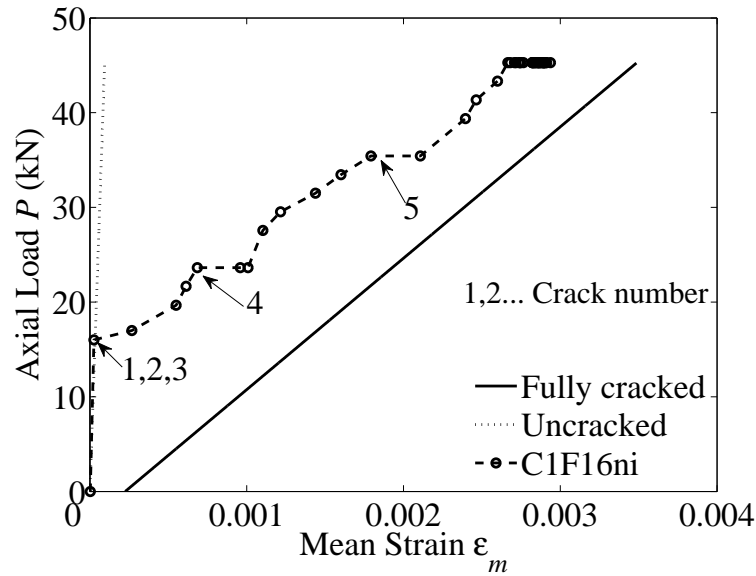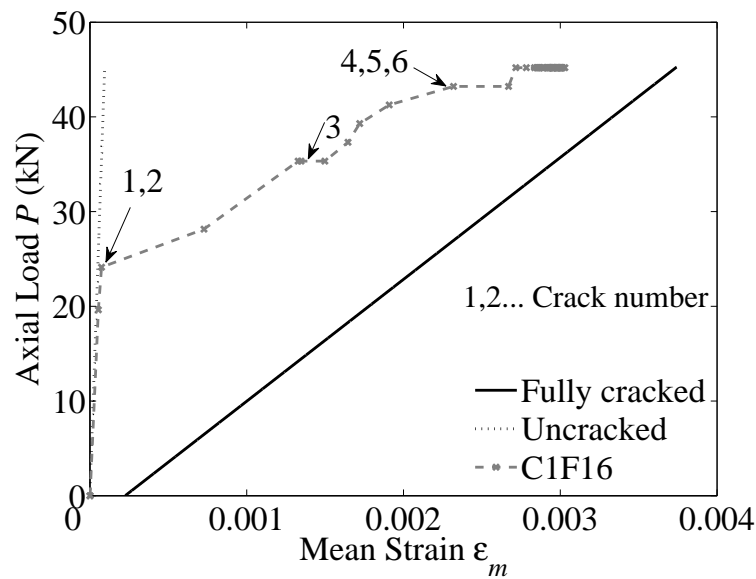

Figure A.14: Experimental load-mean strain curves of specimens C1F16.
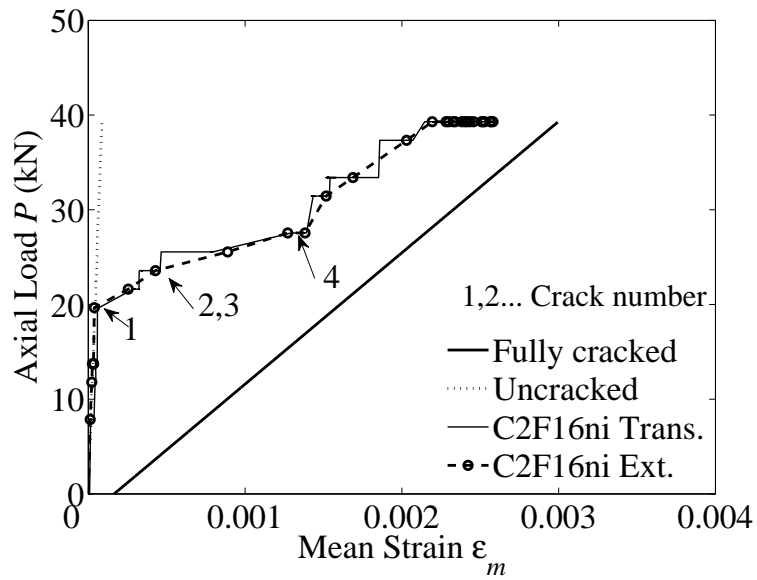
Figure A.15: Experimental load-mean strain curves of specimens C2F16ni.
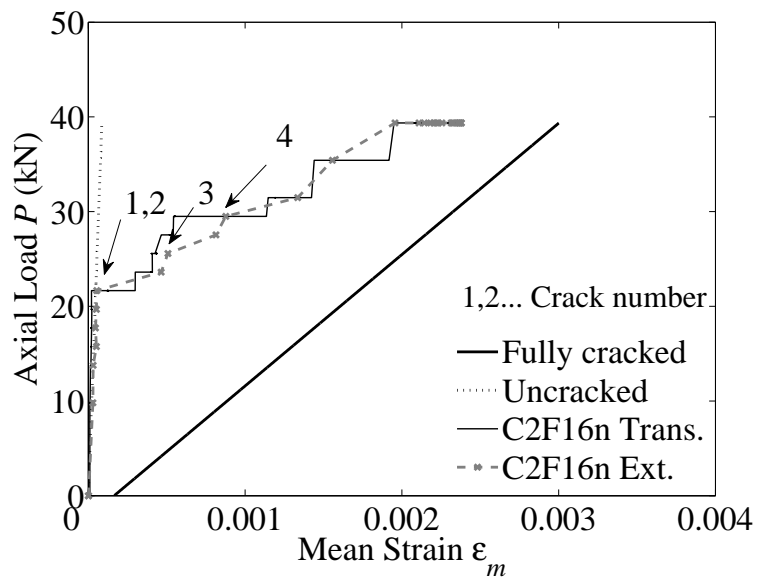
Figure A.16: Experimental load-mean strain curves of specimens C2F16n.
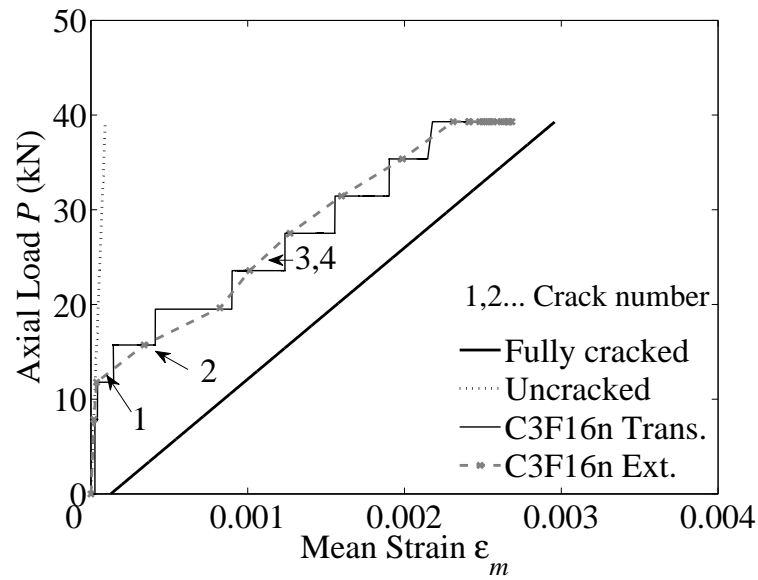
Figure A.17: Experimental load-mean strain curves of specimens C3F16n.
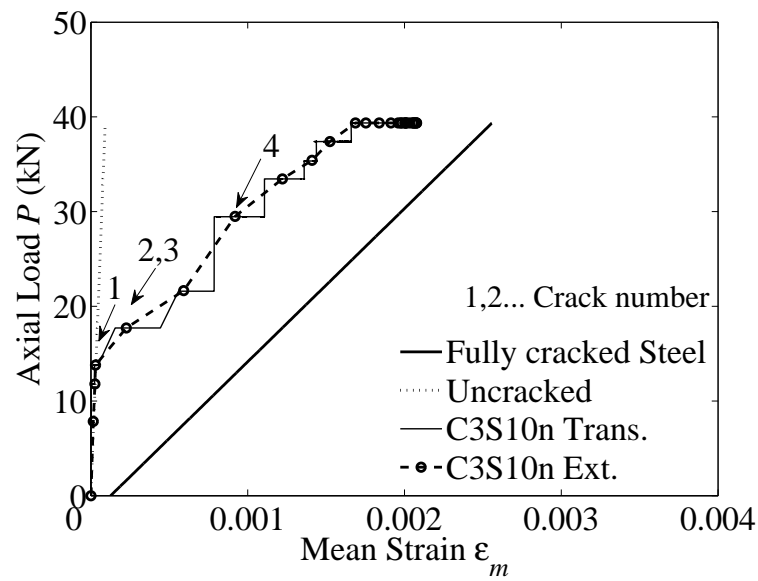
Figure A.18: Experimental load-mean strain curves of specimens C3S10n.

A.3.2 Concrete tensile stress
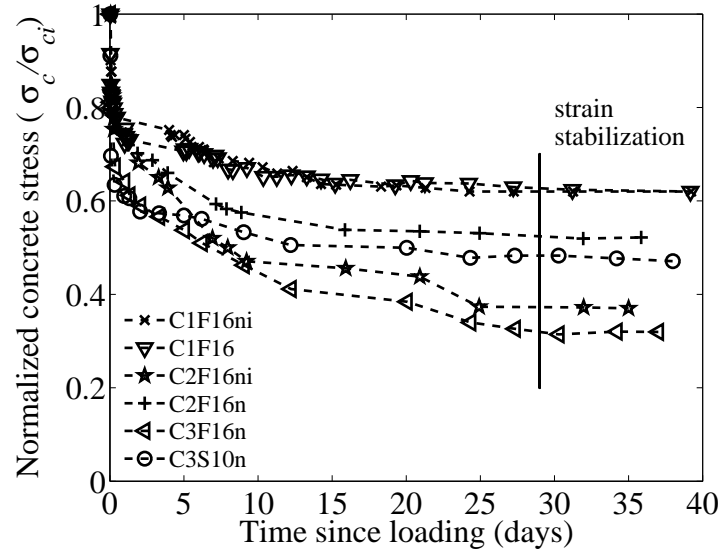
Figure A.19: Evolution of concrete stress over time.

A.3.3 Reinforcement strain and bond stress distributions
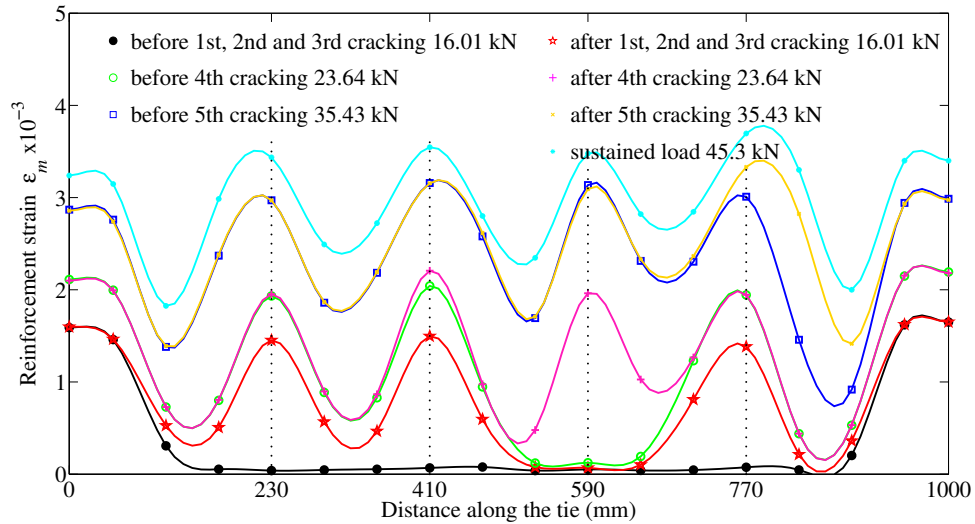
Figure A.20: Experimental reinforcement strain distribution during crack formation in the loading process for specimen C1F16ni.
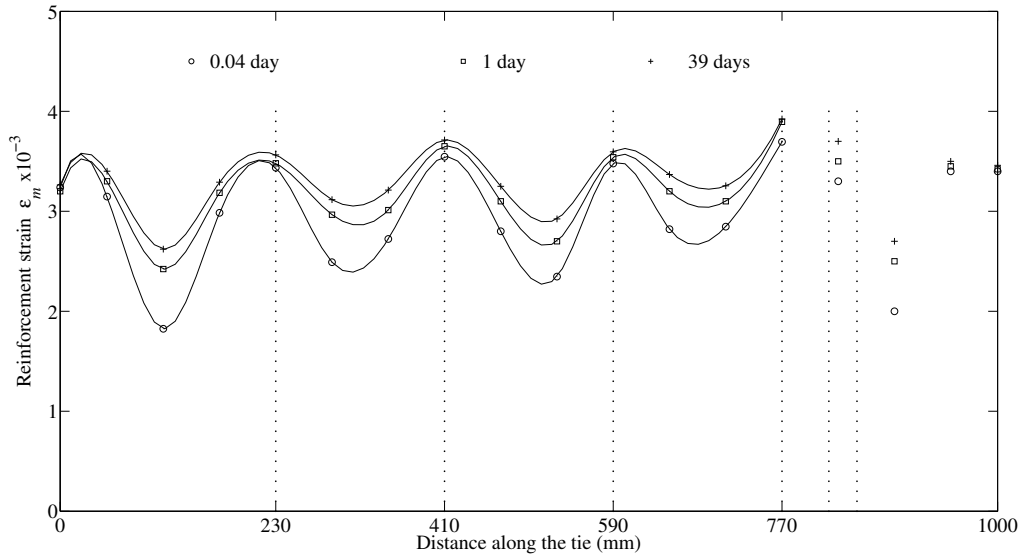
Figure A.21: Experimental reinforcement strain distribution at different times during long-term testing for specimen C1F16ni. (At the right end additional crack is represented).
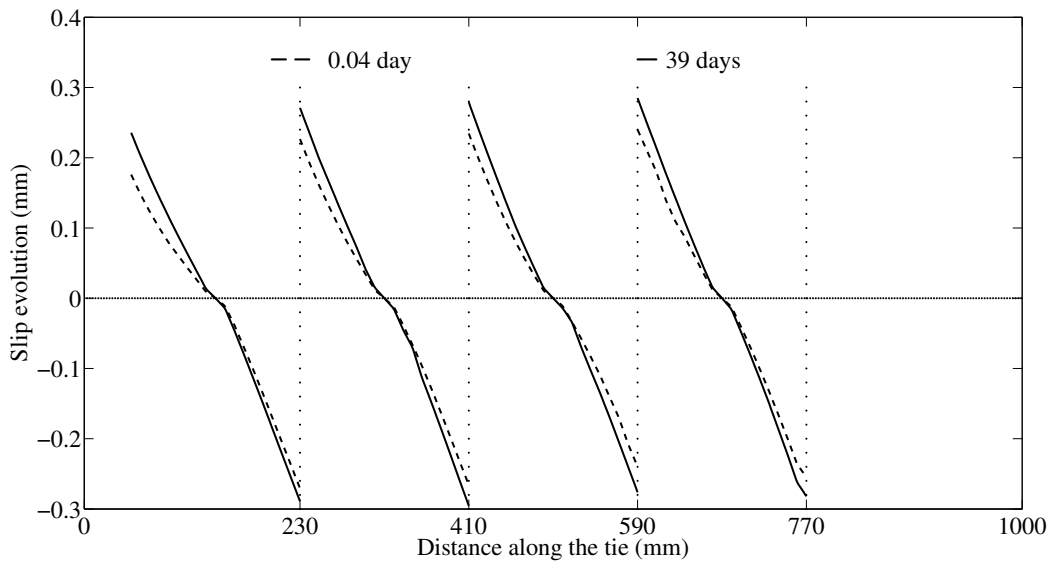
Figure A.22: Experimental slip distribution for specimen C1F16ni at different times during long-term testing.
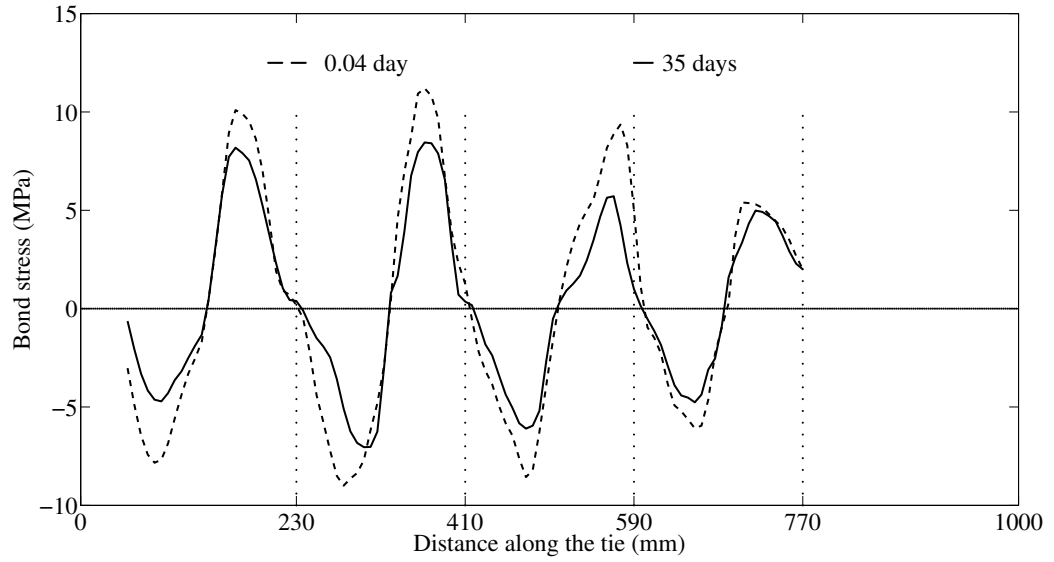
Figure A.23: Experimental bond distribution for specimen C1F16ni at different times during long-term testing.
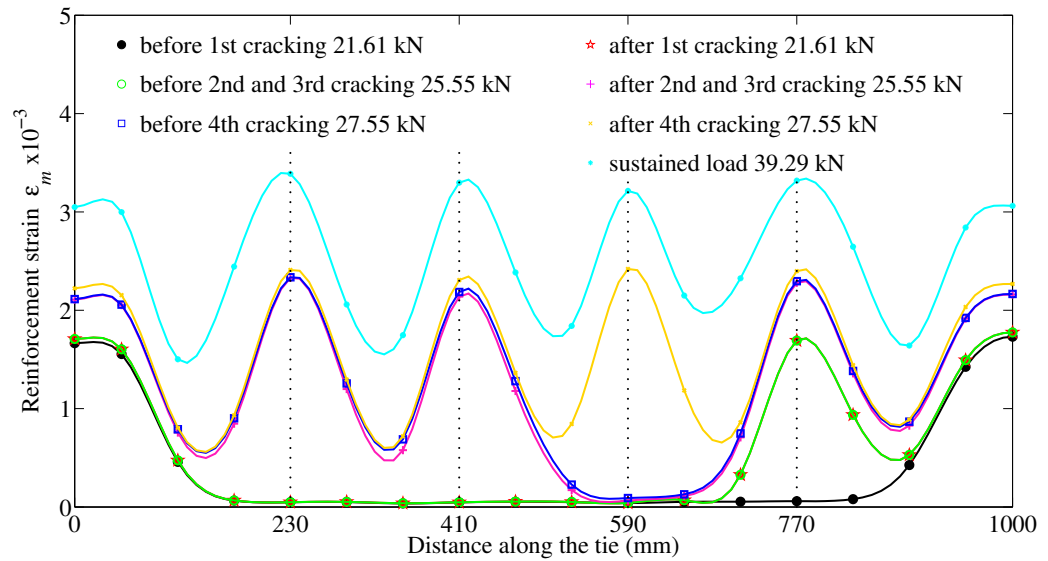
Figure A.24: Experimental reinforcement strain distribution during crack formation in the loading process for specimen C2F16ni.
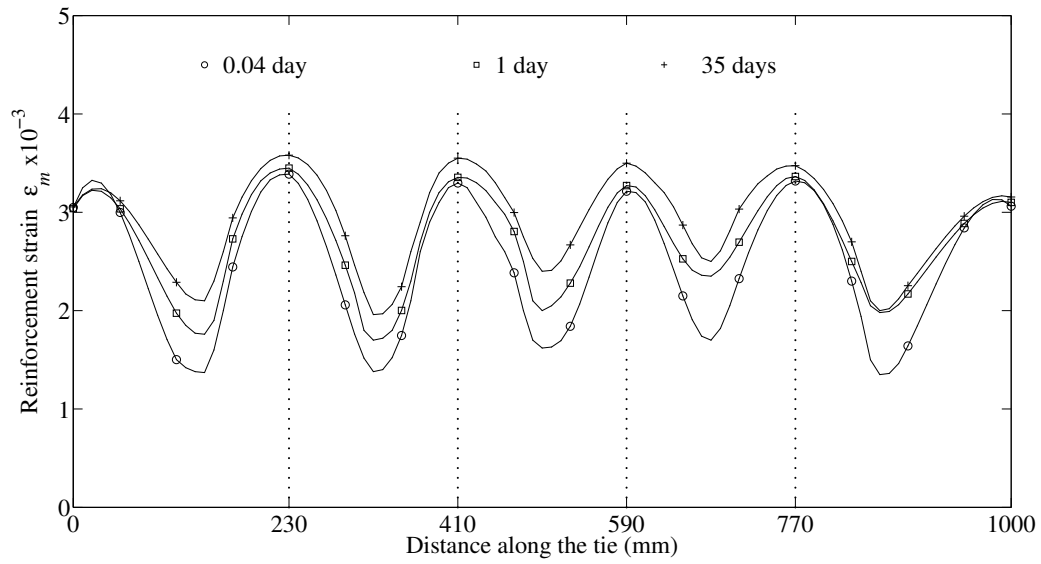
Figure A.25: Experimental reinforcement strain distribution at different times during long-term testing for specimen C2F16ni.
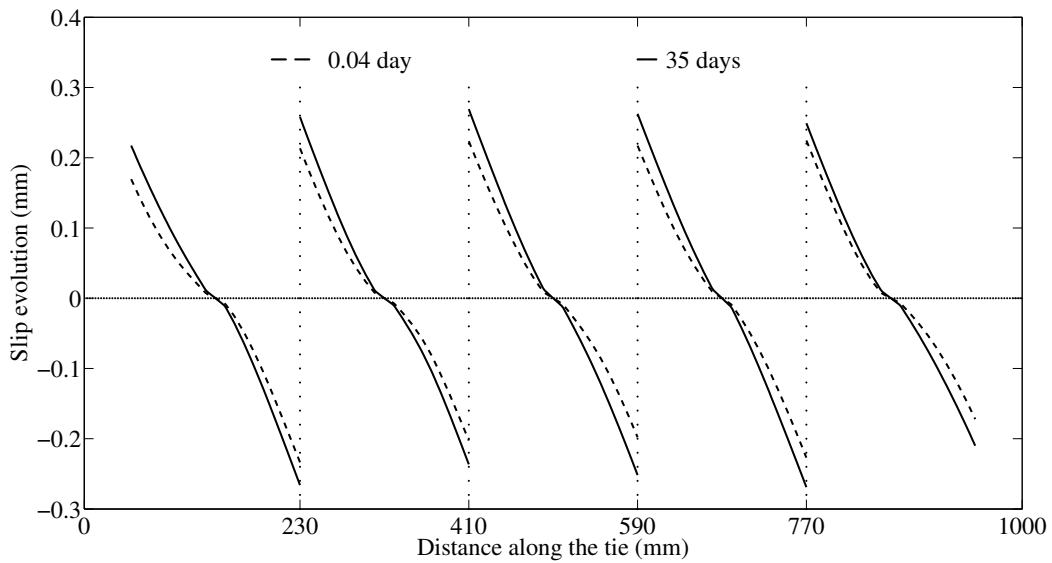
Figure A.26: Experimental slip distribution for specimen C2F16ni at different times during long-term testing.
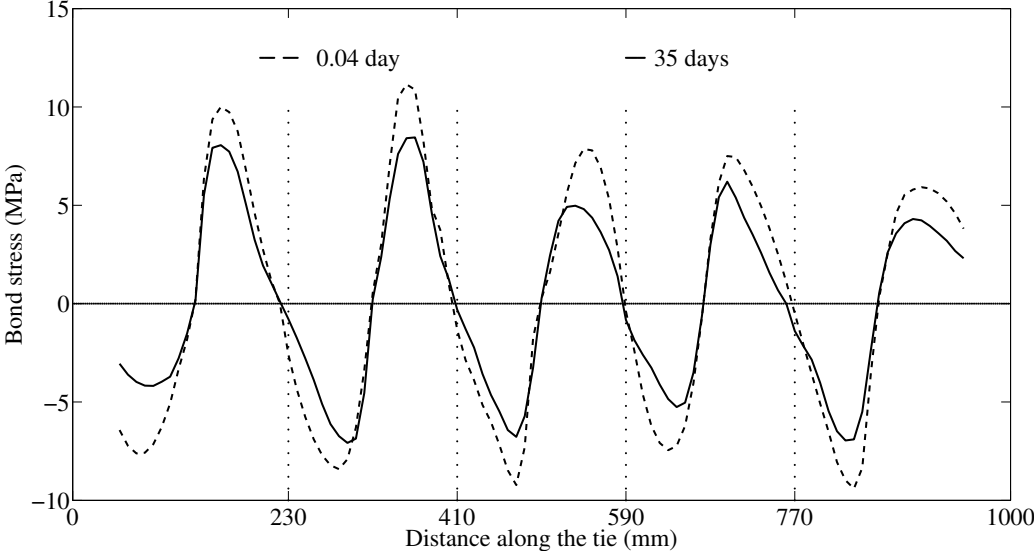
Figure A.27: Experimental bond distribution for specimen C2F16ni at different times during long-term testing.

A.3.4 RC ties during testing.
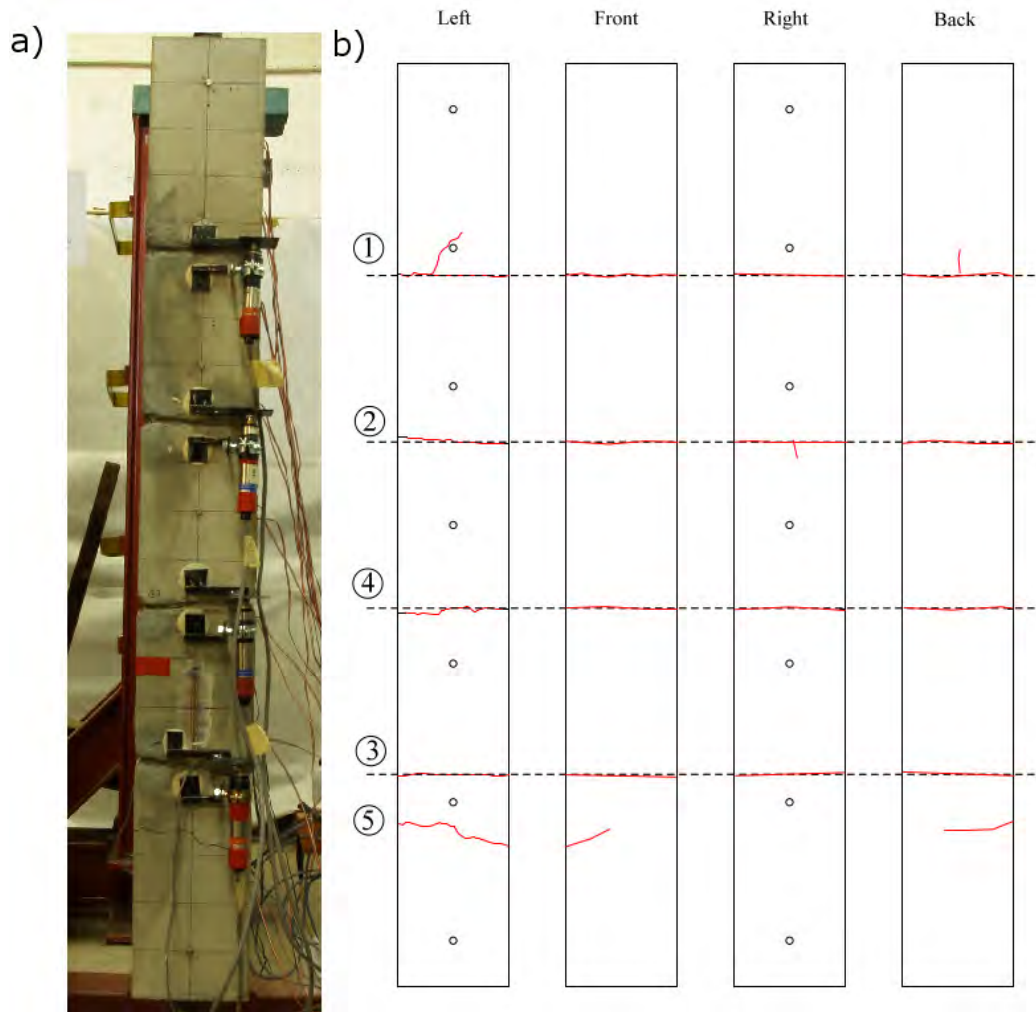
Figure A.28: C1F16ni: a) specimen during testing b) crack pattern.
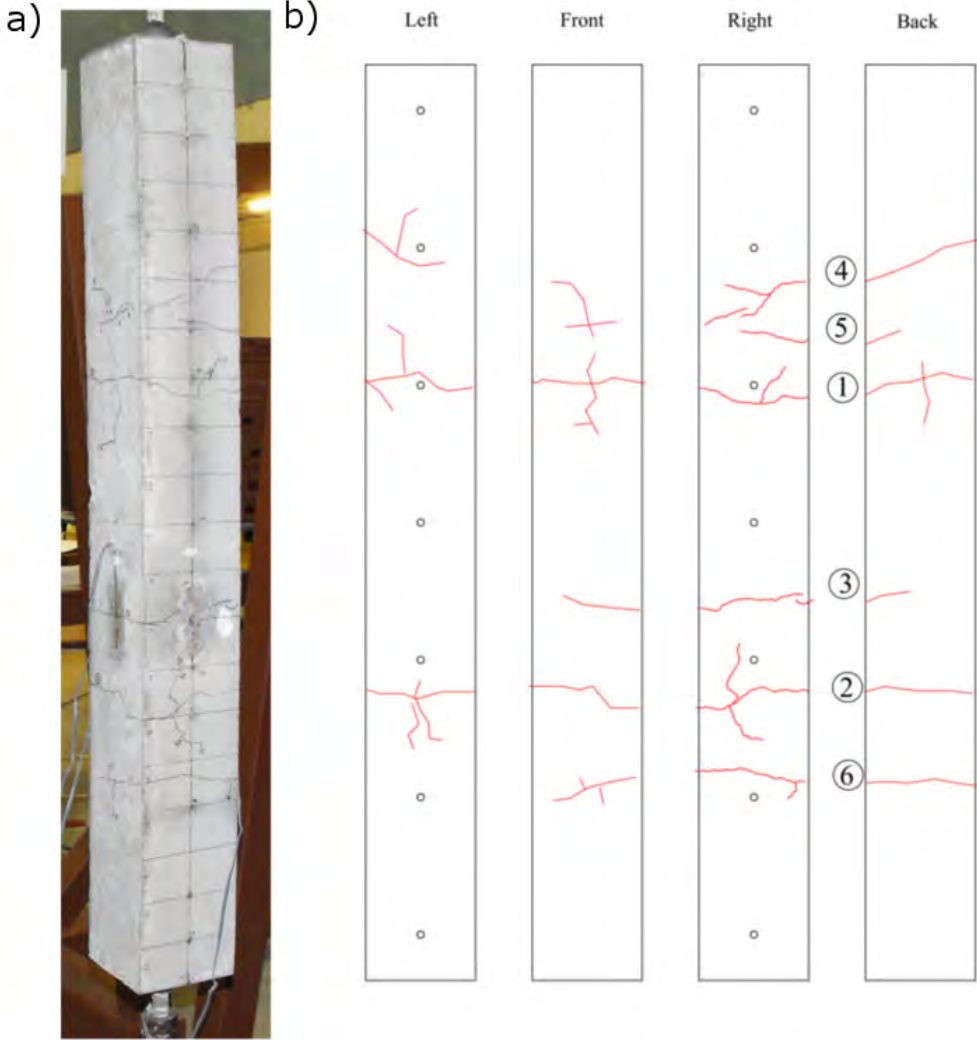
Figure A.29: C1F16: a) specimen during testing b) crack pattern.
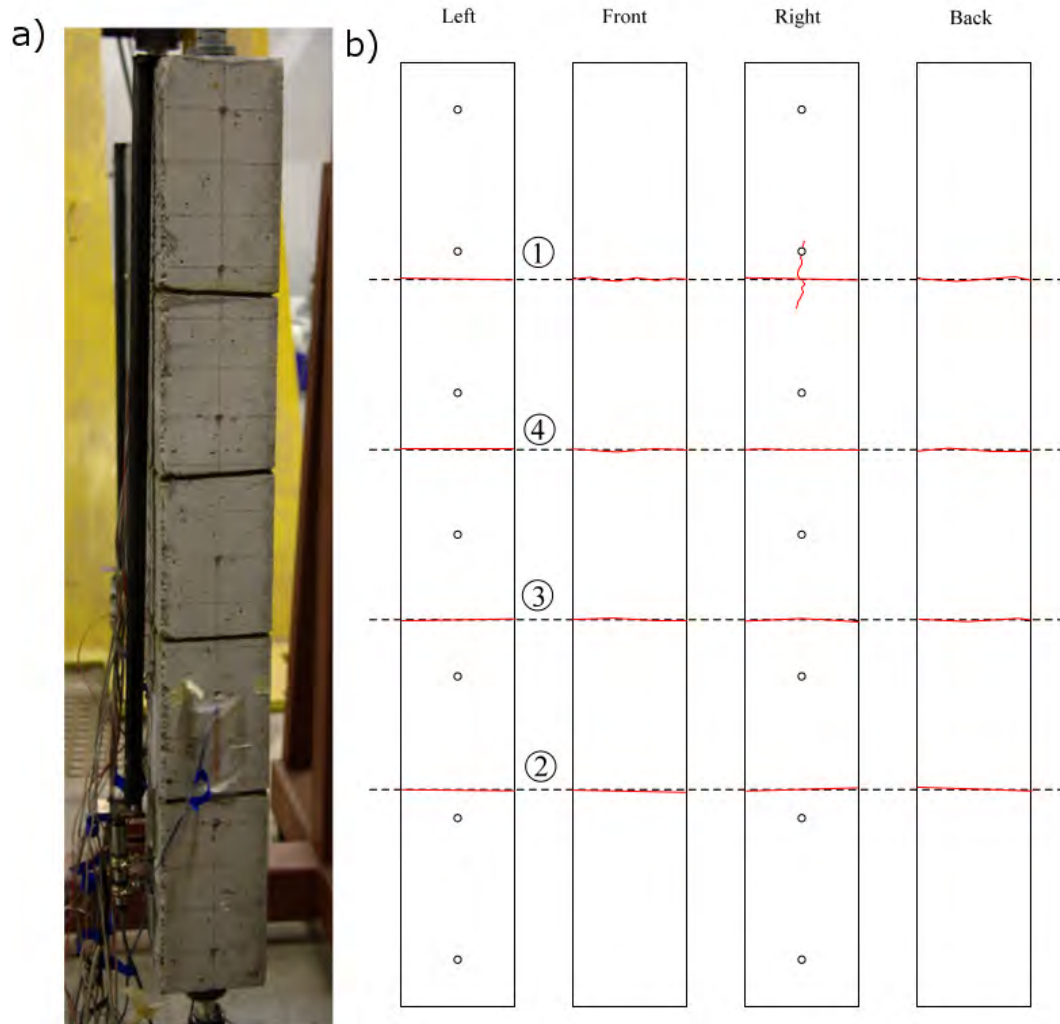
Figure A.30: C2F16ni: a) specimen during testing b) crack pattern.
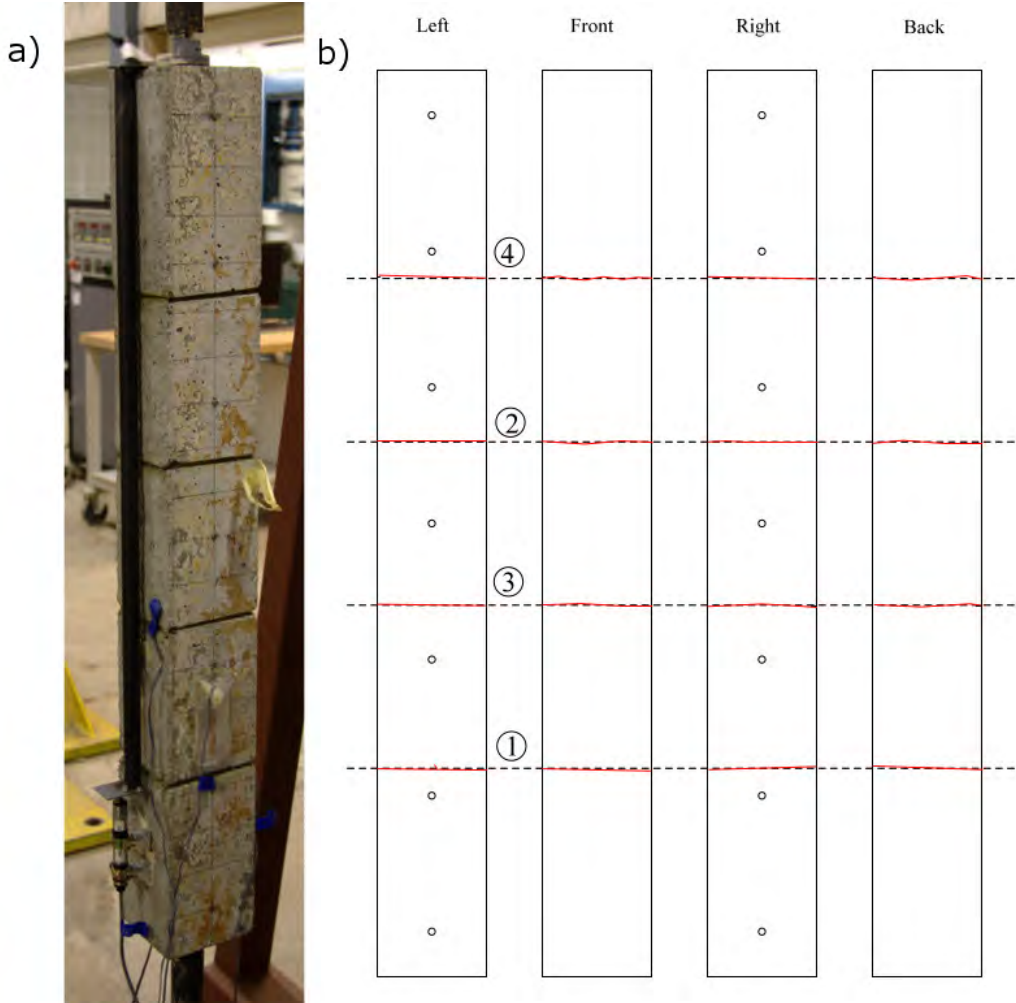
Figure A.31: C2F16n: a) specimen during testing b) crack pattern.
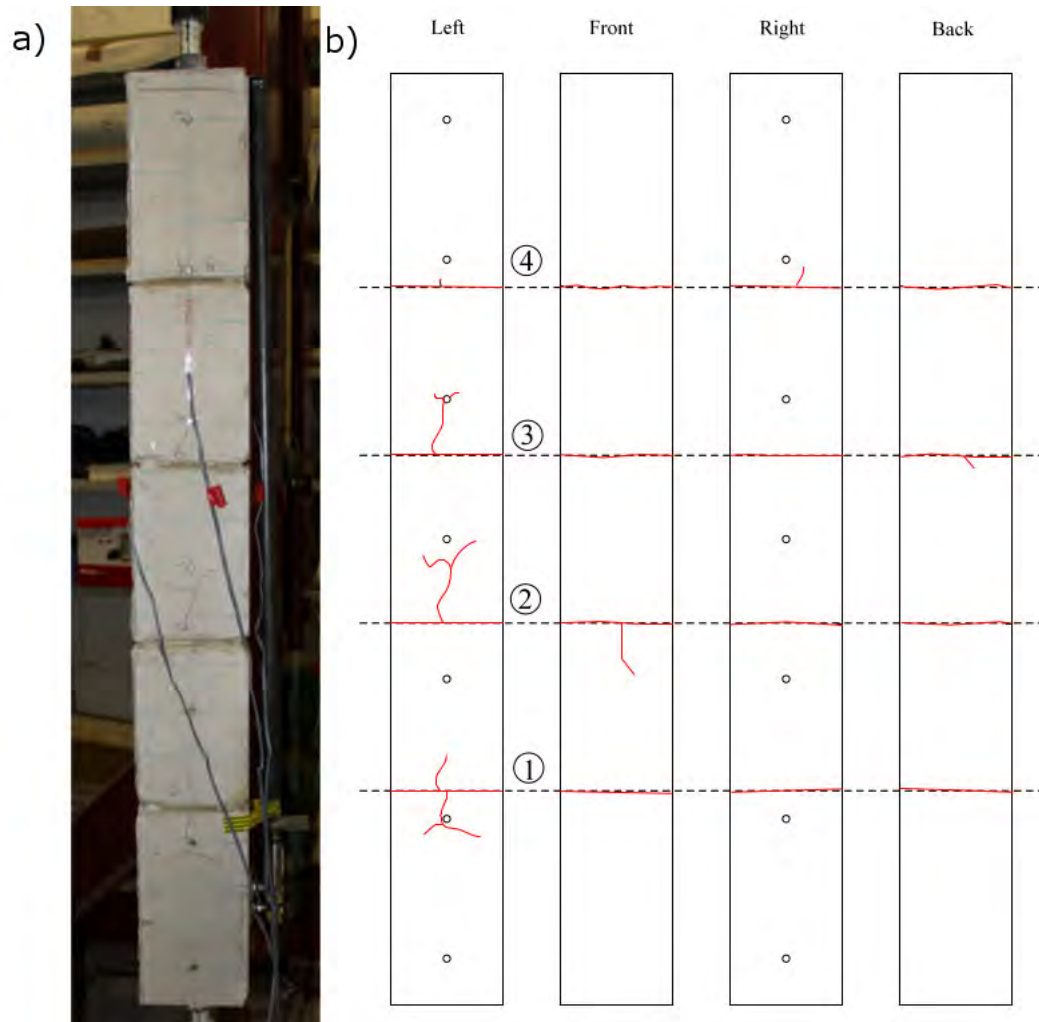
Figure A.32: C3F16n: a) specimen during testing b) crack pattern.
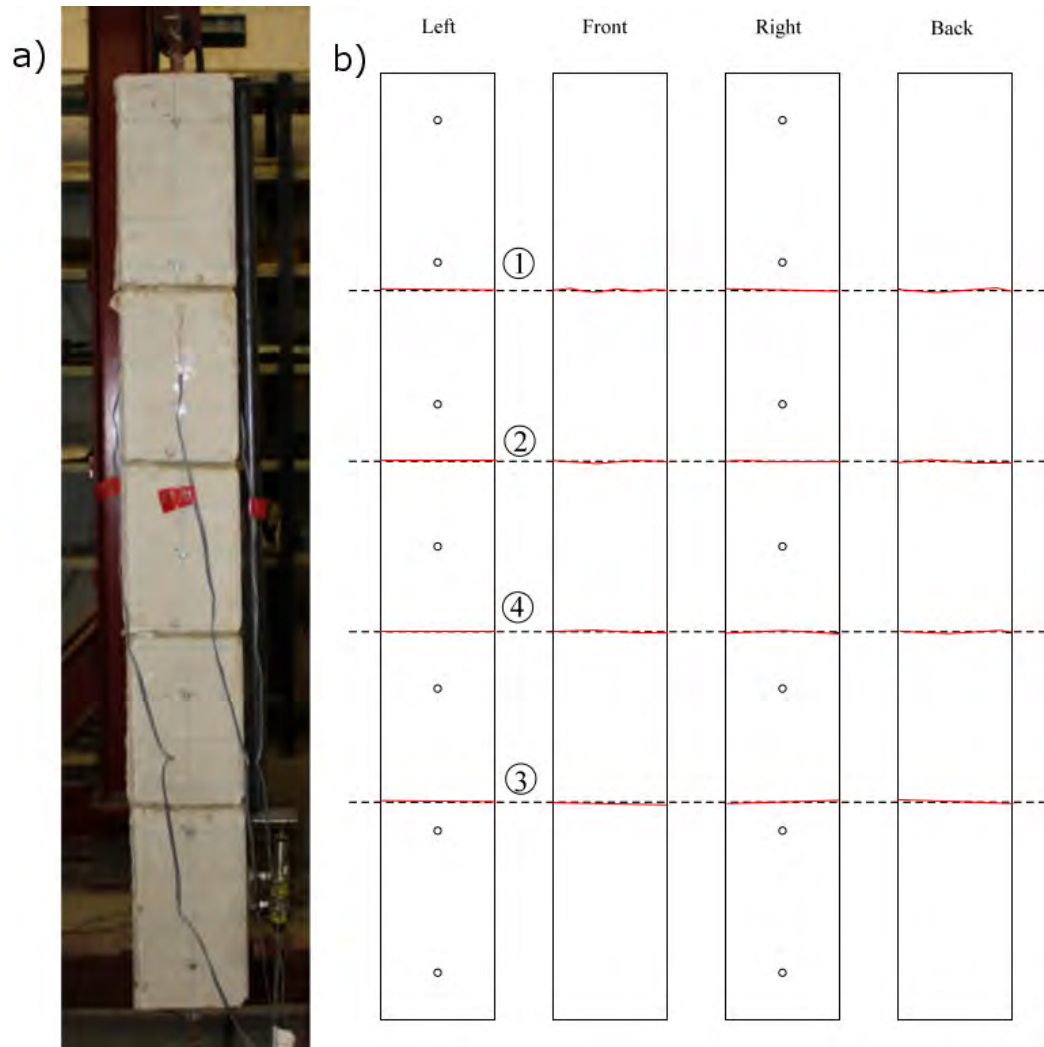
Figure A.33: C3S10n: a) specimen during testing b) crack pattern.

Appendix B

Experimental details of pull-out tests on GFRP RC specimens

B.1 Test Stet up
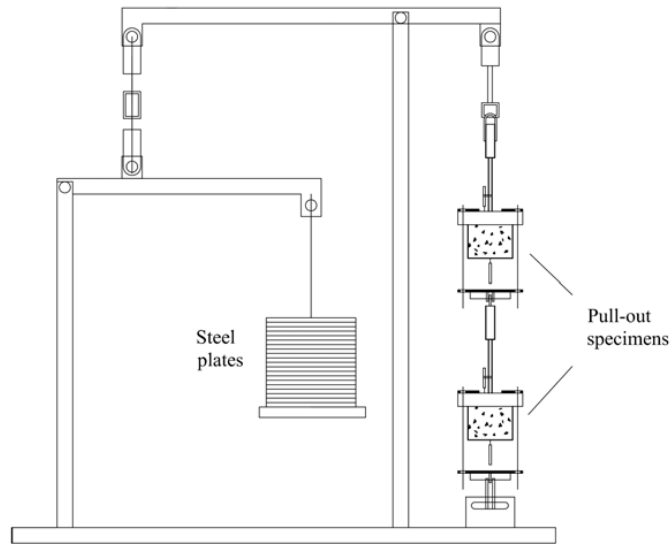
Figure B.1: Frame for long-term testing.

Figure B.2: FRP pull-outs under sustained loads.

Figure B.3: Steel pull-outs under sustained loads.

Figure B.4: Reinforcing bars previous to cast (bond length being already defined).

Figure B.5: Moulds for pull-out specimens' casting.
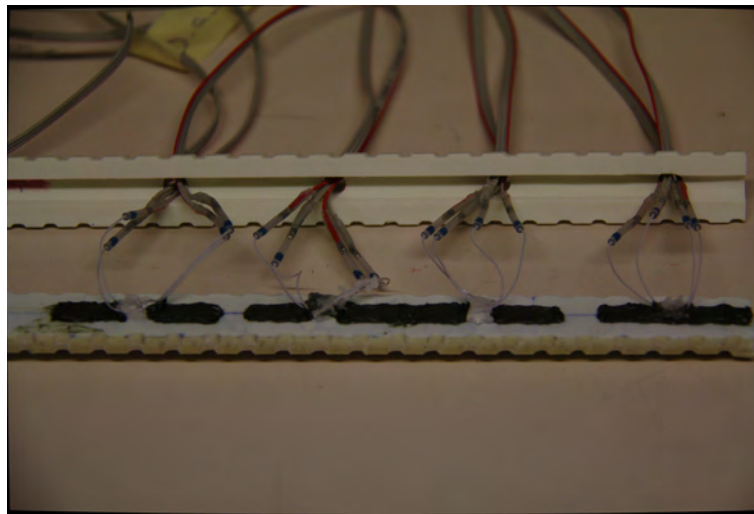
Figure B.6: Internal instrumentation of GFRP bars.

Figure B.7: Pull-out instrumentation during testing.

B.2 Shrinkage and Creep
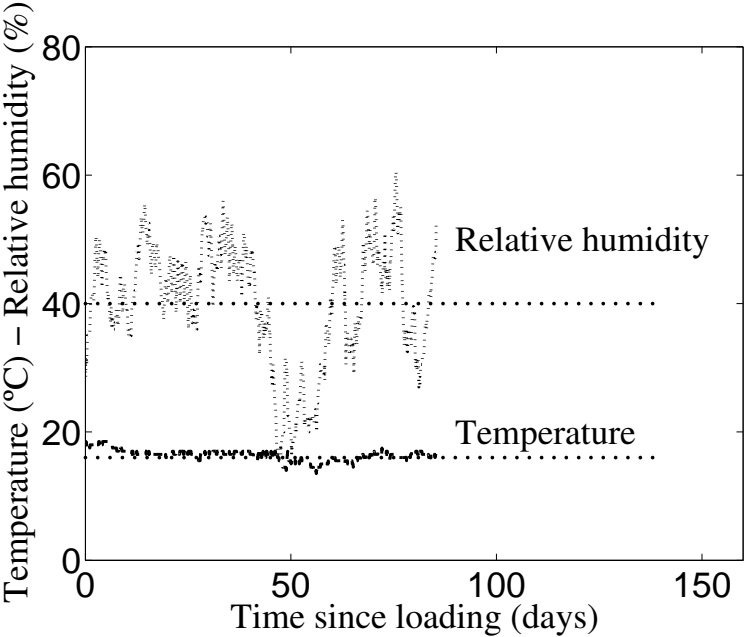
Figure B.8: Temperature and relative humidity registered in the laboratory during C1 tests.
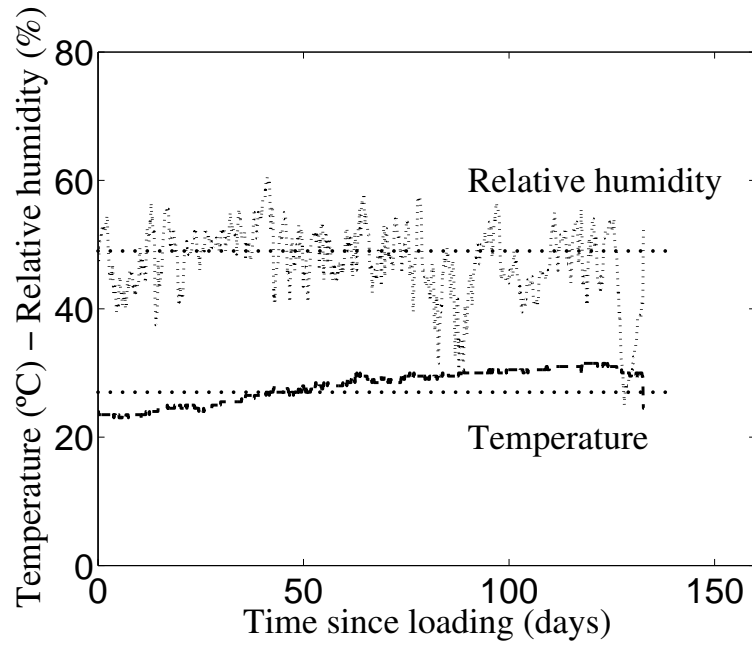
Figure B.9: Temperature and relative humidity registered in the laboratory during C2 tests.
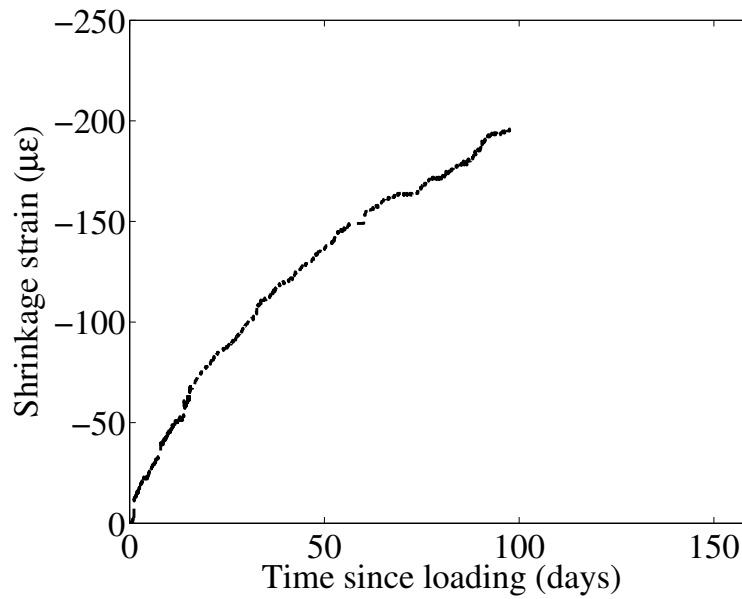
Figure B.10: Experimental free shrinkage strain of C1 series.
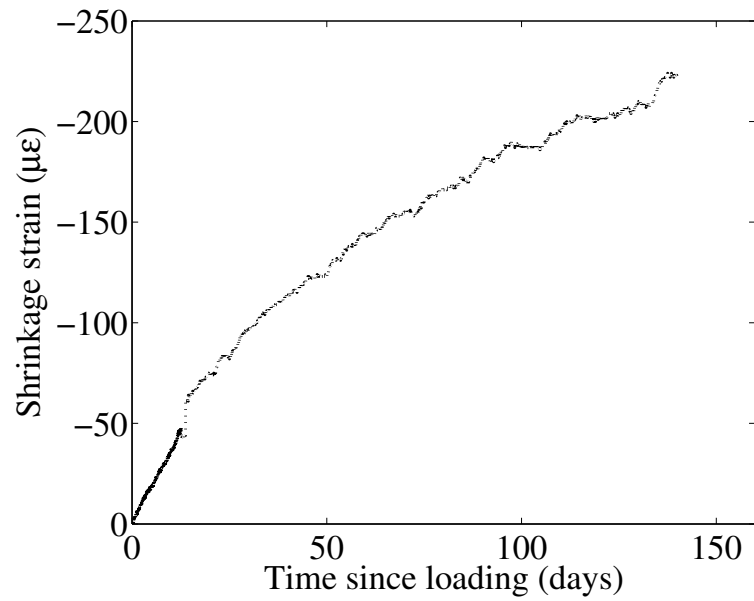
Figure B.11: Experimental free shrinkage strain of C2 series.
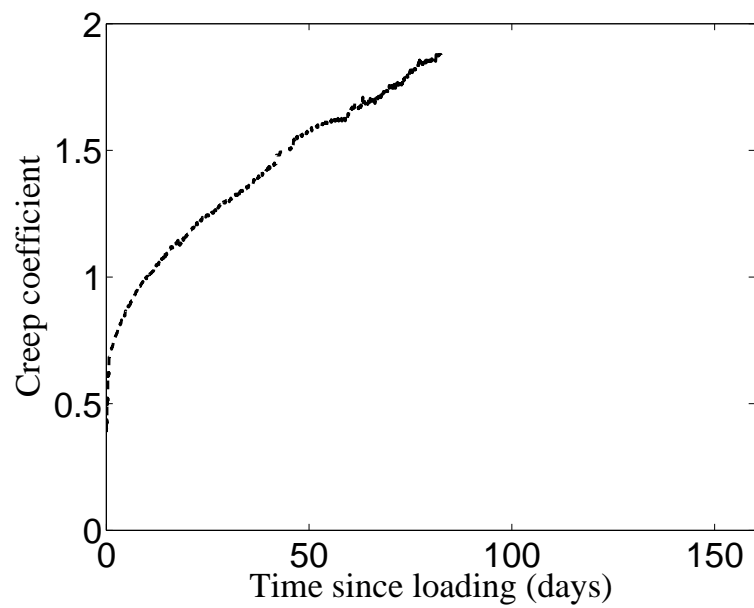
Figure B.12: Experimental creep coefficient of C1 series.
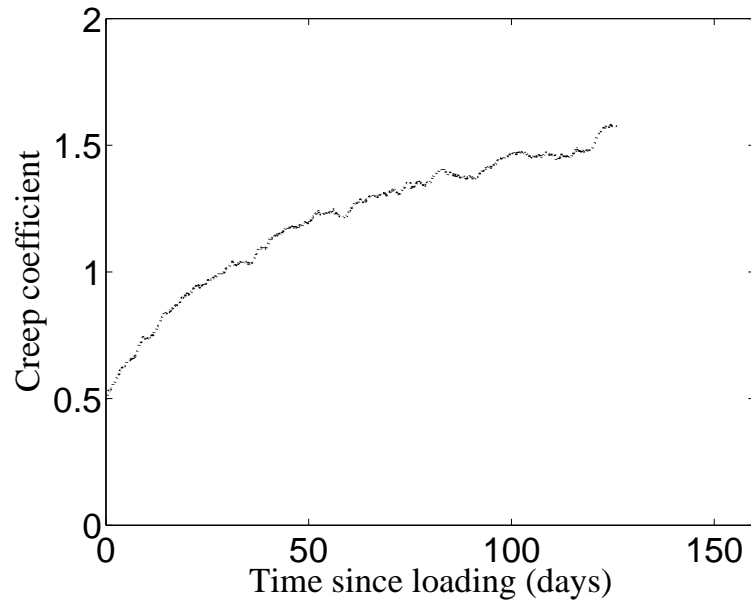
Figure B.13: Experimental creep coefficient of C2 series.

B.3   Results
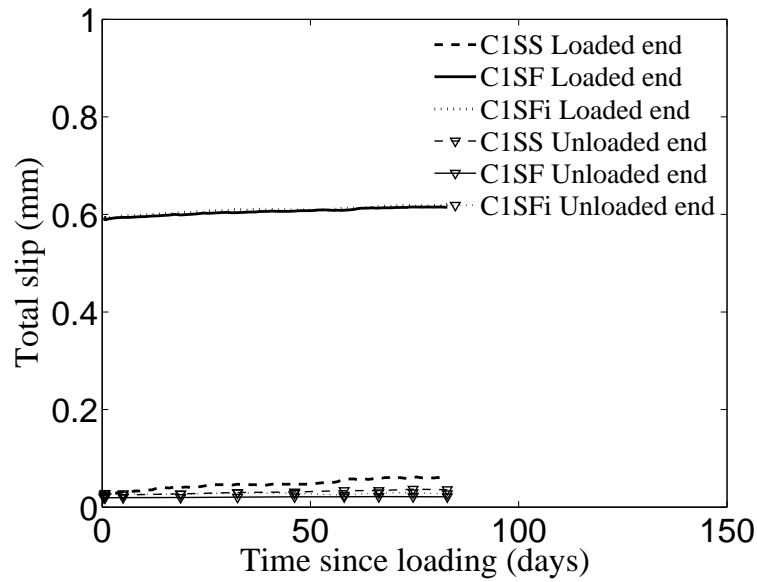
Figure B.14: Experimental total slip vs. time after loading for C1 specimens with short bond length.
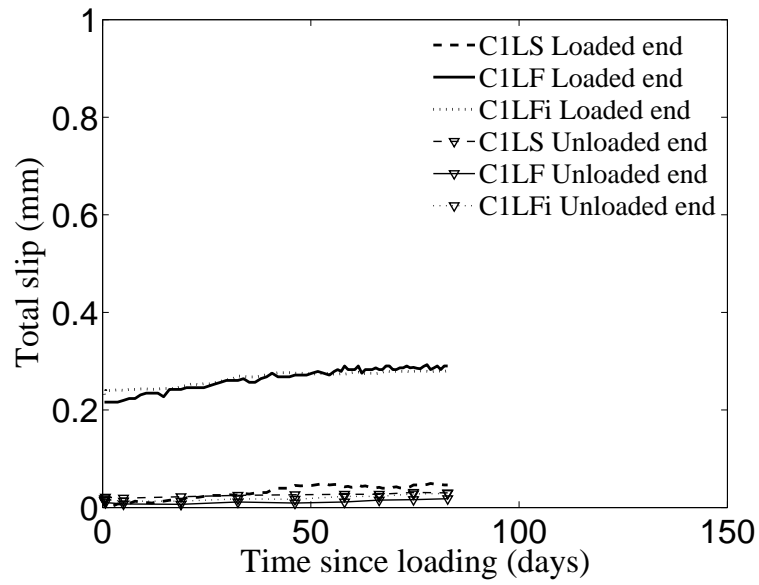
Figure B.15: Experimental total slip vs. time after loading for C1 specimens with long bond length.
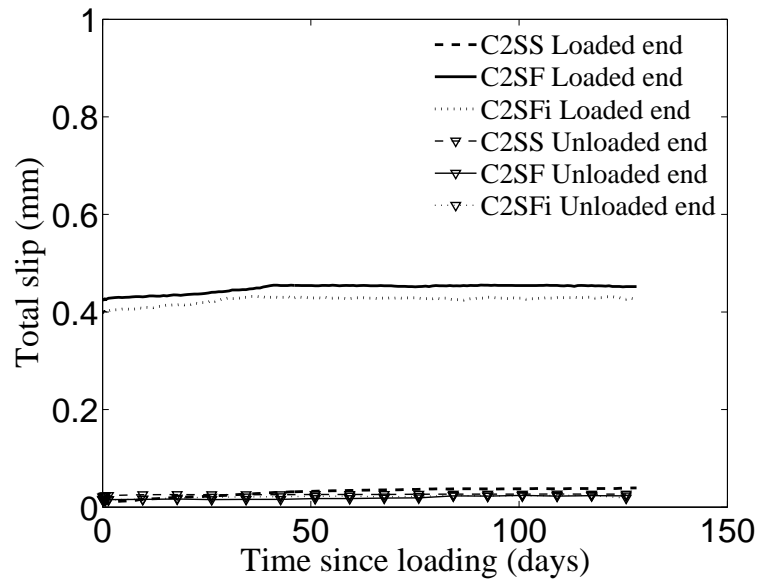
Figure B.16: Experimental total slip vs. time after loading for C2 specimens with short bond length.
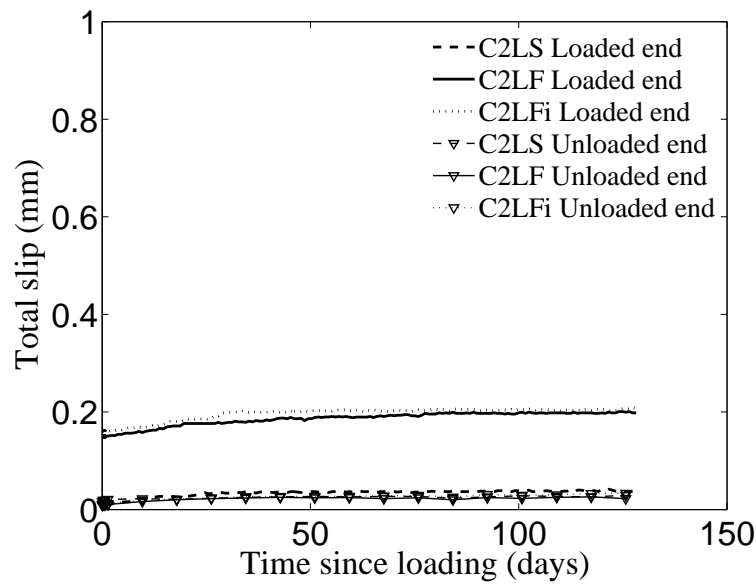
Figure B.17: Experimental total slip vs. time after loading for C2 specimens with long bond length.

B.3.1 Time-dependent slip
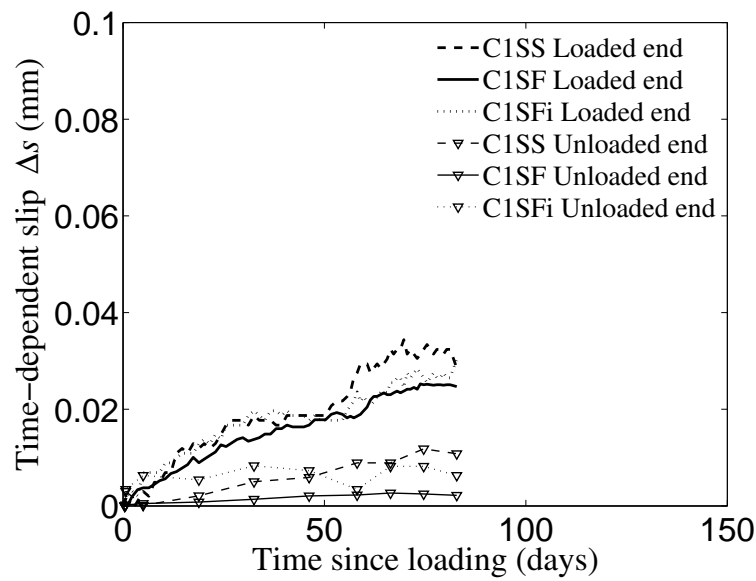
Figure B.18: Experimental time-dependent slip vs. time after loading for C1 specimens with short bond length.
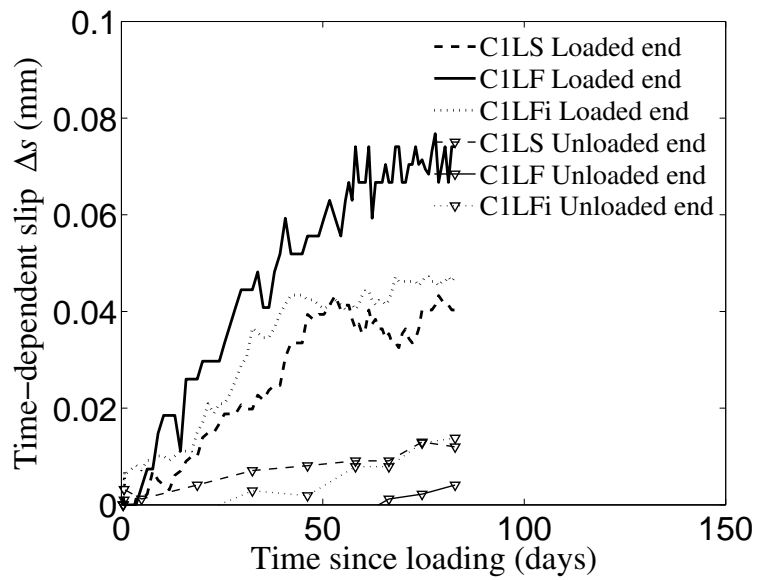
Figure B.19: Experimental time-dependent slip vs. time after loading for C1 specimens with long bond length.
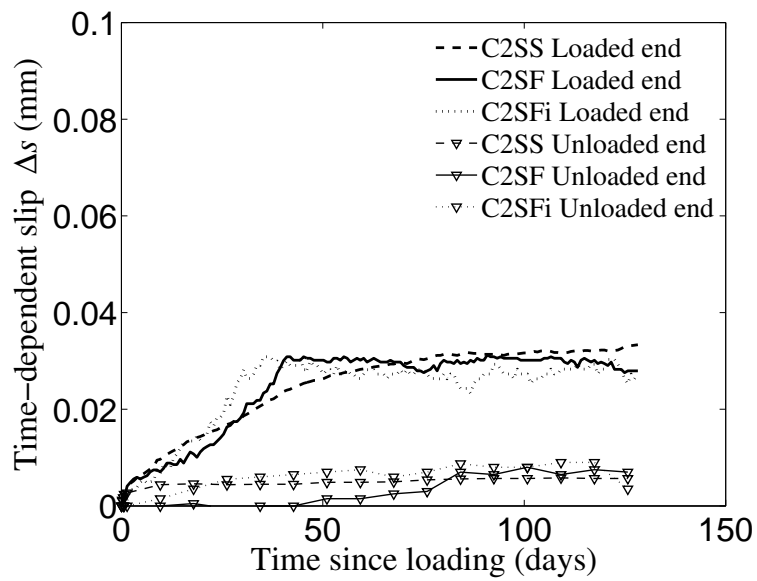
Figure B.20: Experimental time-dependent slip vs. time after loading for C2 specimens with short bond length.
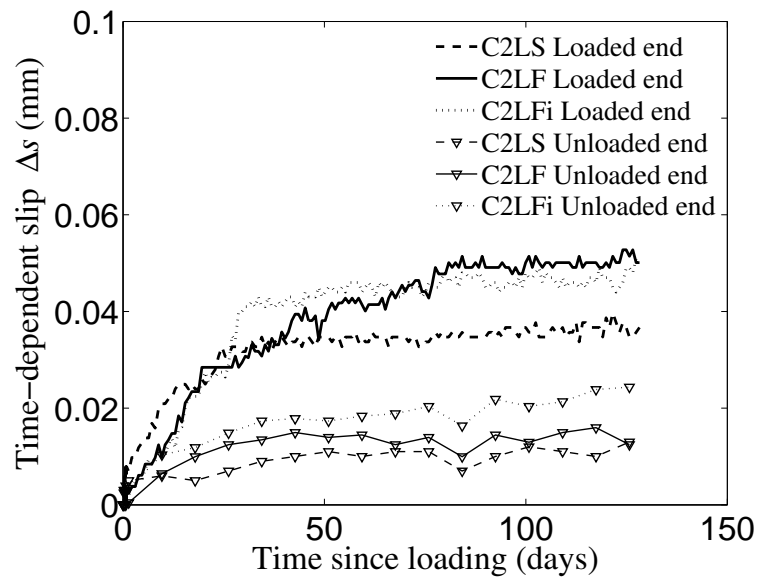
Figure B.21: Experimental time-dependent slip vs. time after loading for C2 specimens with long bond length.

B.3.2   Bond stresses - distribution and evolution
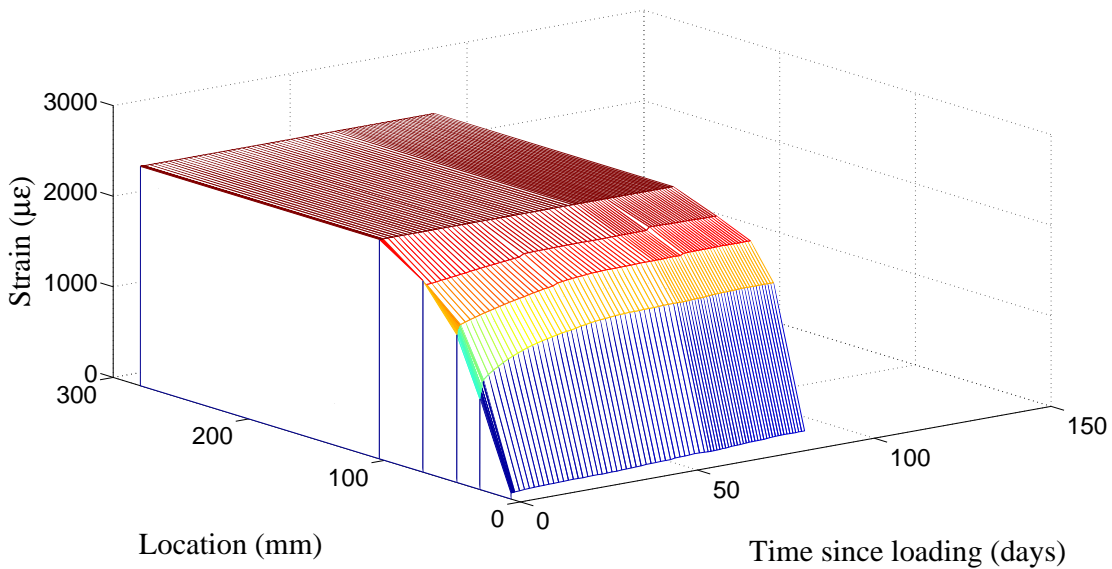
Figure B.22: Experimental reinforcement strain distribution over time for specimen C1SFi.
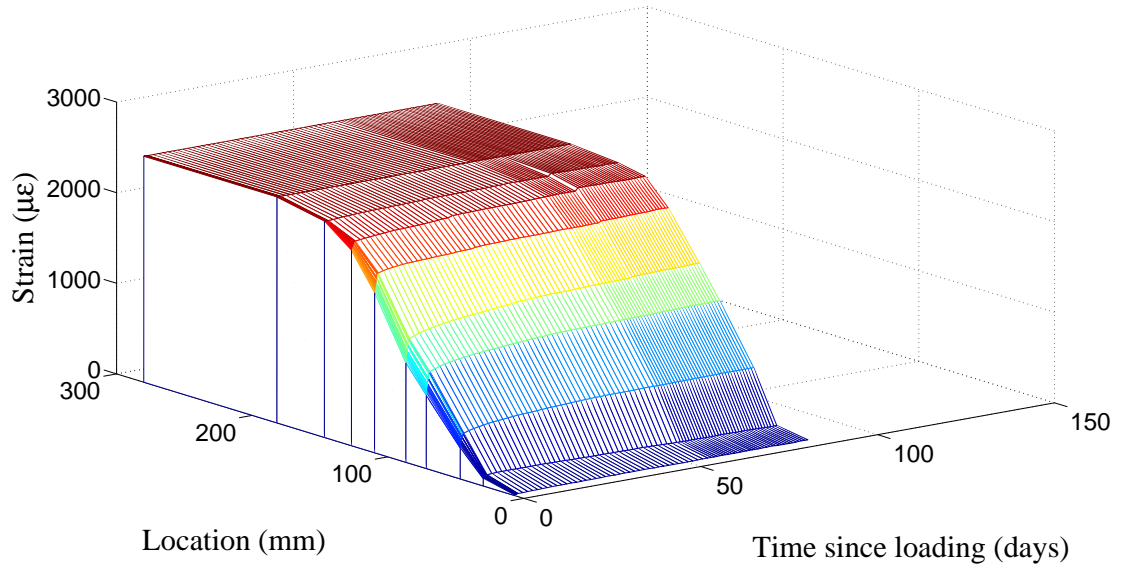
Figure B.23: Experimental reinforcement strain distribution over time for specimen C1LFi.
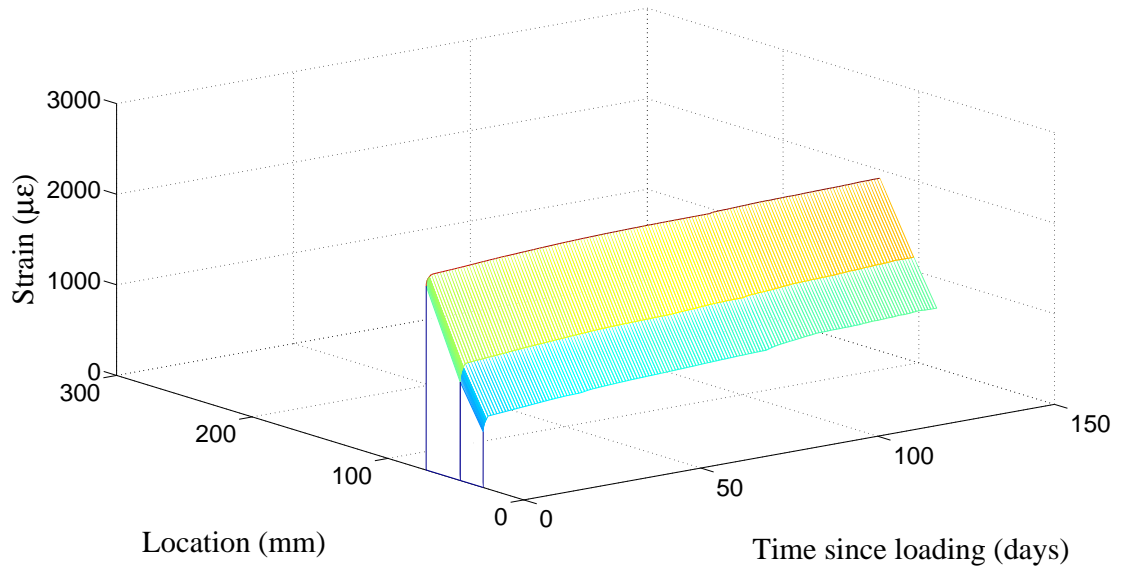
Figure B.24: Experimental reinforcement strain distribution over time for specimen C2SFi.
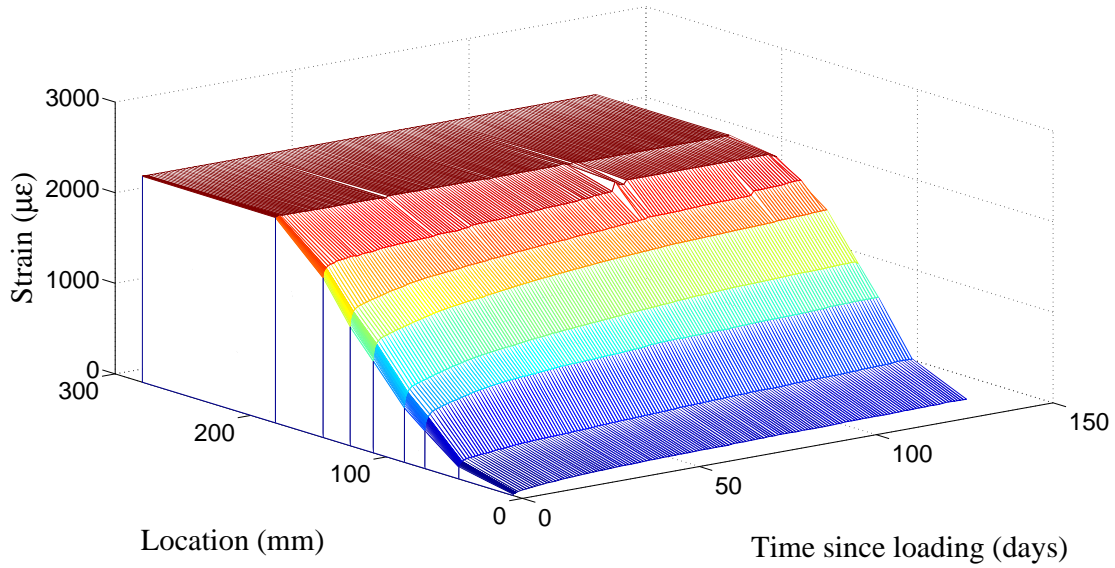
Figure B.25: Experimental reinforcement strain distribution over time for specimen C2LFi.
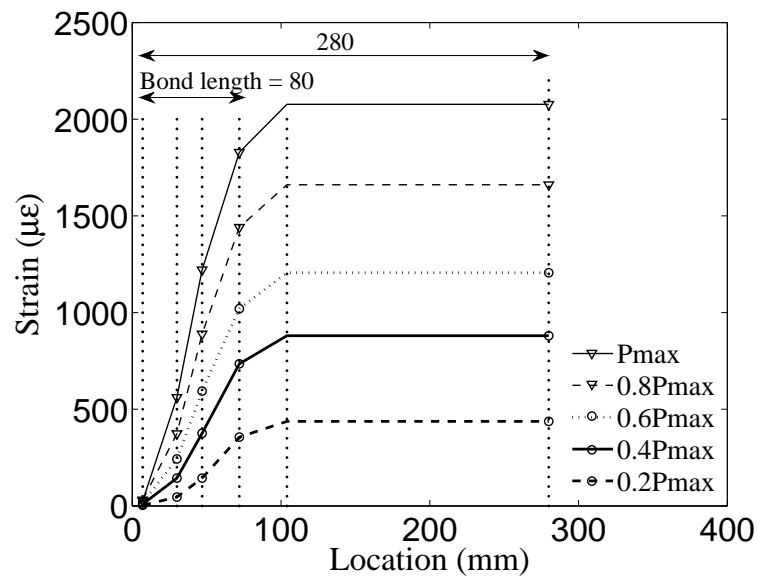
Figure B.26: Experimental reinforcement strain distribution at different loads during instantaneous pull-out test for specimen with short bond length (C1SFi).
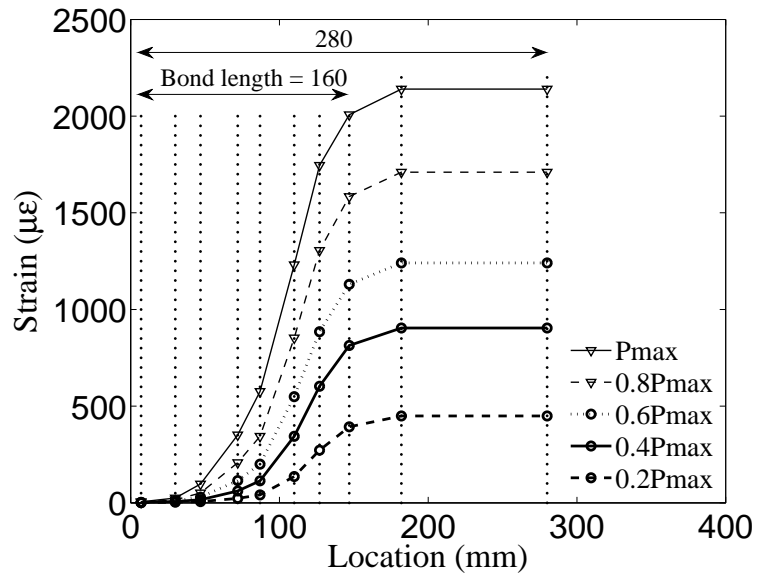
Figure B.27: Experimental reinforcement strain distribution at different loads during instantaneous pull-out test for specimen with long bond length (C1LFi).
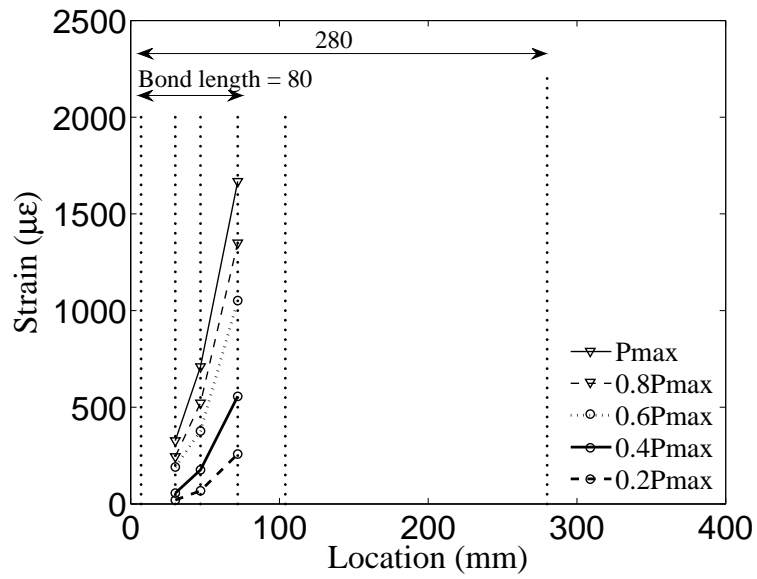
Figure B.28: Experimental reinforcement strain distribution at different loads during instantaneous pull-out test for specimen with short bond length (C2SFi).
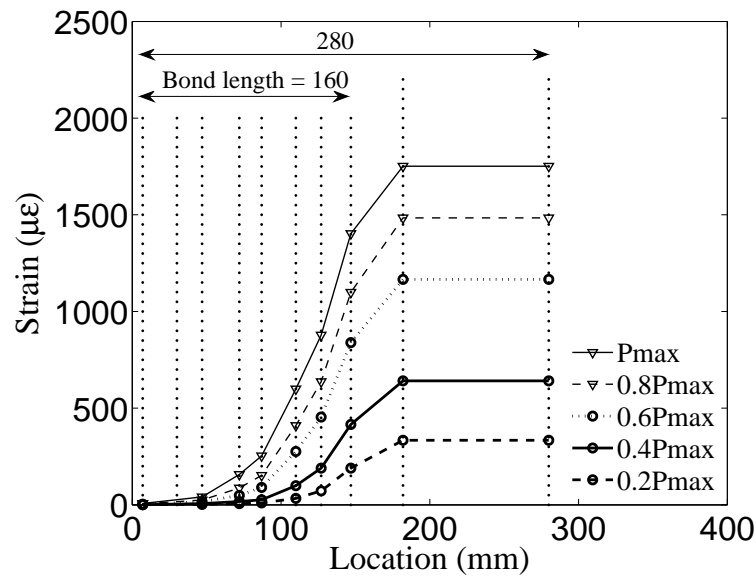
Figure B.29: Experimental reinforcement strain distribution at different loads during instantaneous pull-out test for specimen with long bond length (C2LFi).
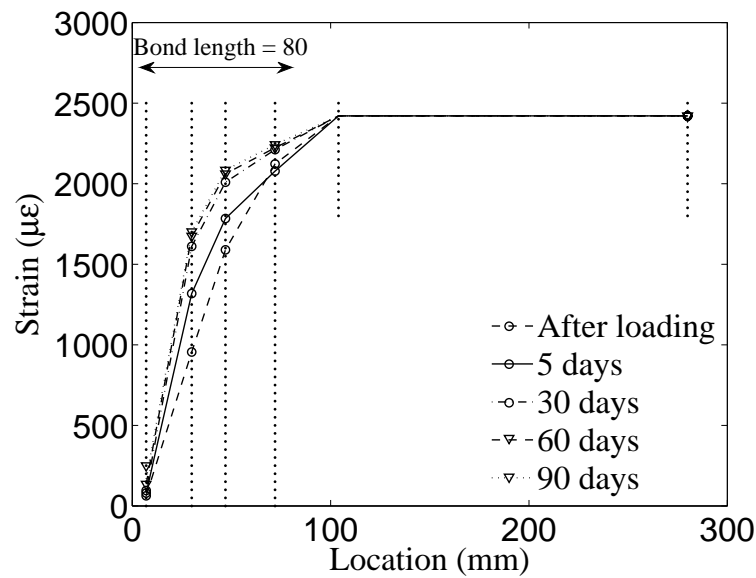
Figure B.30: Experimental reinforcement strain distribution at different times during long-term testing for specimen C1SFi.
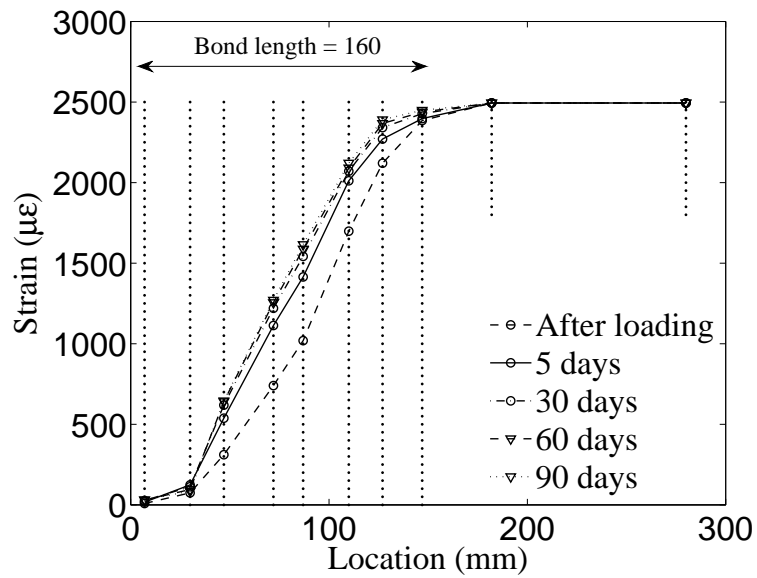
Figure B.31: Experimental reinforcement strain distribution at different times during long-term testing for specimen C1LFi.
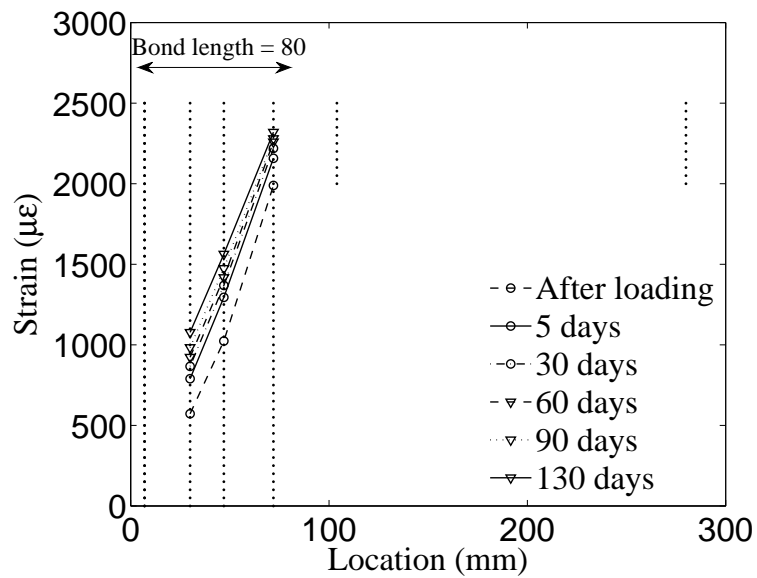
Figure B.32: Experimental reinforcement strain distribution at different times during long-term testing for specimen C2SFi.
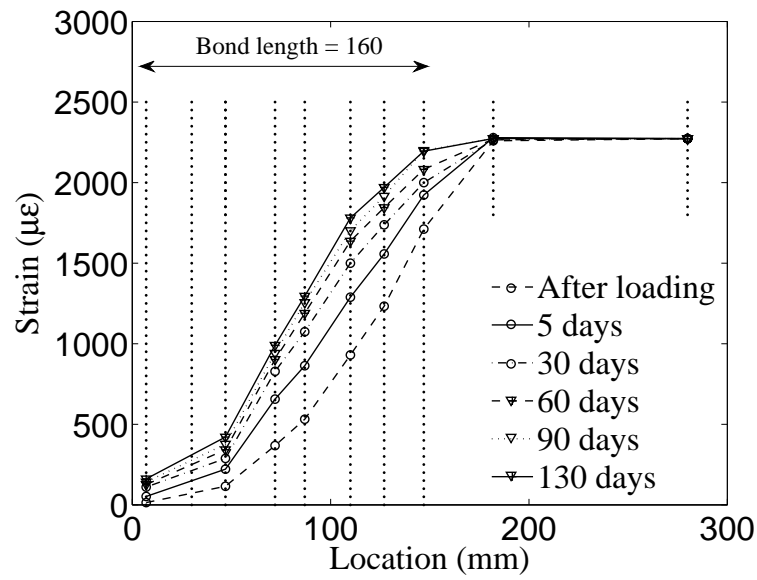
Figure B.33: Experimental reinforcement strain distribution at different times during long-term testing for specimen C2LFi.
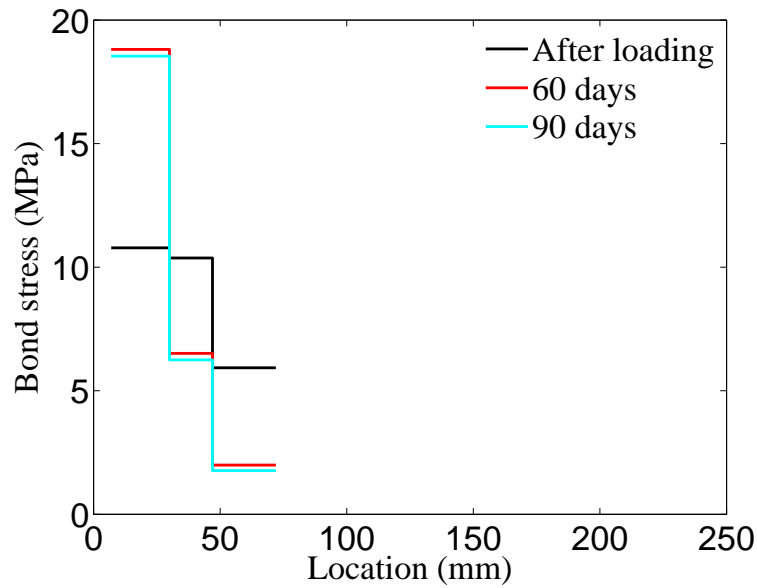
Figure B.34: Experimental bond stress distribution at different times during long-term testing for specimen C1SFi.
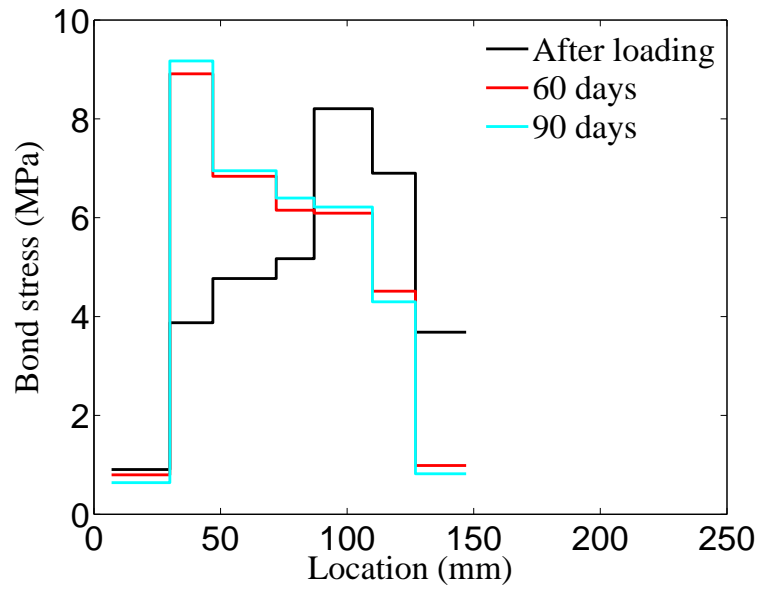
Figure B.35: Experimental bond stress distribution at different times during long-term testing for specimen C1LFi.
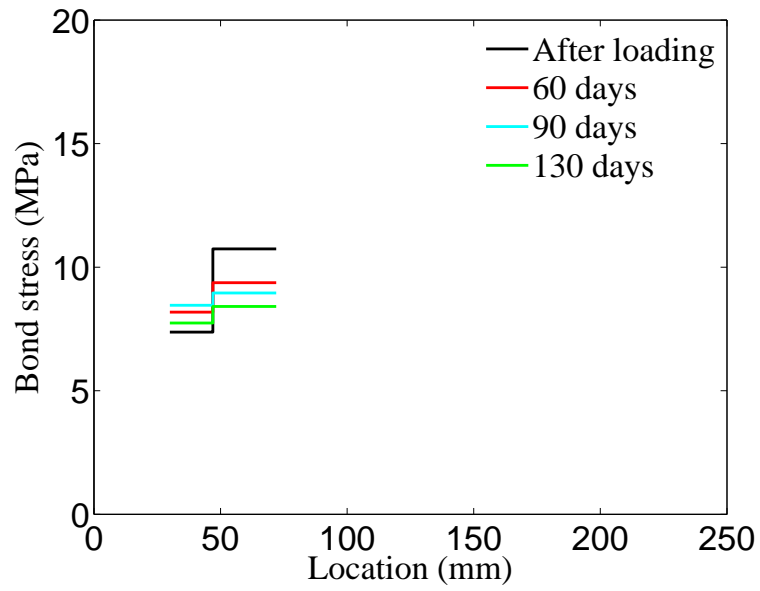
Figure B.36: Experimental bond stress distribution at different times during long-term testing for specimens C2SFi.
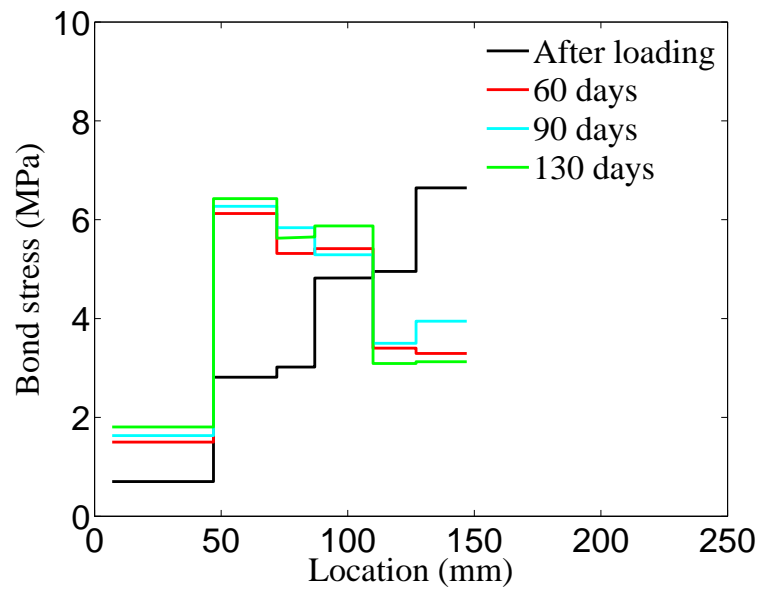
Figure B.37: Experimental bond stress distribution at different times during long-term testing for specimens C2LFi.

Appendix C

Experimental study of tension stiffening in GFRP RC tensile members under sustained load

Contents lists available at ScienceDirect

Engineering Structures

Experimental study of tension stiffening in GFRP RC tensile members under sustained load

CrossMark

I. Vilanova [a], L. Torres [a], M. Baena [a,*], G. Kaklauskas [b], V. Gribniak [b]

[a] Analysis and Advanced Materials for Structural Design (AMADE), Polytechnic School, University of Girona, Campus Montilivi s/n, 17071 Girona, Spain
[b] Vilnius Gediminas Technical University, Vilnius, Lithuania

ABSTRACT

Sustained load effects on steel reinforced concrete structures due to creep and shrinkage in the concrete have been widely studied. However, knowledge of behaviour under sustained loads needs extending to the more recently developed fibre reinforced polymer (FRP) reinforced concrete structures. In this experimental study, the effect of tension stiffening on tensile glass fibre reinforced polymer (GFRP) reinforced concrete elements under sustained load is investigated. A total of six specimens with three different concrete strengths were tested for a period of between 35 and 40 days, when it was seen that deformations stabilized. Some of the specimens included internal instrumentation of the reinforcing bar to capture the reinforcement strain profile and analyse long-term effects. Results confirm bond deterioration due to sustained load, with a reduction in the mean bond stress and concrete tensile stress, and showed how deterioration stabilized at approximately 28 days. The influence of concrete strength on the loss of tension stiffening is also confirmed, with higher concrete compressive strength showing the smallest loss of concrete tensile stresses. The results are compared to predictions using Eurocode 2 approach, in which the effects of sustained load are incorporated by applying the effective modulus method (EMM). Predictions using this methodology compare well with experimental results.

1. Introduction

The use of fibre reinforced polymer (FRP) bars as reinforcement in reinforced concrete (RC) structures has gradually increased in recent decades due to their electromagnetic transparency and resistance to corrosion in aggressive environments [1–4]. In line with this trend, research into FRP RC structures has also increased, a fact reflected in design recommendations in the form of codes and guidelines [5–7]. The existing literature mainly addresses the analysis of flexural behaviour in which the effect of the mechanical properties of FRP rebars is analysed [8–16], and concludes that the general assumptions made for steel RC elements are valid for FRP RC members, but that their specific mechanical properties lead to some changes in equations and design philosophy. The literature also suggests that due to their lower modulus of elasticity, serviceability requirements often govern the design of FRP RC elements. Although fewer studies focus on FRP RC tensile members, the major influence of the tension stiffening effect on load-deformations behaviour has been proved [17–19]. Most of the research carried out so far has focussed on the short-term response of FRP

RC elements; there are not so many studies focussing on long-term behaviour. The analysis of long-term performance has been mainly approached by both studying material durability issues [20–22] and analysing RC flexural behaviour [23–28].

When analysing time effects on the behaviour of RC elements, concrete creep and shrinkage play a crucial role [29–33]. While creep is associated to sustained stresses, shrinkage may be assumed to be independent of load. Both effects cause long-term deformations in concrete. Existing studies allow the influence of long-term effects on tension stiffening, stresses and deformations [34–36] to be analysed, but only limited research into the effects of creep and shrinkage on tensile steel RC elements is available.

Scott and Beeby [34] tested a total of twelve steel RC elements in tension for periods of up to 4 months. The results focussed on creep and shrinkage effects and the loss of tension stiffening. Internal instrumentation of the steel reinforcing bars and external strain gauges were used, allowing the cracking process both for instantaneous and sustained loading to be analysed. The results showed an increase in the strain response until tension stiffening decayed and stabilized in less than one month after first loading [37]. Wu and Gilbert [35] carried out an experimental test campaign on six steel RC elements in tension, four subjected to short-term loading and two to long-term loading for a period of

* Corresponding author.

Nomenclature

A_1	area of a notched section		β_2	loading type coefficient in EC2 proposal
A_2	area of a section without notches		$\Delta\varepsilon$	time dependent strain
A_c	concrete area		ε_1	reinforcement strain for uncracked section
A_r	reinforcement area		ε_2	reinforcement strain for fully cracked section
d_r	reinforcement diameter		ε_c	concrete strain
E_c	concrete modulus of elasticity		$\varepsilon_c(t)$	concrete strain due sustained loading
$E_c(t)$	concrete modulus of elasticity at time t		$\varepsilon_{f,exp}$	experimental strain after sustained load
$E_e(t,t_0)$	concrete effective modulus of elasticity		$\varepsilon_{f,th}$	theoretical strain after sustained load
E_r	reinforcement modulus of elasticity		ε_r	reinforcement strain
f_c	concrete compressive strength		ε_i	the total short-term strain before sustained loading
n	modular ratio between E_r and E_c		$\varepsilon_{i,exp}$	experimental values of strain before sustained load
n^*	modular ratio between E_r and E_e		$\varepsilon_{i,th}$	theoretical strain before sustained load
P	applied load		ε_m	analytical final strain response
P_{add}	initial tensile load due to shrinkage		ε_{mi}	initial shortening due to shrinkage
P_c	load supported by concrete		ε_{sh}	experimental shrinkage
P_{cr}	cracking load		$\varepsilon_{sh}(t,t_0)$	free shrinkage strain
P_{cr}^*	normalised cracking load		$\varepsilon_\varphi(t)$	creep strain
P_r	load supported by reinforcement		$\varepsilon_r(t,t_0)$	total strain
s	slip between concrete and reinforcement		$\varphi(t,t_0)$	creep coefficient
t	time		P	reinforcement ratio
t_0	time of loading		$\sigma_c(t)$	concrete stress
u_c	displacement of concrete		σ_{cr}	reinforcement stress at cracking load
u_r	displacement of reinforcement		σ_r	reinforcement stress at actual load
β_1	bond characteristics coefficient in EC2 proposal		τ	bond stress

about 50 days. The objective was to analyse the influence of creep and shrinkage on long-term behaviour, and to gain a better understanding of the mechanisms involved in tension stiffening, cracking and deformations. According to the experimental results for long-term loading, an increase in reinforcement strain was visible at midway sections between two cracks, and reinforcement strain was found to be approximately constant in cracked sections. Based on the results obtained by Wu and Gilbert [35], Zanuy [36] developed a numerical methodology to predict long-term effects on steel RC elements in tension that included the influence of creep and shrinkage.

The literature dealing with FRP RC elements under sustained loads is even more limited. Nkurunziza et al. [38] tested a total of twenty GFRP bars in tension to study the effect of sustained loads on FRP bars in aggressive environments. The specimens were tested for 417 days at two loading levels (25% and 38% of the ultimate bar tensile strength). The authors observed that long-term loading had a minimal effect on creep strain and elastic modulus, while the effect on residual strength was more dependent on the environmental conditions. Mazzotti and Savoia [39] tested a total of two concrete specimens externally reinforced with CFRP plates. The specimens were subjected to sustained loading for more than 900 days. Three bonded lengths and two load levels were used to analyse the evolution of axial strain and shear stresses with time. Results showed a redistribution of the shear stresses along the anchorage due to creep deformation at the interface level. To the best knowledge of the authors, no studies have been reported into the long-term behaviour of tensile RC members using FRP bars as internal reinforcement.

In this paper, an experimental campaign to study the evolution of strains and stresses in RC elements reinforced with GRFP bars subjected to sustained axial load is presented. A total of six specimens with three different concrete strengths were tested for a period of between 35 and 40 days, when it was seen that deformations stabilized. Some of the specimens were instrumented with internal strain gauges in the reinforcing bar, to better capture the reinforcement strain profile and analyse the long-term effects. Results in

terms of bond, slip, stresses and strains are reported and analysed. Comparison of experimental results with analytical predictions using the effective modulus method (EMM) and Eurocode 2 approach [40] is also reported and discussed.

2. Experimental programme

2.1. Experimental programme

The experimental programme was designed to investigate the effect of concrete strength and reinforcing material on the long-term performance of reinforced concrete elements in tension. The test matrix consisted of six specimens divided into three groups of two specimens each. All the specimens were rectangular in cross-section (120×120 mm) and 1000 mm long with an effective bond length of 900 mm (i.e. 50 mm long plastic tubes were placed at both ends of the specimens before casting to diminish end effects and to try to reproduce bond development better). Two different reinforcing materials (GFRP and steel) and three target concrete strengths (25, 35 and 50 MPa) were used. In order to achieve similar axial stiffness (EA) in all tests, the standardised reinforcement consisted of either a single 16 mm diameter GFRP bar or a single 10 mm diameter steel bar.

Two specimens (Series 1, C1) were cast with a target concrete compressive strength of 50 MPa and GFRP reinforcement. Two specimens (Series 2, C2) were GFRP reinforced and had a target concrete compressive strength of 35 MPa. The last two specimens (Series 3, C3) consisted of one GFRP and one steel RC tie with a target concrete compressive strength of 25 MPa. So that the internal distribution of bond stresses could be analysed, some of the specimens included internal instrumentation in the reinforcing bars. Perimeter notches were included in five of them in order to obtain a controlled crack pattern and force cracks to form at specific locations. The notches were created by placing 3 mm × 2 mm rectangular steel tubes in the moulds prior to casting. A distance of 180 mm between notches was selected based on the cracking

Table 1
Test matrix.

Specimen	Series	Concrete	Target concrete strength (MPa)	Reinforcement	Bar diameter (mm)	Notches	Reinforcement internal instrumentation
C1F16ni	1	C1	50	GFRP	16	Yes	Yes
C1F16	1	C1	50	GFRP	16	No	No
C2F16ni	2	C2	35	GFRP	16	Yes	Yes
C2F16n	2	C2	35	GFRP	16	Yes	No
C3F16n	3	C3	25	GFRP	16	Yes	No
C3S10n	3	C3	25	Steel	10	Yes	No

results obtained in a previous experimental study [18]. Based on this description, the identification of the tested elements was CxRDni, with Cx standing for the type of concrete (C1, C2, C3), R for the type of reinforcement (F = GFRP, S = steel), D for the reinforcement diameter, with "n" identifying specimens with notched sections, and "i" specimens with reinforcement internally instrumented. The test matrix is summarised in Table 1.

2.2. Material properties

Ready-mix concrete was used to cast the specimens. Compressive strength was determined at the time of loading by standard cylinders test (150 × 300 mm) in accordance with UNE 12390-3. The average values of the mechanical properties are summarised in Table 2.

In order to determine the actual characteristics of GFRP and steel reinforcement, three samples for each material were tested under tension in accordance with UNE ISO 15630-1:2011 and ACI

Table 2
Mechanical properties of concrete.

Concrete	Compressive strength, f_c (MPa)	Elastic modulus, E_c (GPa)
C1	48.9	33.8
C2	33.7	32.0
C3	28.5	30.1

Table 3
Mechanical properties of reinforcement.

Material	Elastic modulus, E_r (GPa)	Tensile/yielding strength (MPa)	Axial stiffness, EA (MN)
GFRP	66.5 ± 2.5	1200 ± 61	13.5 ± 0.5
Steel	206 ± 5.0	520 ± 10	16.2 ± 0.4

440.3R-12 respectively. The average values of the mechanical properties of the reinforcing bars are presented in Table 3.

2.3. Test set-up

Two frames with a double lever system were specially designed and manufactured in order to apply a constant tensile load on the specimens (see Fig. 1). The amplification factor of the mechanical system was 11. Steel housings were glued to both ends of the bars to avoid damaging the bars. The load was progressively applied until 20–25% of the ultimate capacity of the reinforcing bar was reached (in the upper bound limit of sustained service loads according to recommendations). The load was applied using 400 × 400 × 15 mm (18.1 kg) steel plates. Smaller plates of 200 × 200 × 15 mm (4.6 kg) were used when approaching the cracking load to determine its value with more accuracy. The tests were stopped whenever a new crack appeared at the concrete surface, and at each stop the strains were recorded in order to plot their evolution. Member strains were measured along the centre line of the element (coinciding with the position of the reinforcing bar) on two opposite faces by means of a mechanical extensometer with a gauge length of 150 mm between Demec points. Additionally, for Series 2 and 3, a linear variable differential transducer (LVDT) was used to measure member deformation; both the mechanical extensometer and the LVDT measured and recorded deformations along the 900 mm bonded length (see Fig. 2). Specimens C1F16ni and C2F16ni allowed strain distribution along the reinforcing bar to be monitored. To this end, two specially manufactured internally strain gauged reinforcing GFRP bars were used. The original bars were cut into two halves and the strain gauges were placed into of 6 × 4 mm grooves at intervals of 60 mm. Small holes were drilled every 120 mm to allow the gauge wiring to come out of the bar. After protecting the gauges against possible humidity, the bar was closed, with the two halves glued together,

Fig. 1. Frames for long-term tensile tests.

Fig. 2. (a) External instrumentation of the concrete specimens. (b) Internal instrumentation of the GFRP reinforcing bar.

to give the appearance of a normal solid round bar. The bar's surface was not modified, and bond performance was not altered due to its instrumentation.

2.4. Creep and shrinkage

Creep coefficient for each series was determined in accordance with ASTM C5 12-02 [41]. Two concrete cylinders (150 mm diameter and 450 mm length) with embedded strain gauges were stacked in a loading frame. The cylinders were loaded at the same time as the tested elements. Additional specimens were left unloaded and were instrumented to determine free shrinkage strain. Temperature and humidity were also recorded.

The evolution of the experimental shrinkage strains of the three types of concrete, C1 (50 MPa), C2 (35 MPa) and C3 (25 MPa), are shown in Fig. 3a. It is worth mentioning that the different evolution of experimental shrinkage strain for C1, reflected in Fig. 3a, is related to the greater age of the concrete at the time of loading (t_0). Specimens were loaded at the ages of 63, 28 and 35 days for Series 1, 2 and 3 respectively. The average values of experimental free shrinkage strain at time t ($\varepsilon_{sh}(t,t_0)$) are tabulated in Table 4. As can be observed, from 10 to 30 days after loading, the shrinkage strain decreased from $-10 \, \mu\varepsilon$ to $-50 \, \mu\varepsilon$ for C1 (50 MPa), from $-39 \, \mu\varepsilon$ to $-95 \, \mu\varepsilon$ for C2 (35 MPa), and from $-41 \, \mu\varepsilon$ to $-100 \, \mu\varepsilon$ for C3 (25 MPa). Experimental results confirm the influence of concrete strength on the free shrinkage strain, with concrete with lower compressive strengths having higher free shrinkage.

The experimental creep coefficient from the strain measurements of the C1, C2 and C3 cylinders, along with their time

evolution, is presented in Fig. 3b. The coefficient is calculated from the ratio of the creep strain to the instantaneous strain. The creep strain at time $t(\varepsilon_{cp}(t))$ is obtained by subtracting the shrinkage strain, $\varepsilon_{sh}(t,t_0)$, from the total strain $\varepsilon_t(t,t_0)$. As seen in the steep slope of Fig. 3b, at the beginning of the tests (up to approximately 5 days after loading), the creep effect increases significantly over time but thereafter tends to increase slowly. The average values of the experimental creep coefficient ($\varphi(t,t_0)$) are indicated in Table 4. At 10 days after loading, the creep coefficient is 1.06 for C1 specimens, 1.22 for C2, and 1.26 for C3. From 10 to 30 days after loading, the creep coefficient increases from 1.06 to 1.59 for C1, from 1.22 to 1.70 for C2, and from 1.26 to 1.78 for C3, corresponding to an increase of 50%, 39% and 41% of the creep coefficient in C1, C2 and C3 specimens respectively. According to these experimental values, an influence of concrete strength on creep coefficient is observed [42].

The effect of shrinkage occurring before initial loading was assessed, since it would be likely to affect test results depending on its absolute value and the sectional characteristics [19,31]. The reinforcement embedded in the concrete provides restraints to concrete shrinkage, leading to compressive stresses in the reinforcement and tensile stresses in the concrete (see Fig. 4). The two main effects of shrinkage on the final response of the RC tie, therefore, are an initial shortening of the member (ε_{mi}) and a lower cracking load (since concrete is under an initial tensile load, hereafter referred to as P_{add}).

$$\varepsilon_{mi} = \varepsilon_{sh}/(1 + n\rho) \qquad (1)$$

$$|P_{add}| = -\varepsilon_{sh}E_rA_r \qquad (2)$$
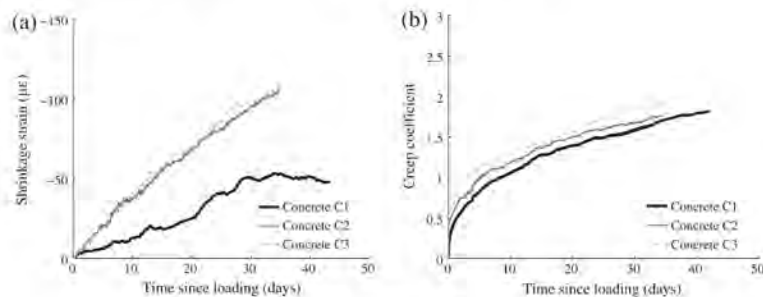
Fig. 3. (a) Experimental free shrinkage strain. (b) Experimental creep coefficient.

Table 4
Experimental time-dependent concrete properties (average values) from the loading day.

Concrete	Time (days) t	Creep coefficient $\varphi(t,t_0)$	Shrinkage strain ($\mu\varepsilon$) $\varepsilon_{sh}(t,t_0)$
C1	10	1.06	−10
C1	30	1.59	−50
C2	10	1.22	−39
C2	30	1.70	−95
C3	10	1.26	−41
C3	30	1.78	−100

Fig. 5. Experimental load-mean strain curves of specimens C1F16ni and C1F16.

Fig. 4. Effect of initial shrinkage [19].

Fig. 6. Experimental load-mean strain curves of specimens C2F16ni and C2F16n.

Table 5
Shrinkage influence on ε_{mi}.

Test Series	ε_{sh}^{*} ($\mu\varepsilon$)	ε_{mi} ($\mu\varepsilon$)
Series 1	−245	−238
Series 2	−171	−166
Series 3 GFRP	−155	−150
Series 3 Steel	−155	−149

* Experimental shrinkage at the time of loading.

Fig. 7. Experimental load-mean strain curves of specimens C3S10n and C3F16n.

where ε_{sh} is the experimental shrinkage at the time of loading, n is the modular ratio ($n = E_r/E_c$) and ρ is the reinforcement ratio.

As noted above, specimens were loaded at the ages of 63, 28 and 35 days for Series 1, 2 and 3 respectively. The experimental values of the recorded shrinkage at the time of loading are used to estimate the initial shortening, ε_{mi}, in accordance with Eq. (1). As shown in Table 5, the higher the shrinkage previous to loading, the higher the values of initial shortening (for bars of similar EA stiffness).

Initial member shortening, ε_{mi}, resulting from shrinkage effects is taken into account when representing the member tensile behaviour (Figs. 5–7) by offsetting the bare bar response with the shortening value ε_{mi} [19].

3. Test results

3.1. Tensile behaviour

Load-strain responses measured during the experimental tests are presented in Figs. 5–7. Mean member strain has been computed as member elongation divided by the 900 mm bonded

length. For comparison purposes, the theoretical uncracked and the fully cracked responses are also plotted.

All the specimens have an initial linear branch with a steep slope corresponding to the uncracked condition. After cracking load (P_{cr}) is reached, a drop in the slope is observed due to the progressive cracking of the element. At this stage, the load–strain response gradually tends towards fully cracked behaviour. The load was progressively applied until the stress in the reinforcing bar reached 20–25% of its tensile strength. This maximum load was thereafter kept constant until the end of the test. The cracking load, the corresponding tensile strength, the number of cracks that

Table 6
Cracking load, number of cracks and time under sustained load.

Specimen	P_{cr} (kN)	f_{cr} (MPa)	Number of cracks	Time under sustained load (days)
C1F16ni	19.6	1.46	5	39
C1F16	24.1	1.65	6	39
C2F16ni	19.6	1.46	4	35
C2F16n	23.6	1.76	4	35
C3F16n	15.7	1.31	4	37
C3S10n	17.7	1.16	4	37

Table 7
Experimental total short-term strain (ε_i), time dependent strain ($\Delta\varepsilon$), sustained load and sustained stress at reinforcement.

Specimen	ε_i ($\mu\varepsilon$)	$\Delta\varepsilon$ ($\mu\varepsilon$)	Sustained load (kN)	Sustained stress in the bar (MPa)
C1F16ni	2666	198	45.3	225
C1F16	2716	274	45.2	224
C2F16ni	2239	388	39.3	195
C2F16n	1956	424	39.4	196
C3F16n	2310	375	39.3	195
C3S10n	1687	390	39.4	501

appeared during the loading process and the time under sustained load are summarised in Table 6, while Figs. 5–7 show the load–mean strain response of test specimens. Markers in the curves represent pauses in the specimen loading process for elongation measurements, while sudden elongations indicate the appearance of new cracks. The order of appearance of cracks is indicated by numbers in the figures.

3.1.1. Series 1

Experimental responses for Series 1 elements are presented in Fig. 5, and similar behaviour can be observed for the two specimens. The differences in cracking load can be attributed to the reduced transversal section and scatter in the cracking load (P_{cr}) of specimen C1F16ni (notched). After cracking, both specimens tend towards fully cracked section behaviour. During the cracking stage, 5 and 6 transversal cracks appeared in specimens C1F16ni and C1F16 respectively. The loading process was stopped at a load of 45.3 kN, equivalent to stress in the reinforcement bar of 225 MPa. At this point, the load was kept constant at a total short-term strain (ε_i) of 2666 $\mu\varepsilon$ and 2716 $\mu\varepsilon$ for specimens C1F16ni and C1F16 respectively, with the load sustained for 39 days for both specimens. The plateau at the end of the load–strain curves shows the deformation increment caused by long-term effects, hereafter referred to as time dependent strain $\Delta\varepsilon$, which was 198 $\mu\varepsilon$ and 274 $\mu\varepsilon$ for specimens C1F16ni and C1F16 respectively.

3.1.2. Series 2

Experimental responses for Series 2 are presented in Fig. 6. During the loading process 4 transversal cracks appeared at the notched sections in both specimens. In this series, the loading process was stopped at a load of 39.3 kN, when there was a stress in reinforcement of 195 MPa. With these loading conditions, the total short-term strains read ε_i = 2239 $\mu\varepsilon$ and ε_i = 1956 $\mu\varepsilon$ for specimens C2F16ni and C2F16n respectively. From these initial conditions, similar long-term deformations were observed during the 35 days of sustained loading, with time dependent strain reading $\Delta\varepsilon$ = 388 $\mu\varepsilon$ and 424 $\mu\varepsilon$ for specimens C2F16ni and C2F16n respectively.

3.1.3. Series 3

Experimental responses for Series 3 are presented in Fig. 7. One of the specimens in this series was reinforced with a 16 mm GFRP bar and the other with a 10 mm steel bar, so that their axial stiffness was as similar as possible (see Table 3). This can be noticed in the curves for fully cracked behaviour in Fig. 7. Despite an unavoidable difference in stiffness, the experimental responses were similar for the two tests, with an analogous cracking load (P_{cr}) and four transverse cracks at the notched sections. The loading process was stopped at a load of 39.3 kN, meaning there was a stress of 501 MPa in steel reinforcement and 195 MPa in GFRP reinforcement (in accordance with their respective sectional areas). The sustained load was maintained for 37 days under these conditions. The total short-term strains were ε_i = 1687 $\mu\varepsilon$ and ε_i = 2310 $\mu\varepsilon$ for specimens

C3S10n and C3F16n respectively, while the time dependent strains for these two specimens were $\Delta\varepsilon$ = 390 $\mu\varepsilon$ and $\Delta\varepsilon$ = 375 $\mu\varepsilon$. According to the experimental results, similar time dependent strain is obtained for a fixed axial stiffness irrespective of the reinforcement material.

Table 7 presents a summary of long-term behaviour exhibited in all the tests. The total short-term strain was bigger for the specimens in Series 1 because of the larger applied load, (which was adapted to the higher value of the cracking load observed). By contrast, specimens in Series 2 and 3 had larger time dependent strains. This can be explained by the lower compressive strength of the concrete in Series 2 and 3, and it being loaded under sustained loads at an earlier age.

3.2. Reinforcement strain and bond stress distributions

The cracking process and the evolution of strains and stresses in the tested specimens can be analysed by looking at the evolution of the reinforcement strain distribution. To this end, two of the GFRP RC elements incorporated internal instrumentation in the reinforcing bar (see Table 1). The locations of the strain gauges allowed the reinforcement strain at the four notched sections and the intermediate sections (Fig. 2b) to be registered.

Experimental reinforcement strain distribution along the bar before and after each crack formation, based on strain gauge readings for specimen C2F16ni, is shown in Fig. 8. The vertical dashed lines represent the location of the notches and every marker in the curves represents a reading from a strain gauge. Before the first cracking, a peak in reinforcement strain distribution can be found at both ends of the RC tensile element. The value of this peak in strain corresponds to that of a fully cracked section. From this section on, reinforcement strain decreases until composite action is attained. At this point the reinforcement strain value equals that of an uncracked section. The first crack appears at P = 21.61 kN, and a maximum peak in reinforcement strain distribution is

Fig. 8. Experimental reinforcement strain distribution during crack formation in the loading process for specimen C2F16ni.

Fig. 9. Experimental reinforcement strain distribution at different times during long-term testing for specimen C2F16ni.

Fig. 10. Experimental slip distribution for specimen C2F16ni at different times during long-term testing.

Fig. 11. Experimental bond distribution for specimen C2F16ni at different times during long-term testing.

displayed at $x = 770$ mm. The second and third cracks, occurring at $P = 25.55$ kN, are captured in reinforcement strain distribution with new peak values of $x = 230$ mm and $x = 410$ mm respectively. Finally, the fourth (and last) crack appears at $P = 27.55$ kN at $x = 590$ mm. This is finally reflected in Fig. 8, where the cracking process and experimental distribution on strains along the member are represented for different load levels.

Once all the cracks are formed, the load is further increased until it reaches about 39 kN, or 20% of the reinforcement tensile strength. This load was kept constant for long-term testing for 35 days. The comparison between experimental reinforcement strain distributions at different times of long-term testing is shown in Fig. 9. Experimental results show an increase in reinforcement strain due to long-term loading, with higher variations at intermediate sections between cracks. This means a reduction in concrete stresses at these sections, and therefore a reduction in the tension stiffening effect.

Further analysis of reinforcement strain distribution makes it possible to study the distribution of bond stresses and concrete-reinforcement slip. The slip can be defined as the difference between the displacement of the reinforcement (u_r) and the displacement of concrete (u_c) as follows:

$$s = u_r - u_c \tag{3}$$

Differentiating Eq. (3) leads to:

$$\frac{ds}{dx} = \varepsilon_r - \varepsilon_c \tag{4}$$

where ε_r is the reinforcement strain and ε_c is the concrete strain for the same section.

Assuming that concrete strain can be disregarded in front of that of the reinforcement, the slip between concrete and reinforcement can be computed as:

$$s = \int_0^x \varepsilon_r(x)\,dx \tag{5}$$

Bond stresses can also be obtained from experimental data on reinforcement strain distribution. Taking the definition of bond as the force transferred between the reinforcing bar and the concrete per unit surface area, and performing equilibrium calculations on a piece of bar of length dx, along with the assumption of linear elastic behaviour of the bar, leads to:

$$\tau = \frac{E_r d_r}{4} \frac{d\varepsilon_r(x)}{dx} \tag{6}$$

where τ is the bond stress, d_r is the reinforcing bar diameter and E_r is the elastic modulus of reinforcement.

Using experimental data of specimen C2F16ni and Eqs. (5) and (6), the experimental slip and bond stress distributions along the reinforcing bar can be obtained as shown in Figs. 10 and 11, respectively. The vertical dashed lines represent the notched sections. The results in Fig. 10 show an increase in slip with time under a sustained load. Moreover, maximum slip matches with the location of the cracks and zero slip values are found in the middle of two consecutive cracks, as expected. Similarly, results in Fig. 11 show that maximum bond stresses are located near the cracked sections and zero bond stresses are found at the midway section between two cracks. Comparison between the curves of bond stresses at the time of application of sustained loading and at the end of the test reveals a deterioration in bond performance due to long-term loading. As an example, the mean value for bond stress at 0.04 days reads 5.3 MPa, and decreases to 3.8 MPa at 35 days. Similarly, the mean value for maximum bond stress decreases from 8.4 MPa to 6.2 MPa over the same period – a reduction in bond stresses of 28.30% and 26.19% respectively. Similar tendencies were observed for specimen C1F16ni, with a mean value for bond stress decreasing from 4.7 MPa to 3.4 MPa, and a mean value for maximum bond stress decreasing from 7.9 MPa to 5.7 MPa, meaning a reduction in the two bond stresses of 27.66% and 27.85%, respectively.

3.3. Concrete tensile stress

The effects of sustained load on RC tensile elements can also be analysed by studying the evolution over time of concrete tensile stresses. This alternative is based on an equilibrium equation for a block of reinforced concrete reading:

$$P = P_c + P_r \tag{7}$$

where P is the applied load, P_c is the force supported by concrete and P_r is the force supported by the reinforcing bar.

Table 8
Comparison between experimental mechanical extensometer and strain gauge readings at different testing times (specimen C2F16ni).

Time (days)	Mechanical extensometer ($\mu\varepsilon$)	Strain gauges ($\mu\varepsilon$)	Difference (%)
0.09	2326	2342	0.68
0.16	2342	2374	1.35
0.26	2371	2408	1.54
0.56	2385	2407	0.91
1.93	2427	2519	3.65
3.29	2446	2546	3.93
3.92	2459	2557	3.83
6.92	2478	2648	6.42
7.95	2502	2659	5.90
9.22	2553	2670	4.38
15.92	2562	2709	5.72
20.92	2572	2730	5.79
24.92	2611	2745	4.88
29.97	2612	2756	5.22

Based on Eq. (7), the evolution of concrete tensile stresses over time can be analysed by means of two different methodologies. The first uses experimental reinforcement strain values. From these readings, bar tensile stresses can be computed and, consequently, concrete stresses can be obtained. The second method requires the assumption of average reinforcement strain being equal to average surface strains computed by means of a mechanical extensometer as performed in [41]. Using this methodology, readings from the extensometer were averaged over the length of the specimen. Based on these average surface strains, concrete stresses were calculated using the following equations:

$$P_r = E_r \varepsilon_r A_r \tag{8}$$

$$\sigma_c = \frac{P - E_r \varepsilon_r A_r}{A_c} \tag{9}$$

where A_r is the reinforcement area and A_c is the concrete area.

For comparison purposes, the average reinforcement strain gauge readings and those of the mechanical extensometer at different times after loading are presented for specimen C2F16ni in Table 8. There is little difference between the measurements. Therefore, and because not all the specimens included internal instrumentation of the reinforcing bar, readings from the mechanical extensometer are used for the study of the evolution of concrete tensile stress for all the specimens. This evolution is presented in Fig. 12, where the concrete stress has been normalised to its initial value. As a general trend, there is a marked decrease in concrete stress (of between 20% and 40%) in a short time period immediately after the application of the sustained load

(around 10 h). Stresses continue decreasing over time at a lower rate and stabilise at approximately 28 days. According to the experimental results, Series 1 specimens (with the highest concrete compressive strength) show the smallest variation in concrete tensile stress due to long-term testing, with a decay of around 38%. For Series 2 and 3 specimens, a greater decrease in concrete tensile stress can be observed, with specimens from Series 3 (with the lowest concrete compressive strength) showing the greatest variation with a decay of around 53%. It should be noted that specimens C2F16ni and C3F16n showed splitting cracks during short-term testing, which explains their even larger loss. Based on these results, the influence of concrete strength on the loss of concrete tensile stress, and therefore on the tension stiffening effect, is clear.

4. Comparison with the EMM approach

In this section, the experimental load–strain behaviour of the tested specimens is compared to theoretical predictions based on the smeared crack approach procedure of Eurocode 2 [40], using the effective modulus method (EMM) for estimating long-term deformations. The mean reinforcement strain at a certain applied load reads:

$$\varepsilon_m = \varepsilon_1 \left[\beta_1 \beta_2 \left(\frac{\sigma_{cr}}{\sigma_r} \right)^2 \right] + \varepsilon_2 \left[1 - \beta_1 \beta_2 \left(\frac{\sigma_{cr}}{\sigma_r} \right)^2 \right] \tag{10}$$

where β_1 stands for the bond characteristics of the internal reinforcing bars (1 for ribbed and 0.5 for smooth bars), β_2 represents the loading type (1 for short term and 0.5 for sustained load), σ_{cr} is the tensile stress in the reinforcing bar for a fully-cracked section when the first crack occurs ($\sigma_{cr} = P_{cr}/A_r$), σ_r is the stress in the reinforcing bar for a fully-cracked section at the actual load ($\sigma_r = P/A_r$), and ε_1 and ε_2 are the reinforcement strains calculated for the uncracked and the fully-cracked states respectively. This equation is applicable both for short and long-term loading.

For the calculation of ε_1 in the uncracked state, the strains between concrete and reinforcement can be considered compatible ($\varepsilon_1 = \varepsilon_c$). To include in Eq. (10) long-term effects in accordance with the concrete constitutive relationship used in the EMM, the concrete strain caused by sustained loading can be computed as:

$$\varepsilon_c(t) = \frac{\sigma_c(t)}{E_c(t, t_0)} + \varepsilon_{sh}(t, t_0) \tag{11}$$

where $\sigma_c(t)$ is the concrete stress, $\varepsilon_{sh}(t, t_0)$ is the free shrinkage strain and $E_c(t, t_0)$ is the effective modulus of elasticity given by:

$$E_c(t, t_0) = \frac{E_c(t)}{1 + \varphi(t, t_0)} \tag{12}$$

where $E_c(t)$ is the modulus of elasticity of concrete at time t and $\varphi(t, t_0)$ the creep coefficient at time t.

Taking the equilibrium equation for a block of reinforced concrete:

$$P = \sigma_c(t)A_c + \sigma_r(t)A_r \tag{13}$$

the reinforcement strain in the uncracked state is found to be:

$$\varepsilon_1(t) = \frac{P - \sigma_c(t)A_c}{A_r E_r} \tag{14}$$

where P is the applied load, A_c is the area of concrete and A_r is the area of reinforcement.

Equating Eqs. (11) and (14) the following expression can be obtained:

$$\frac{\sigma_c(t)}{E_c(t, t_0)} + \varepsilon_{sh}(t, t_0) = \frac{P - \sigma_c(t)A_c}{A_r E_r} \tag{15}$$
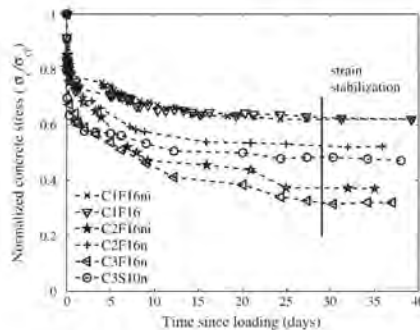
Fig. 12. Evolution of concrete stress over time.
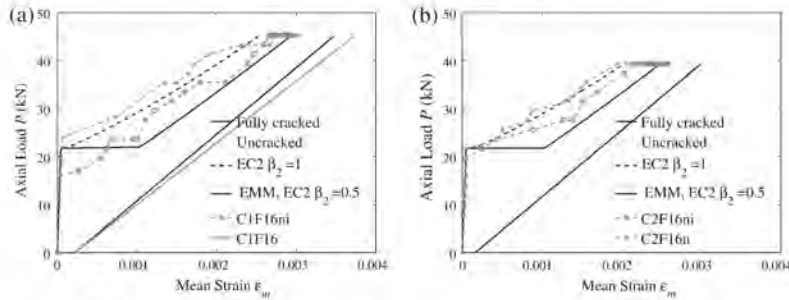
Fig. 13. Comparison of experimental responses and theoretical predictions for specimens of a) Series 1 and b) Series 2.
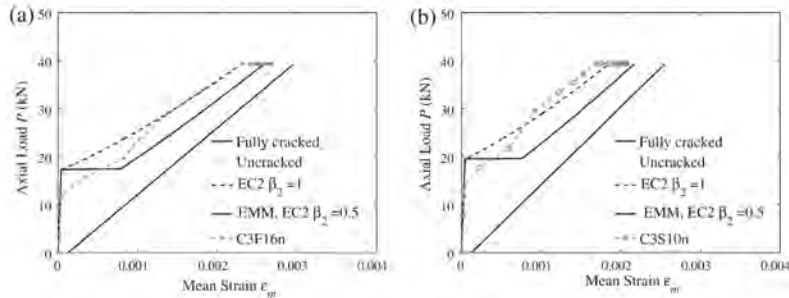
Fig. 14. Comparison of experimental responses and EMM predictions for specimens (a) C3F16n and (b) C3S10n.

Rearranging Eq. (15) results in [43]:

$$\sigma_c(t) = \frac{P}{A_c(1 + n^* \rho)} - \frac{\varepsilon_{csh}(t,t_0) E_r \rho}{1 + n^* \rho} \tag{16}$$

where n^* is the modular ratio between E_r and $E_c(t,t_0)$ and ρ is the reinforcement ratio. Eq. (16) is then substituted in Eq. (11), to obtain the strain in the uncracked state due to sustained loading ($\varepsilon_c(t)$), which finally is used to replace ε_1 in Eq. (10). The experimental values of the aforementioned parameters have been used in this study.

Predictions using this methodology are presented and compared with experimental results in Figs. 13 and 14, under the label "EMM, EC2 $\beta_2 = 0.5$". Additionally, Eurocode 2 predictions for a short-term response and the non-inclusion of long-term effects

are also plotted under the label "EC2 $\beta_2 = 1$". For comparison purposes, the uncracked and the fully cracked responses are also plotted. It should be noted that the cracking load (P_{cr}) used in the predictions for specimens with notched sections has been normalised in accordance with:

$$P_{cr}^* = P_{cr} \frac{A_2(1 + n\rho_2)}{A_1(1 + n\rho_1)} \tag{17}$$

where P_{cr}^* is the normalised cracking load, A_1 is the area of a notched section and A_2 is the area of a section without notches.

Predictions for specimens of Series 1 are presented in Fig. 13a. As can be seen in the plot, Eurocode 2 predictions for short-term testing compare reasonably well with experiments. Regarding long-term analysis, the methodology predicts reasonably accurately

Table 9
Comparison between experimental and analytical long term predictions.

Specimen	ε_{GFRP} ($\mu\varepsilon$)	ε_{cth}^* ($\mu\varepsilon$)	$\varepsilon_{cth}^* / \varepsilon_{cexp}$	ε_{cexp} ($\mu\varepsilon$)	ε_{cth}^{**} ($\mu\varepsilon$)	$\varepsilon_{cth}^{**} / \varepsilon_{cexp}$
C1F16ni	2666	2522	0.95	2864	2925	1.02
C1F16	2716	2522	0.93	2990	2925	0.98
C2F16ni	2239	2028	0.91	2626	2482	0.95
C2F16n	1956	2028	1.04	2380	2482	1.04
C3F16n	2310	2295	0.99	2685	2586	0.96
C3S10n	1687	1854	1.09	2077	2172	1.05
Mean			0.97			1.00
Standard deviation			0.07			0.04

* EC2, $\beta_2 = 1$.
** EEM, EC2, $\beta_2 = 0.5$.

the effect of long-term testing, with predicted time dependent strains ($\Delta\varepsilon$) being similar to the experimental ones.

Experimental and theoretical values for Series 2 specimens are presented in Fig. 13b. While the short-term response for specimen C2F16n is predicted accurately, there is a slight underestimation for specimen C2F16ni. Apart from this, the methodology is again effective in predicting the long-term effects.

Results for Series 3 are plotted in separate figures (see Fig. 14a and b) due to a stiffness difference (see Table 3). The figures demonstrate a good prediction of the cracking process in both short-term and long-term testing.

For the sake of clarity, Table 9 presents a summary of experimental and predicted values for short-term strain (ε_i) and the strain after a sustained load (ε_f). This last strain is computed as the sum of short-term strain and time dependent strain (i.e. $\varepsilon_f = \varepsilon_i + \Delta\varepsilon$). The ratios between experimental and predicted strains are also shown along with the mean and the standard deviation. From these ratios, it can be concluded that the combination of the Eurocode 2 proposal and EMM methodology for the analysis of long-term testing is valid.

5. Conclusions

An experimental study to investigate the tension stiffening effect on GFRP RC tensile elements under sustained loading has been presented. The experiment consisted of an initial short-term loading and a subsequent test under sustained load for a period of between 35 and 40 days. A total of six tensile members with three concrete strengths were tested and analysed. Two specimens included internal instrumentation of the reinforcing bar that allowed monitoring of the strain distribution in both the short-term and the long-term tests.

Based on data from the internal strain gauges, the slip and the bond stresses were computed and analysed. Results show an increase in reinforcement strain due to sustained loading and a degradation in the tension stiffening effect. This reflects the impact of long-term loading on bond deterioration, with 28% reduction in mean bond stresses and increase in slip along the specimen.

Behaviour under sustained load was also studied by analysing the evolution of concrete tensile stresses. A sharp decrease in such stresses was found during the first 10 h after imposing the sustained loading, followed by a smaller reduction that stabilized at approximately 28 days. The experimental results confirm the influence of concrete strength on the loss of tension stiffening, with higher concrete compressive strength showing the smallest decrease of concrete tensile stresses, with a value of around 38% compared to approximately 53% for the lowest concrete strength.

Experimental results from both short and long-term tests have been compared to predictions using Eurocode 2 by applying EMM methodology. The predictions using the methodology compare well with experimental results.

Acknowledgements

References

[1] Nanni A, editor. Fiber reinforced plastic (FRP) reinforcement for concrete structures: properties and applications. Amsterdam: Elsevier; 1993.
[2] GangaRao HVS, Taly N, Vijay PV. Reinforced concrete design with FRP composites. London: Taylor & Francis Group; 2006.
[3] Bank LC. Composites for construction: structural design with FRP materials. New Jersey: John Wiley & Sons; 2006.
[4] Hollaway LC. A review of the present and future utilisation of FRP composites in the civil infrastructure with reference to their important in-service properties. Constr Build Mater 2010;24(12):2419–45.
[5] ACI 440.1R-06. Guide for the design and construction of concrete reinforced with FRP bars. Farmington Hills: American Concrete Institute; 2006.
[6] CSA. Design and construction of building structures with fibre-reinforced polymers (CAN/CSA-S806-012). Canadian Standards Association, Mississauga, Ontario, Canada; 2012. 206p.
[7] CNR. Guide for the design and construction of concrete structures reinforced with fiber-reinforced polymer bars (CNR-DT 203/2006). National Research Council, Rome, Italy; 2007.
[8] Benmokrane B, Chaallal O, Masmoudi R. Flexural response of concrete beams reinforced with FRP reinforcing bars. ACI Struct J 1996;91(2):46–55.
[9] Matthys S, Taerwe L. Concrete slabs reinforced with FRP grids. I: One-way bending. J Compos Construct 2000;4(3):145–52.
[10] Pecce M, Manfredi G, Cosenza E. Experimental response and code models of GFRP RC beams in bending. ASCE J Compos Construct 2000;4(4):182–90.
[11] Al-Sunna R, Pilakoutas K, Hajirasouliha I, Guadagnini M. Deflection behaviour of FRP reinforced concrete beams and slabs: an experimental investigation. Compos B Eng 2012;43(5):2125–34.
[12] Bischoff PH. Deflection calculation of FRP reinforced concrete beams based on modifications to the existing Branson equation. ASCE J Compos Construct 2007;11(1):4–14.
[13] Muhamad R, MS Mohamed A, Oehlers D, Hamid Sheikh A. Load-slip relationship of tension reinforcement in reinforced concrete members. Eng Struct 2011;33(4):1098–106.
[14] Barris C, Torres L, Baena M, Pilakoutas K, Giadagnini M. Serviceability limit state of FRP RC beams. Adv Struct Eng 2012;15:653–63.
[15] Barris C, Torres L, Miàs C, Vilanova I. Design of FRP reinforced concrete beams for serviceability requirements. J Civ Eng Manage 2012;18(6):843–57.
[16] Gribniak V, Kaklauskas G, Torres L, Daniunas A, Timinskas E, Gudonis E. Comparative analysis of deformations and tension-stiffening in concrete beams reinforced with GFRP or steel bars and fibers. Compos B Eng 2013;50:158–70.
[17] Aiello AM, Leone M. Bond performances of FRP rebars-reinforced concrete. J Mater Civ Eng 2007;19(3):205–13.
[18] Baena M, Torres L, Turon A, Mias C. Experimental study and code predictions of fibre reinforced polymer reinforced concrete (FRP RC) tensile members. Compos Struct 2011;93:2511–20.
[19] Bischoff PH. Effects of shrinkage on tension stiffening and cracking in reinforced concrete. Can J Civ Eng 2001;28(3):363–74.
[20] Robert M, Benmokrane B. Combined effects of saline solution and moist concrete on long-term durability of GFRP reinforcing bars. Constr Build Mater 2013;38:274–84.
[21] Masmoudi R, Masmoudi A, Ouezdou MB, Daoud A. Long-term bond performance of GFRP bars in concrete under temperature ranging from 20 °C to 80 °C. Constr Build Mater 2011;25(2):486–93.
[22] Robert M, Benmokrane B. Effect of aging on bond of GFRP bars embedded in concrete. Cem Concr Compos 2010;32(6):461–7.
[23] Hall T, Ghali A. Long-term deflection prediction of concrete members reinforced with glass fibre reinforced polymer bars. Can J Civ Eng 2000;27(5):890–8.
[24] Arockiasamy M, Chidambaram S, Amer A, Shahawy M. Time-dependent deformations of concrete beams reinforced with CFRP bars. Compos B Eng 2000;31(6–7):577–92.
[25] Al-Salloum YA, Almusallam TH. Creep effect on the behavior of concrete beams reinforced with GFRP bars subjected to different environments. Constr Build Mater 2007;21(7):1510–9.
[26] Mias C, Torres L, Turon A, Baena M, Barris C. A simplified method to obtain time-dependent curvatures and deflections of concrete members reinforced with FRP bars. Compos Struct 2010;92:1833–8.
[27] Torres L, Mias C, Turon A, Baena M. A rational method to predict long-term deflections of FRP reinforced concrete members. Eng Struct 2012;40:230–9.
[28] Mias C, Torres L, Turon A, Sharaky IA. Effect of material properties on long-term deflections of GFRP reinforced concrete beams. Constr Build Mater 2013;41:99–108.
[29] Mari AR. Numerical simulation of the segmental construction of three dimensional concrete frames. Eng Struct 2000;22:585–96.
[30] Torres L, López-Almansa F, Cahis X, Bozzo LM. A numerical model for sequential construction, repairing and strengthening of 2-D concrete frames. Eng Struct 2003;25(3):323–36.
[31] Kaklauskas G, Gribniak V, Bacinskas D, Vainiunas P. Shrinkage influence on tension stiffening in concrete members. Eng Struct 2009;31(6):1305–12.
[32] Visintin P, Oehlers DJ, Haskett M. Partial-interaction time dependent behaviour of reinforced concrete beams. Eng Struct 2013;49:408–20.

[33] Gribniak V, Bacinskas D, Kacianauskas R, Kaklauskas G, Torres L. 2012 Long-term deflections of reinforced concrete elements: accuracy analysis of predictions by different methods. Mech Time-Depend Mater 2013;17(3): 297–313.

[34] Scott RH, Beeby AW. Long-term tension-stiffening effects in concrete. ACI Struct J 2005;102(6):904–5.

[35] Wu H, Gilbert R. An experimental study of tension stiffening in reinforced concrete members under short-term and long-term loads. Tech rep. The University of New South Wales; 2008.

[36] Zanuy C. Analytical approach to factors affecting long-term tension stiffening. Mag Concr Res 2010;62:869–78.

[37] Beeby AW, Scott RH. Mechanisms of long-tern decay of tension stiffening. Mag Concr Res 2006;58(5):255–66.

[38] Nkurunziza G, Benmokrane B, Debaiky AS, Masmoudi R. Effect of sustained load and environment on long-term tensile properties of glass fiber-reinforced polymer reinforcing bars. ACI Struct J 2005;102(4):615–21.

[39] Mazzotti C, Savoia M. Stress redistribution along the interface between concrete and FRP subjected to long-term loading. Adv Struct Eng 2009;12(5):651–61.

[40] CEN. Eurocode 2 design of concrete structures – Part 1: General rules and rules for buildings. ENV 1992-1-1 Brussels; 1992.

[41] ASTM. Standard test method for creep of concrete in compression, vol. 04.02; 2008.

[42] Neville AM. Properties of concrete. 4th ed. Harlow, England: Longman Group Limited; 1995.

[43] Gilbert R. Time effects in concrete structures. Amsterdam: Elsevier Science Ltd.; 1988.

Appendix D

Experimental study of bond-slip of GFRP bars in concrete under sustained loads

Contents lists available at ScienceDirect

Composites Part B

composites

Experimental study of bond-slip of GFRP bars in concrete under sustained loads

CrossMark

I. Vilanova, M. Baena*, L. Torres, C. Barris

Analysis and Advanced Materials for Structural Design (AMADE), Polytechnic School, University of Girona, Campus Montilivi s/n, 17071 Girona, Spain

ARTICLE INFO

ABSTRACT

The structural behaviour of reinforced concrete (RC) elements depends heavily on the bond performance between the concrete and the reinforcing material. Bond behaviour under short-term testing has been extensively analysed for steel reinforcement and many studies have been carried out for fibre reinforced polymer (FRP) reinforcement. However, there has only been limited investigation of the long-term effects of this interaction. Several factors can affect the long-term bond behaviour of these elements, the most important being bond length and the immediate and time-dependent properties of reinforcement and concrete (concrete grade, creep, shrinkage and stiffness). This time-dependent behaviour is likely to cause changes and redistributions in bond stresses not properly considered in the limited existing literature. In this experimental study, the bond performance of GFRP RC under sustained load is investigated through pull-out tests. A total of 12 pull-out specimens were tested for a period of between 90 and 130 days. Two concrete strengths (35 MPa and 50 MPa), two bond lengths (5 and 10 times the diameter of the reinforcing bar) and two reinforcing materials (glass fibre reinforced polymer (GFRP) and steel) were used. Experimental results regarding immediate and time-dependent slip are presented and analysed here. In addition, some specimens were instrumented, with internal strain gauges in the reinforcing bar to provide data on the reinforcement strain, thus allowing the distribution of bond stresses and their evolution during sustained loading to be also presented and analysed.

© 2015 Elsevier Ltd. All rights reserved.

1. Introduction

Fibre reinforced polymer (FRP) bars are increasingly being used as an alternative to steel reinforcement for reinforced concrete (RC) elements in corrosive environments or when the effects of electromagnetic fields may be present [1–3]. This has led to an increasing interest in the knowledge of properties and the study of different aspects of behaviour of FRP RC structures [4–14]. The viability of these recently introduced materials largely depends on the effectiveness of the bond between the FRP bar and the concrete. In this regard, pull-out tests are probably one of the tests most extensively used to characterize the behaviour of the interface between the reinforcement and the concrete by means of bond-slip response. In the last two decades, considerable experimental research has gone into investigating the short-term response of FRP-to-concrete interfaces [15–24], with it being generally concluded that the pull-out mechanism of the many existing types of FRP reinforcement differs from that of deformed steel bars and is dependent on even more parameters [20,25].

When analysing time effects on the behaviour of RC elements, concrete creep and shrinkage play a crucial role [26–32]. While creep is associated with sustained stresses, shrinkage may be assumed to be independent of load, but both cause long-term deformations in concrete. For common steel RC no additional long-term effects need to be considered because steel undergoes neither shrinkage nor creep. Few studies have focused on the possible effect of creep in FRP reinforcement. An experimental programme with regard to such an effect in aggressive environments was presented in Ref. [33]. The programme consisted of testing twenty GFRP bars in tension for 417 days at two loading levels (25% and 38% of the ultimate bar tensile strength). The results showed that creep strain in the GFRP bars was less than 5% of the initial strain value. It was also concluded that long-term loading had a minimal effect on the elastic modulus, whilst the effect on residual strength was more dependent on the environmental conditions. A more recent programme was presented in Ref. [34], where GFRP pultruded laminates were tested under a tensile

* Corresponding author. Tel.: +34 972419517; fax: +34 972418098.
E-mail address: marta.baena@udg.edu (M. Baena).

sustained load for 500 days. The authors observed that the largest increments in longitudinal stresses due to long-term testing were less than 2%. The components (matrix and reinforcement or polyester resin and glass fibres) were tested separately to check their individual long-term responses. A significant increase in longitudinal strain was observed for the polyester resin while only a negligible increase was obtained for the glass fibres.

The literature dealing with time effect on the bond behaviour of FRP reinforcement and concrete is also limited in extent [35–38]. An experimental study of long-term behaviour of CFRP externally reinforced concrete elements covering three bond lengths and two loading levels was presented in Ref. [35], where the evolution of reinforcement axial stresses and bond stresses under constant tensile load was analysed over 900 days of testing. Results showed a redistribution of bond stresses along the anchorage due to creep deformations at the interface. In respect of internal reinforcement, degradation of the bond between FRP bars and concrete under sustained load was analysed in Ref. [36] through a pull-out testing procedure. The experimental work included four different reinforcing materials as well as different environmental conditions, with pull-out specimens being loaded for one year at different loading levels. Results showed an increase in slip with time, with this increase being dependent on the bar surface treatment and the level of sustained load. A more recent experimental study of the bond behaviour of internal GFRP reinforcement and concrete under sustained loading was presented in Ref. [37]. The pull-out specimens, which combined three different bar diameters, were preloaded until one millimetre of slip was observed at the unloaded end. Following this, the specimens were loaded until slip stabilization. The tests were considered to be acceptable if no increase in slip was observed after 2000 h. To simulate accelerated long-term testing, the tests were conducted at 60 °C, and a design value of bond strength was proposed by the authors based on the experimental data. The long-term effect on steel and GFRP internally reinforced concrete members under tension has been analysed in a study made by the present authors [38]. The experimental programme included three different concrete strengths and two different reinforcing materials. The evolution of reinforcement strains was monitored, and slips and bond stresses were analysed. Results showed that long-term testing caused a reduction in mean bond stress of about 28%, which highlights the importance of analysing and understanding bond behaviour in the long term. Since limited literature exists on this issue, an experimental long-term bond test programme is needed.

This paper presents the results of an experimental campaign consisting of twelve pull-out specimens tested under sustained axial load for a period between 90 and 130 days. The programme included two concrete strengths, two reinforcing materials and two bond lengths. The sustained load level was set at 15% of the ultimate capacity of the GFRP reinforcing bar to ensure it corresponded to the service load range. Experimental results in terms of immediate and time-dependent slip are presented and analysed. Some specimens were instrumented, with internal strain gauges in the reinforcing bar, to provide data on the reinforcement strain, thus allowing the distribution of bond stresses and their evolution during sustained loading to be analysed.

2. Experimental programme

2.1. Test matrix

The experimental programme was aimed at studying the effect of concrete strength, reinforcing material and bond length on the bond response of pull-out tests under sustained loading. Two different target concrete compressive strengths (35 and 50 MPa),

two different bond lengths (equal to $5d_r$ and $10d_r$, with d_r being the nominal diameter of the reinforcing bar) and two reinforcing materials (GFRP and steel) were considered. So that axial stiffness (EA) would be similar in all tests, the reinforcement consisted of either a single 16 mm diameter GFRP bar or a single 10 mm diameter steel bar. The combination of these variables gave a total of eight specimens. So that the internal distribution of bond stresses could be analysed, four additional specimens were manufactured that included internal instrumentation of the GFRP reinforcing bar. Thus, the test matrix consisted of twelve pull-out specimens divided into two groups of six specimens each according to concrete grade.

Based on this description, the tested elements are identifiable by the formula CxBRi, with Cx standing for the type of concrete (C1 = 35 MPa, C2 = 50 MPa), B for the bond length (S = $5d_r$, L = $10d_r$), R for the type of reinforcement (F = GFRP, S = Steel), and "i" for the identification of specimens with internally instrumented reinforcement. The test matrix is summarized in Table 1.

All the specimens were cubic (200 mm sides) with a 600 mm bar located in the middle. Before casting, the bond length was appropriately marked, and a plastic tube was positioned to prevent contact along the remaining bar length. Steel housings were glued to the GFRP bars so that the pull-out load could be applied without damaging the bars.

2.2. Material properties

Ready-mixed concrete was used to cast the specimens. Compressive strength was determined at the time of loading (35 days after casting) by a standard cylinder test (150 × 300 mm) according to UNE 12390-3 [39]. The average values of the mechanical properties are summarized in Table 2.

In order to determine the characteristics of the GFRP and steel reinforcement, three samples for each material were tested under tension according to UNE ISO 15630-1:2011 [40] and ACI 44.3R-12 [41] respectively. The average values of the mechanical properties of the reinforcing bars are given in Table 3.

2.3. Test set-up

Three frames with a double lever system were used to apply a constant tensile load on the pull-out specimens (see Fig. 1). The amplification factor of the mechanical system was 11. In each frame, two pull-out specimens with the same reinforcing bar and concrete grade but of different bond length were connected in series (i.e. specimen C1SS was connected in series with specimen C1LS), which meant that the same load was applied to both

Table 1
Test matrix.

Specimen	Concrete	Bond length, l_b (mm)	Reinforcement	Reinforcement internal instrumentation
C1SS	C1	50	Steel	No
C1SF	C1	80	GFRP	No
C1SFi	C1	80	GFRP	Yes
C1LS	C1	100	Steel	No
C1LF	C1	160	GFRP	No
C1LFi	C1	160	GFRP	Yes
C2SS	C2	50	Steel	No
C2SF	C2	80	GFRP	No
C2SFi	C2	80	GFRP	Yes
C2LS	C2	100	Steel	No
C2LF	C2	160	GFRP	No
C2LFi	C2	160	GFRP	Yes

Table 2
Mechanical properties of concrete.

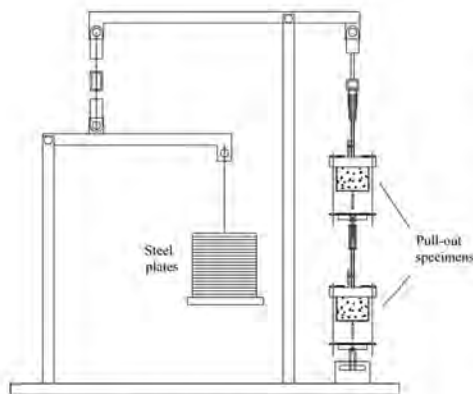| Concrete	Compressive strength, f_c (MPa)	Elastic modulus, E_c (GPa)
C1	35.5	32.1
C2	48.5	35.3

Table 3
Mechanical properties of reinforcement.

Material	Elastic modulus, E_r (GPa)	Tensile/Yielding strength (MPa)	Axial stiffness, EA (MN)
GFRP	66.5 ± 2.5	1200 ± 61	13.5 ± 0.5
Steel	206 ± 5.0	520 ± 10	16.2 ± 0.4

Table 4
Maximum loads.

Specimens	P_{max} (kN)
C1SS, C1LS	10.5
C1SF, C1LF	29.5
C1SFi, C1LFi	29.5
C2SS, C2LS	10.5
C2SF, C2LF	29.5
C2SFi, C2LFi	29.5

specimens. A maximum load equal to 15% of the ultimate capacity of the GFRP bar was selected (see Table 4), in order to correspond to the service load range (ACI 440 1.R-06 [42] fixes a limit of 20% for GFRP bars). The sustained load applied to the steel reinforced specimens was adapted (by means of the bond perimeter) so as to obtain similar bond stresses to those of GFRP reinforced pull-outs.

To perform the test the load was applied progressively using $400 \times 400 \times 15$ mm (18.1 kg) steel plates, until the loads indicated in Table 4 were reached. These maximum loads were thereafter sustained for 90 days in the case of series C1 and 130 days in series C2.

To measure the slip at both the loaded and the unloaded end, two displacement transducers (HLS) were used for each pull-out specimen (see Fig. 2a). Four of the twelve pull-out specimens allowed monitoring of the strain distribution along the bar. These specimens were cast using specially manufactured internally strain gauged GFRP bars [38,43]. The location of the internal instrumentation is shown in Fig. 2b. In the case of the short bond length specimens, four and two strain gauges were placed along and outside the bond length respectively. For long bond length specimens, the number of gauges located along the bond length was doubled to eight.

Fig. 1. Frame for long-term testing.

2.4. Shrinkage and creep

The creep coefficient for each series was determined in accordance with ASTM C5 12-02 [44]. Two concrete cylinders (150 mm in diameter and 450 mm in length) with embedded strain gauges were stacked in a loading frame. The cylinders were loaded at the same time as the pull-out specimens. An additional 200 mm cubic concrete specimen was instrumented and left unloaded to determine free shrinkage strain.

Temperature and humidity were also recorded. An average temperature and relative humidity of 16 ± 2.5 °C and $40 \pm 23.5\%$ were registered for the C1 series. These registers changed to 27 ± 3.5 °C and $49 \pm 15\%$ for the C2 series. Recorded values are shown in Fig. 3.

The evolution of the shrinkage strains recorded for the two types of concrete is shown in Fig. 4a. The values of free shrinkage strains recorded at time t ($\epsilon_{sh}(t,t_0)$) are indicated in Table 5. As can be observed, from 10 to 90 days the shrinkage strain increased from -46 με to -190 με for C1 (35 MPa), and from -36 με to -182 με for C2 (50 MPa). At 90 days, the shrinkage strain of concrete C1 was 4.2% greater than that of concrete C2.

The experimental creep coefficient obtained from the strain measurements of the C1 and C2 series, calculated from the ratio of creep strain to instantaneous strain, is shown in Fig. 5. The creep strain at time t ($\epsilon_\varphi(t)$) is obtained by subtracting the shrinkage strain, $\epsilon_{sh}(t,t_0)$ from the total strain $\epsilon_t(t,t_0)$ [30,38]. At the beginning of the test the creep effect increases considerably with time, but thereafter tends to increase slowly. The average values of experimental creep coefficient ($\varphi(t,t_0)$) are indicated in Table 5. At 10 days after loading, the creep coefficient reads 1.00 and 0.74 for C1 and C2 respectively. From 10 to 90 days after loading, it increases from 1.00 to 1.88 for C1 and from 0.74 to 1.37 for C2, corresponding to increases of 88% and 85% respectively. The influence of concrete strength on creep coefficient is observable in these values, with the creep coefficient at 90 days of C1 being around 1.37 times greater than that of C2.

3. Test results

The results obtained in the experimental tests described in Section 2 are presented and discussed in the following. Particularly, the immediate value and the time-development of the relative slip measured at the bar–concrete interface are specifically considered. As stress distribution is not constant along the bond length in a pull-out test, an average bond stress is defined as:

$$\tau_{av} = \frac{P_{max}}{\pi d_r l_b} \tag{1}$$

where τ_{av} is the average bond stress applied to the interface, P_{max} is the maximum load applied to the bar, d_r is the bar diameter and l_b is the bond length.

For the test set-up, the pull-out specimens were loaded in pairs of equal concrete grade and with the same reinforcing bar, but

45
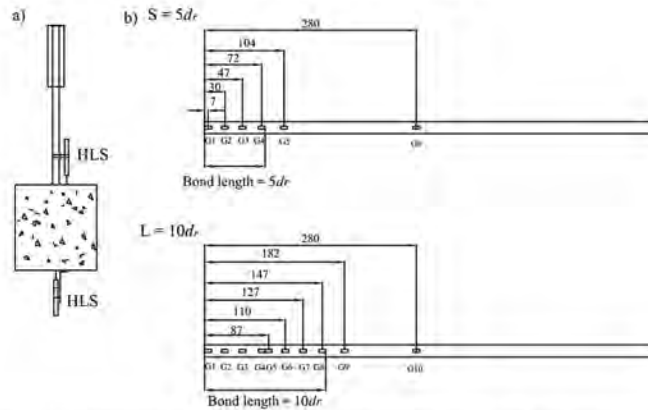
Fig. 2. a) External instrumentation of the pull-out specimens b) Internal instrumentation of the GFRP reinforcing bar (distance in mm).
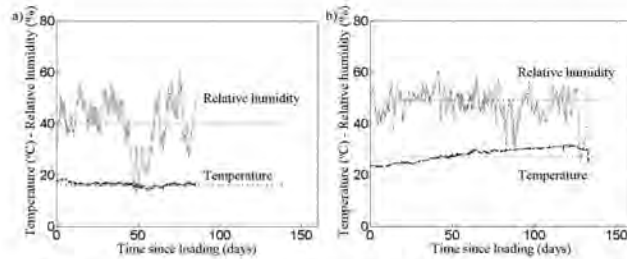
Fig. 3. Temperature and relative humidity registered in the laboratory during a) C1 tests and b) C2 tests.

different bond length (i.e. specimen C1SS and C1LS in series, specimens C1SF and C1LF in series, and so on). As a result, the average bond stress induced in short bond length specimens was twice that in long bond length specimens (see Table 6).

Experimental total slips versus time after loading are shown in Figs. 6 and 7. The total slip includes both the immediate slip due to instantaneous loading and the time-dependent slip due to sustained loading. As can be observed, the curves have a similar trend, with a larger immediate slip for short bond length specimens.

3.1. Immediate slip

Experimental data on the immediate response is given in Table 3 and analysed in this section. As can be seen values of registered slips are influenced by bond length, concrete strength and type of bar as has been reported in previous studies [19–24].

Irrespective of the type of bar and bond length, slips are larger for lower concrete strength which is a consequence of larger local deformability and damage in the concrete surrounding the bar.
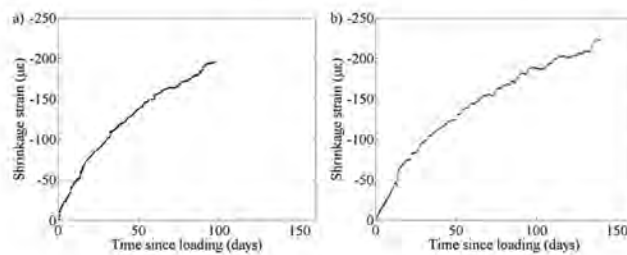
Fig. 4. Experimental free shrinkage strain of a) C1 series and b) C2 series.

Table 5
Experimental time-dependent concrete properties (average values) from the loading day.

Concrete	Time, t (days)	Creep coefficient, $\varphi(t,t_0)$	Shrinkage strain, $\varepsilon_{sh}(t,t_0)$ (µε)
C1	10	1.00	−46
C1	50	1.57	−134
C1	90	1.88	−190
C2	10	0.74	−36
C2	50	1.19	−123
C2	90	1.37	−182
C2	130	1.57	−223

Table 6
Maximum applied loads and average bond stresses at the interface.

Specimen	P_{max} (kN)	Average bond stress, τ_{av} (MPa)
C1SS	10.5	6.71
C1SF	29.5	7.33
C1SFi	29.5	7.32
C1LS	10.5	3.35
C1LF	29.5	3.67
C1LFi	29.5	3.66
C2SS	10.5	6.71
C2SF	29.5	7.33
C2SFi	29.5	7.32
C2LS	10.5	3.35
C2LF	29.5	3.67
C2LFi	29.5	3.66

Likewise, slips are larger for specimens with lower bond lengths due to the higher bond stresses needed to transfer similar loads. It is also observed that the difference in slips between loaded and unloaded end is larger for the FRP bars as reported in Refs. [19,21]. This may be attributable to the higher deformability of the FRP bars jointly with a more effective mechanical interlock between bars and concrete due to the material and surface characteristics. Comparing similar specimens with different type of bar, slips are generally higher for the FRP bars, which indicates a lower slope in the bond stress-slip response. The only exception is for the slip at the unloaded end in specimens with short bond length and C1 concrete, which may be attributable to the combination of higher bar stiffness and damage introduced in the concrete for this short bond length. Globally, these differences in slips between both ends indicate a non-uniform distribution of stresses along the bonded length, which is more pronounced for larger bond lengths [23,24].

3.2. Time-dependent slip

For the sake of clarity and to make analysing the long-term experimental results easier, in Figs. 8 and 9 the immediate slip has been removed, so that only the experimental time-dependent slip (Δs) is presented. In addition, representative time-dependent slips at different times during long-term testing have been tabulated in Table 8.

Both Figs. 8 and 9 and Table 8 confirm the minimal effect of long-term testing on the slip at the unloaded end. As an example, time-dependent slip at 90 days (Δs_{90}) is below 0.012 mm for steel specimens and below 0.022 mm for GFRP specimens. Larger time-dependent slips are observed for the loaded end. An analysis of the evolution of these slips is presented below.

Experimental time-dependent slip results for C1 specimens are given in Fig. 8. As can be seen in the slopes of the curves, at the beginning of the sustained loading test the slip increases considerably over time, but thereafter tends to increase more slowly. Changeover takes place at around 60 days, when an average of

89.7% and 97.8% of the time-dependent slip at 90 days (Δs_{90}) is achieved for short and long bond length specimens respectively. Finally, the time-dependent slip at 90 days (Δs_{90}) for specimens with a long bond length is 1.94 times that of specimens with a short bond length.

Similar trends can be observed in C2 specimens (see Fig. 9 and Table 8). In this series, the sustained load was applied for a total of 130 days, making stabilization much clearer. In fact, based on the stabilization observed previously in this series, the C1 series was designed to consist of 90 days' testing. At 60 days an average of 95.5% and 95.9% of the time-dependent slip at 90 days (Δs_{90}) was achieved for short and long bond length specimens respectively. In this series, the time-dependent slip at 90 days (Δs_{90}) for specimens with long bond length was 1.49 times that of short bond length specimens. According to these results, the time-dependent slip at 90 days (Δs_{90}) in the C2 series is around 23.3% lower than in the C1 series. This difference could be attributable to the mechanical properties of concrete (immediate and time-dependent), where lower concrete strength produces higher time-dependent slips, as would be expected.

A summary of experimental time-dependent slips at 60 and 90 days after loading (Δs_{60}, and Δs_{90}) is shown in Table 8. Additionally, the time-dependent slip at 130 days (Δs_{130}) is also reported for the C2 series.

3.3. Bond stresses — distribution and evolution

Experimental results show an increase in pull-out slips due to sustained loading, attributable to bond deterioration. There are no means of directly registering the bond taking place at an interface, but bond can be estimated from strain distribution along the bond length, as shown in previous works [35,38,43].
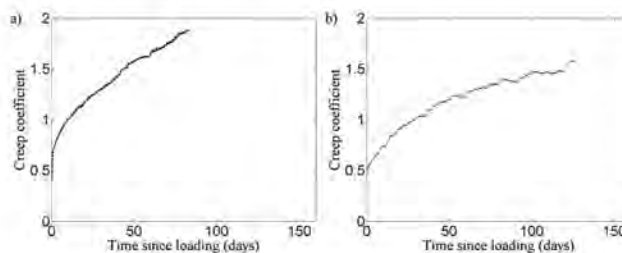
Fig. 5. Experimental creep coefficient of a) C1 series and b) C2 series.
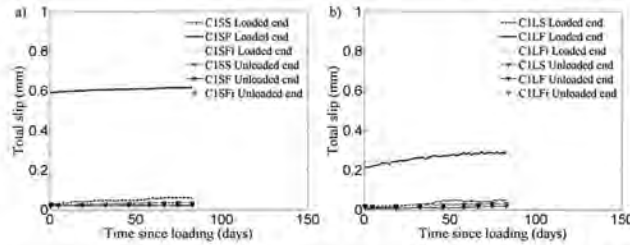
Fig. 6. Experimental total slip vs. time after loading for C1 specimens with a) short bond length and b) long bond length.

Fig. 7. Experimental total slip vs. time after loading for C2 specimens with a) short bond length and b) long bond length.

Table 7
Experimental results for immediate slip.

Specimen	Immediate slip (mm)	
	Loaded end	Unloaded end
C1SS	0.028	0.025
C1SF	0.590	0.019
C1SFi	0.591	0.021
C1LS	0.018	0.006
C1LF	0.216	0.014
C1LFi	0.233	0.015
C2SS	0.021	0.006
C2SF	0.424	0.016
C2SFi	0.401	0.015
C2LS	0.016	0.002
C2LF	0.148	0.010
C2LFi	0.158	0.009

As indicated previously, this experimental investigation included four pull-out specimens whose reinforcement was internally strain gauged so that data on the reinforcement strains along the bond length would be available. In this section, the reinforcement strain distributions are presented and analysed. In a further step, these strain distributions are used for the analysis of the bond profile and redistribution of bond stresses over time which take place due to sustained loading.

3.3.1. Reinforcement strain distribution

Fig. 10 shows the strain gauge readings at various locations along the bond and unbonded length (see Fig. 2b), with location 0 mm representing the unloaded end of the pull-out specimen. The figure includes two different sets of information. First, strain development with load is represented at the very first curves (plotted at 0 days after loading). These curves were registered during the instantaneous test, where load was progressively applied until 15% of the ultimate capacity of the GFRP reinforcing

Fig. 8. Experimental time-dependent slip vs. time after loading for C1 specimens with a) short bond length and b) long bond length.
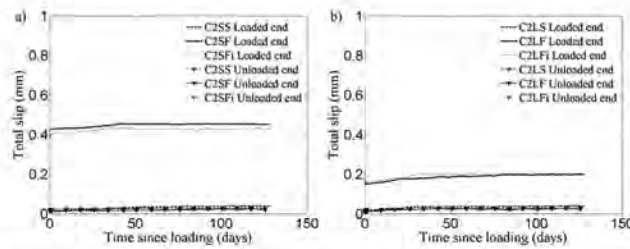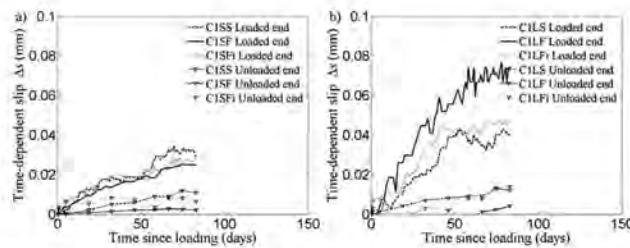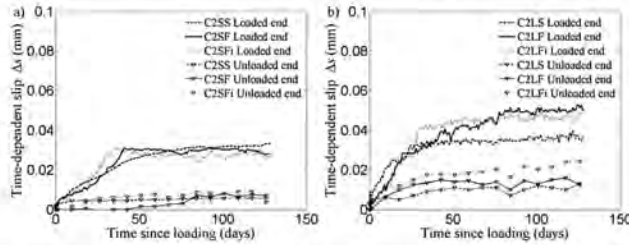
Fig. 9. Experimental time-dependent slip vs. time after loading for C2 specimens with a) short bond length and b) long bond length.

Table 8
Experimental time-dependent slip at different times during long-term testing.

Specimen	Δs_{60} (mm)		Δs_{90} (mm)		Δs_{130} (mm)	
	Loaded	Unloaded	Loaded	Unloaded	Loaded	Unloaded
C1SS	0.029	0.009	0.029	0.011	–	–
C1SF	0.023	0.002	0.024	0.002	–	–
C1SFi	0.022	0.007	0.030	0.006	–	–
C1LS	0.040	0.009	0.040	0.012	–	–
C1LF	0.074	0.003	0.074	0.004	–	–
C1LFi	0.044	0.008	0.047	0.010	–	–
C2SS	0.028	0.005	0.031	0.006	0.030	0.006
C2SF	0.030	0.002	0.030	0.007	0.031	0.008
C2SFi	0.026	0.008	0.027	0.008	0.030	0.009
C2LS	0.036	0.010	0.036	0.010	0.037	0.011
C2LF	0.043	0.014	0.049	0.014	0.050	0.013
C2LFi	0.046	0.018	0.046	0.022	0.048	0.021

bar was reached. Second, strain development with time is represented with the help of the third axis. These curves were registered during the long-term test, when load was sustained for 90 days in the case of the C1 series and 130 days for the C2 series. For practical reasons, only data regarding specimen C1LFi is shown in Fig. 10, although this information is also available for specimens C1SFi, C2SFi and C2LFi.

Fig. 11 shows the reinforcement strain distribution at different load levels at the time of loading (instantaneous pull-out corresponding to 0 days in Fig. 10), with location 0 mm representing the unloaded end of the pull-out specimen and the vertical dashed lines representing the location of strain gauges (see Fig. 2b). The

bond length is clearly marked to help in the analysis of the results. Some of the strain gauges failed during the test, and therefore no data is recorded at some locations. For example, the strain gauge at 104 mm from the unloaded end of specimen C1SFi failed, and this is evident in Fig. 11a, where no marker exists at that location. In this case, for illustrative purposes, and because this gauge was located outside the bond length, its value was assumed to be the same as that of location 280 mm, also located outside the bond length.

A significant difference can be observed between Fig. 11a and b. The loading process in the short bond length is characterized by a quasi linear distribution of strains (see Fig. 11a) along the bond length, whereas in the case of long bond length a clearer non-linear distribution is obtained (see Fig. 11b). According to these results, bond stresses are more evenly distributed in a short bond length, with the entire bond region contributing to the stress transfer process. On the other hand, for specimens with long bond length the transfer length increases with the applied load.

Reinforcement strain distribution at different times during long-term testing is shown in Table 9 and Figs. 12 and 13. As in previous figures, location 0 mm represents the unloaded end, vertical dashed lines represent the location of strain gauges and bond length is clearly marked.

Irrespective of the length of the bond zone and the concrete grade, experimental results show that no significant increase in the readings of the strain gauges located in the unbonded zone is visible at the service load levels applied in the present work (see section 2.3). This means that no appreciable creep due to sustained loading occurred in the GFRP bar as expected. In the region within the bond length, the effect of sustained load is reflected in an
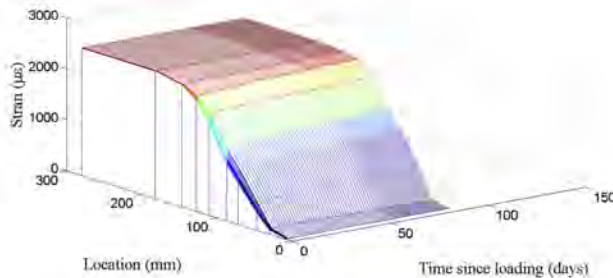

Fig. 10. Experimental reinforcement strain distribution over time for specimen C1LFi.
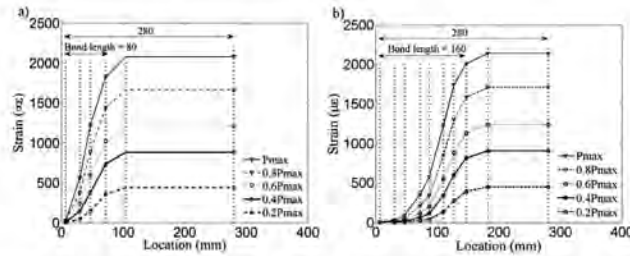
Fig. 11. Experimental reinforcement strain distribution at different loads during instantaneous pull-out test for specimen with a) short bond length (C1SFi) and b) long bond length (C1LFi).

increase in the strain gauge readings, with higher rates occurring at the intermediate zone between loaded and unloaded ends. This can be attributed to bond deterioration and redistribution of stresses, which is lower in more damaged zones (i.e. close to loaded end) and in zones with low levels of stress (i.e. unloaded end in specimens with larger bond length). This is indicated by the area between curves after loading and 90 days in Figs. 12 and 13. The stabilization of this redistribution occurs at approximately 30 days after loading in the case of the C1 series (see Fig. 12). For the C2 series, the increase in strains slows down and stabilizes at the end of long-term testing (see Fig. 13). In situations in which creep could not be ignored, higher deformations and therefore larger redistributions and slips would be expected.

Table 9
Experimental instantaneous strain and time-dependent strain at different times during long-term testing.

Specimen	Strain gauge	Position (mm)	Instantaneous strain, ε_{inst} (µε)	Strain at 60 days, ε_{60} (µε)	Strain at 90 days, ε_{90} (µε)	Strain at 130 days, ε_{130} (µε)
C1SFi	G1	7	63	150	276	–
	G2	30	948	1680	1702	–
	G3	47	1582	2070	2084	–
	G4	72	2123	2250	2243	–
	G5	104	Failed			
	G6	280	2421	2422	2423	–
C1LFi	G1	7	8	30	31	–
	G2	30	73	90	87	–
	G3	47	307	660	645	–
	G4	72	731	1260	1270	–
	G5	87	1008	1590	1615	–
	G6	110	1688	2091	2121	–
	G7	127	2115	2370	2390	–
	G8	147	2385	2438	2449	–
	G9	182	2494	2496	2497	–
	G10	280	2493	2496	2495	–
C2SFi	G1	7	Failed			
	G2	30	567	930	983	1077
	G3	47	1013	1417	1474	1563
	G4	72	1981	2260	2280	2319
	G5	104	Failed			
	G6	280	Failed			
C2LFi	G1	7	14	126	142	161
	G2	30	Failed			
	G3	47	115	342	377	422
	G4	72	368	902	941	990
	G5	87	531	1189	1256	1319
	G6	110	930	1637	1702	1781
	G7	127	1233	1845	1916	2037
	G8	147	1711	2082	2239	2215
	G9	182	2269	2270	2272	2274
	G10	280	2272	2273	2273	2274

Reinforcement strains both at the beginning (ε_{inst}) and at 90 days (ε_{90}) of the sustained loading tests are greater for C1 series specimens, as might be expected. However, larger increments in strains due to long-term testing ($\Delta\varepsilon_{90}$) are found for C2 series specimens with long bond lengths (see Table 9). This is a sign of greater stress transfer, which is related to better bond behaviour attributable to a higher concrete grade.

3.3.2. Bond stress distribution

The experimental data shown in the previous section was used to analyse bond deterioration due to sustained loading. Taking the definition of bond as the force transferred between the reinforcing bar and the concrete per unit of surface area, and performing equilibrium calculations on a piece of bar of length dx, along with the assumption of linear elastic behaviour of the bar, leads to:

$$\tau = \frac{EA}{\pi d_r} \frac{d\varepsilon_T(x)}{dx} \tag{2}$$

where τ is the bond stress, EA is the axial stiffness of the reinforcement and d_r is the nominal bar diameter.

Eq. (2) was applied to experimental reinforcement strains registered during long-term testing, and experimental bond stress distributions were obtained for internally strain-gauged specimens (i.e. specimens C1SFi, C1LFi, C2SFi and C2LFi). Information regarding bond stress distributions for specimens of series C1 and C2 at different stages of long-term testing is presented in Figs. 14 and 15 respectively, with location 0 mm representing the unloaded end as in previous figures. When Eq. (2) is applied between two consecutive strain gauges, $dx = \Delta x$, $d\varepsilon_r = \Delta\varepsilon_r$, and discrete constant values of bond stresses are obtained. It should be noted that bond stress distributions for specimen C2SFi is only partially represented due to the failure of one of the strain gauges (Fig. 15a).

Comparison of the plots of bond stresses at the time of application of sustained loading and at 90 days reveals a general trend of redistribution of bond stresses due to long-term loading. Within this redistribution, different trends can be found if short and long bond specimens are compared.

For short bond length specimens, bond stresses decrease at the loaded end and increase near the unloaded end, which is due to an increase of bar-concrete interface damage in the loaded end zone. This is a sign of the whole bond length contributing to the bond phenomenon. As an example, bond stress decreases from 5.9 MPa to 1.7 MPa at the loaded end and increases from 10.8 MPa to 18.5 MPa at the unloaded end in specimen C1SFi (see Fig. 14a), meaning a decrease of 70% and an increase of 71% respectively. Similar trends can be observed for specimen C2SFi (see Fig. 15a), with bond stress at the loaded end decreasing from 10.7 MPa to

Fig. 12. Experimental reinforcement strain distribution at different times during long-term testing for specimen a) C1SFi and b) C1LFi.

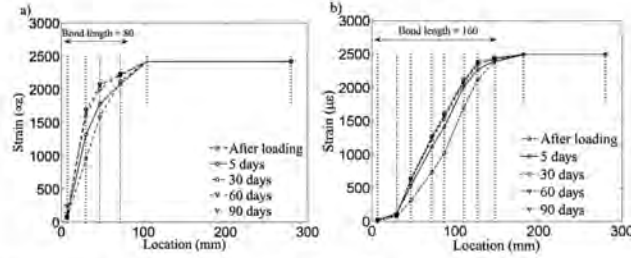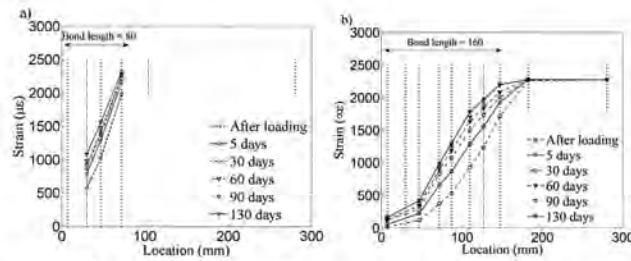**Fig. 13.** Experimental reinforcement strain distribution at different times during long-term testing for specimen a) C2SFi and b) C2LFi.
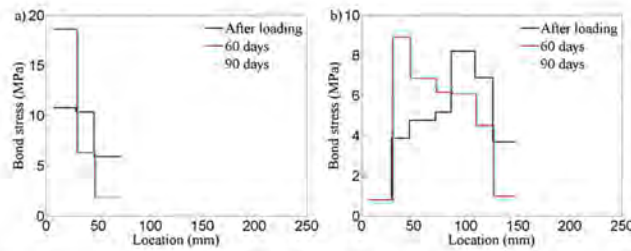

Fig. 14. Experimental bond stress distribution at different times during long-term testing for specimen a) C1SFi and b) C1LFi.
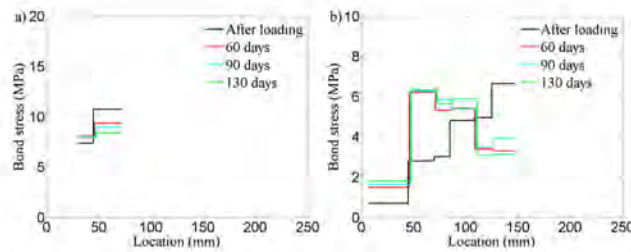

Fig. 15. Experimental bond stress distribution at different times during long-term testing for specimens a) C2SFi and b) C2LFi.

8.9 MPa, a reduction of 16%. No percentage can be defined at the unloaded end due to the failure of one of the strain gauges.

In the case of long bond length specimens, a redistribution of bond stresses is also visible, with bond stresses decreasing at the loaded end, and larger bond stresses developing in neighbouring sections. As an example, bond stress at the loaded end decreases from 3.7 MPa to 0.8 MPa and from 6.6 MPa to 3.9 MPa in specimens C1LFi (see Fig. 14b) and C2LFi (see Fig. 15b) respectively, representing a reduction in bond stress of 78% and 41% respectively. However, such redistribution does not take place at the unloaded end of the specimens, indicating that the stress transfer process does not affect the entire length of the bond in the same way.

4. Conclusions

The results of an experimental programme to investigate the bond stress-slip behaviour of GFRP bars in concrete under sustained load have been presented and discussed. A total of 12 pull-out specimens with two concrete strengths (35 and 50 MPa), two bond lengths ($5d_r$ and $10d_r$) and two reinforcement materials (GFRP and steel) were tested. The specimens were initially subject to short-term loading, which was sustained for a period of between 90 and 130 days. A load corresponding to 15% of the ultimate capacity of the GFRP bar was selected so as to correspond to the service range. Based on the results of this study, the following conclusion can be drawn:

- Experimental results on immediate slip due to short-term loading confirm results from previous studies with larger slips for specimens with either lower concrete compressive strength or shorter bond length, attributable to larger local deformability and damage in the concrete surrounding the bar. At the same time the tendency for GFRP pull-out specimens to bars to have larger slips than steel specimens is also confirmed, which may attributed to the deformability jointly with the mechanical interlock characteristics of the bars. Globally, the differences in slips between both ends indicate a non-uniform distribution of stresses along the bonded length, which is more pronounced for larger bond lengths.
- Data from the internal strain gauges during short-term testing shows that bond stresses are more evenly distributed in a short bond length where a quasi linear distribution of strains can be observed. This is not the case in a long bond length, where distribution is more clearly non-linear.
- As regards time-dependent slip due to sustained loading, results show an increase in the slip that stabilizes at approximately 60 days after loading, irrespective of the concrete strength, with higher increments for long bond length specimens. This can be attributed to bond deterioration and redistribution of stresses, which is more pronounced at the intermediate zone between loaded and unloaded ends. The experimental results confirm the influence of concrete strength on the deterioration of bond performance, with higher concrete compressive strength showing a time-dependent slip around 23.3% lower than that of lower concrete compressive strength.
- The evolution of bond stresses under sustained load was analysed using data from internal strain gauges. The experimental results confirm the influence of concrete strength on the stress transfer process and the redistribution of stresses along the bond length, decreasing in neighbouring loaded end zones due to an increase of bar-concrete interface damage. Specimens with the greatest concrete compressive strength showed a smaller loss of bond stresses at the loaded end, with values of 16% and 41% (for short and long bond length respectively) compared to 70% and 78% for the lowest concrete strength. In addition,

irrespective of the concrete compressive strength, bigger variations of bond stresses were found in long bond length specimens, a sign of greater bond stress redistribution along the bond length.

References

[1] Bank LC. Composites for construction: structural design with FRP materials. New Jersey: John Wiley & Sons; 2006.
[2] GangaRao HVS, Taly N, Vijay PV. Reinforced concrete design with FRP composites. London: Taylor & Francis Group; 2006.
[3] Nanni A, De Luca A, Zadeh HJ. Reinforced concrete with FRP bars: mechanics and design. CRC Press; 2014.
[4] Matthys S, Taerwe L. Concrete slabs reinforced with FRP grids. I: one-way bending. ASCE J Compos Constr 2000;4(3):145–52.
[5] Pecce M, Manfredi G, Cosenza E. Experimental response and code models of GFRP RC beams in bending. ASCE J Compos Constr 2000;4(4):182–90.
[6] Alsayed SH, Al-Salloum YA, Almusallam TH. Performance of glass fiber reinforced plastic bars as a reinforcing material for concrete structures. Compos Part B Eng 2000;31(6–7):555–67.
[7] Bischoff PH. Deflection calculation of FRP reinforced concrete beams based on modifications to the existing Branson equation. ASCE J Compos Constr 2007;11(1):4–14.
[8] Barris C, Torres L, Turon A, Baena M, Catalan A. An experimental study of the flexural behaviour of GFRP RC beams and comparison with prediction models. Compos Struct 2009;91(3):286–95.
[9] Al-Sunna R, Pilakoutas K, Hajirasouliha I, Guadagnini M. Deflection behaviour of FRP reinforced concrete beams and slabs: an experimental investigation. Compos Part B Eng 2012;43(5):2125–34.
[10] Kara IF, Ashour AF, Dundar C. Deflection of concrete structures reinforced with FRP bars. Compos Part B Eng 2013;44(1):375–84.
[11] Pepe M, Mazaheripour H, Barros J, Sena-Cruz J, Martinelli E. Numerical calibration of bond law for GFRP bars embedded in steel fibre-reinforced self-compacting concrete. Compos Part B Eng 2013;50:403–12. http://www.scopus.com/record/display.url?eid=2-s2.0-84877707714&origin=resultslist&sort=plf-f&src=s&st1=sena+cruz&st2=GFRP&sid=A193EC417D819EE6935192FA51CFD169.WXhD7YyTQ6A7Pvk9AlA%3a20&sot=b&sdt=b&sl=48&s=%28AUTHOR-NAME%28sena+cruz%29+AND+TITLE-ABS-KEY%28GFRP%29%29&relpos=4&relpos=4&citeCnt=1&searchTerm=%28AUTHOR-NAME%28sena+cruz%29+AND+TITLE-ABS-KEY%28GFRP%29%29.
[12] Mias C, Torres L, Turon A, Barris C. Experimental study of immediate and time dependent deflections of GFRP reinforced concrete beams. Compos Struct 2013;96:279–85.
[13] Zadeh HJ, Nanni A. Reliability analysis of concrete beams internally reinforced with fiber-reinforced polymer bars. ACI Struct J 2013;110(6):1023–31.
[14] Hassan M, Ahmed EA, Benmokrane B. Punching-shear design equation for two-way concrete slabs reinforced with FRP bars and stirrups. Constr Build Mater 2014;66:522–32.
[15] Larralde J, Silva-Rodriguez R. Bond and slip of FRP rebars in concrete. ASCE J Mater Civ Eng 1993;5(1):30–40.
[16] Benmokrane B, Tighiouart B, Chaallal O. Bond strength and load distribution of composite GFRP reinforcing bars in concrete. ACI Mater J 1996;93(3):246–53.
[17] Cosenza E, Manfredi G, Realfonzo R. Behavior and modeling of bond of FRP rebars to concrete. ASCE J Compos Constr 1997;1(2):40–51.
[18] Tighiouart B, Benmokrane B, Gao D. Investigation of bond in concrete member with fibre reinforced polymer (FRP) bars. Constr Build Mater 1998;12:453–62.
[19] Pecce M, Manfredi G, Realfonzo R, Cosenza E. Experimental and analytical evaluation of bond properties of GFRP bars. J Mater Civ Eng 2001;13(4):282–90.
[20] Achillides Z, Pilakoutas K. Bond behaviour of fiber reinforced polymer bars under direct pull out conditions. ASCE J Compos Constr 2004;8(2):173–81.
[21] Aiello AM, Leone M, Pecce M. Bond performance of FRP rebars-reinforced concrete. ASCE J Mater Civ Eng 2007;19:205–13.
[22] Lee JY, Kim TY, Kim TJ, Yi CK, Park JS, You YC, et al. Interfacial bond strength of glass fiber reinforced polymer bars in high-strength concrete. Compos Part B Eng 2008;39:258–70.
[23] Baena M, Torres L, Turon A, Barris C. Experimental study of bond behaviour between concrete and FRP bars using a pull-out test. Compos Part B Eng 2009;40(8):784–97.
[24] Mazaheripour H, Barros J, Sena-Cruz J, Pepe M, Martinelli E. Experimental study on bond performance of GFRP bars in self-compacting steel fiber reinforced concrete. Compos Struct 2013;95:202–12.

[25] Tepfers R. Bond clause proposal for FRP-bars/rods in concrete based on CEB/FIP model code 90. Part 1: design bond stress for FRP reinforcing bars. Struct Concr 2006;7(2):47–55.

[26] Marí AR. Numerical simulation of the segmental construction of three dimensional concrete frames. Eng Struct 2000;22:585–96.

[27] Torres L, López-Almansa F, Cahís X, Bozzo LM. A numerical model for sequential construction, repairing and strengthening of 2-D concrete frames. Eng Struct 2003;25(3):323–36.

[28] Kaklauskas G, Gribniak V, Bacinskas D, Vainiunas P. Shrinkage influence on tension stiffening in concrete members. Eng Struct 2009;31(6):1305–12.

[29] Torres L, Miàs C, Turon A, Baena M. A rational method to predict long-term deflections of FRP reinforced concrete members. Eng Struct 2012;40:230–9.

[30] Mias C, Torres L, Turon A, Sharaky IA. Effect of material properties on long-term deflections of GFRP reinforced concrete beams. Constr Build Mater 2013;41:99–108.

[31] Visintin P, Oehlers DJ, Haskett M. Partial-interaction time dependent behaviour of reinforced concrete beams. Eng Struct 2013;49:408–20.

[32] Gribniak V, Bacinskas D, Kacianauskas R, Kaklauskas G, Torres L. Long-term deflections of reinforced concrete elements: accuracy analysis of predictions by different methods. Mech Time-Dependent Mater 2013;17:297–313.

[33] Nkurunziza G, Benmokrane B, Debaiky AS, Masmoudi R. Effect of sustained load and environment on long-term tensile properties of glass fiber-reinforced polymer reinforcing bars. ACI Struct J 2005;102(4):615–21.

[34] Ascione L, Berardi VP, D'Apont A. Creep phenomena in FRP materials. Mech Reserch Commun 2012;43:15–21.

[35] Mazzotti C, Savoia M. Stress redistribution along the interface between concrete and FRP subjected to long-term loading. Adv Struct Eng 2009;12(5):651–61.

[36] Shahidi F. Bond degradation between FRP bars and concrete under sustained loads [PhD Thesis]. Saskatoon, Canada: University of Saskatchewan; 2003.

[37] Juette A, Weber A, Witt C. Long-term bond behaviour of GFRP rebars in severe environments [Quebec City, Canada]. In: Proceedings of the 4th International Conference on Durability and Sustainability of fibre reinforced polymer (FRP) Composites for Construction and Rehabilitation (CDCC 2011); July 2011. p. 10.

[38] Vilanova I, Torres L, Baena M, Kaklauskas G, Gribniak V. Experimental study of FRP RC tensile members under sustained load. Eng Struct 2014;79:390–400.

[39] UNE-EN 12390–3:2003. Testing hardened concrete – part 3: compressive strength of test specimens. AENOR 2003:20.

[40] UNE-EN ISO 15630–1:2011. Steel for the reinforcement and prestressing of concrete – test methods – part 1: reinforcing bars, wire rod and wire (ISO15630–1:2010). AENOR 2011:28.

[41] ACI 440.3R-12. Guide test methods for fiber-reinforced polymer (FRPs) composites for reinforcing or strengthening concrete structures. Am Concr Inst 2012:23.

[42] ACI 440.1R-06 Guide for the design and construction of concrete reinforced with FRP bars. American Concrete Institute; 2006. p. 45.

[43] Baena M, Torres L, Turon A, Mias C. Analysis of cracking behaviour and tension stiffening in FRP reinforced concrete tensile elements. Compos Part B Eng 2013;45:1360–7.

[44] ASTM C512-02. Standard test method for creep of concrete in compression. ASTM 2002:4.

AMADE

ANALYSIS AND ADVANCED MATERIALS
FOR STRUCTURAL DESIGN